Springer Geology Field Guides

Timothy Lawton · Katherine Giles · Mark Rowan

La Popa Basin, Nuevo León and Coahuila, Mexico

Halokinetic Sequences and Diapiric Structural Kinematics in the Field

Springer

Springer Geology

Springer Geology Field Guides

FieldGuides

Series Editor

Soumyajit Mukherjee, Department of Earth Sciences, Indian Institute of Technology Bombay, Mumbai, Maharashtra, India

Springer Geology Field Guides is a book series that provides the details of both well-known and little known transects to discover the beauty and knowledge of Geology, worldwide. Springer Geology Field Guides aims to bring geology field trips to professionals, students, and amateurs to find the most interesting geology worldwide. This series includes carefully crafted guidebooks that help generations of geologists explore the terrain with minimum or no guidance. In this series, the audience will also find field methodologies and case studies as examples.

This book series will welcome both authored and edited field guides of all geology disciplines, including structural geology, tectonics, sedimentology, stratigraphy, paleontology, economic geology, among others. Photo-atlases are also welcome.

More information about this subseries at http://www.springer.com/series/16656

Timothy Lawton · Katherine Giles · Mark Rowan

La Popa Basin, Nuevo León and Coahuila, Mexico

Halokinetic Sequences and Diapiric Structural Kinematics in the Field

Springer

Timothy Lawton
Quantitative Clastics Laboratory
Bureau of Economic Geology
Jackson School of Geosciences
The University of Texas at Austin
Austin, TX, USA

Katherine Giles
Department of Earth, Environmental,
and Resource Sciences
Institute of Tectonic Studies
The University of Texas at El Paso
El Paso, TX, USA

Mark Rowan
Rowan Consulting Inc.
Boulder, CO, USA

ISSN 2197-9545 ISSN 2197-9553 (electronic)
Springer Geology
ISSN 2730-7344 ISSN 2730-7352 (electronic)
Springer Geology Field Guides
ISBN 978-3-030-79396-8 ISBN 978-3-030-79397-5 (eBook)
https://doi.org/10.1007/978-3-030-79397-5

Above all, we are grateful to the people of northeastern Mexico, who met us with a range of reactions that included bemusement, trepidation, and intense interest, but who were always uncommonly generous and proud of the magnificent landscape that is their home.

Acknowledgments

The concepts included in these excursions have been assembled over several decades of research and would not have been possible without the contributions, insights, and financial support of many people and organizations. We thank the following graduate students of New Mexico State University for their detailed field work, much of which is included in this guide: Joe Andrie, Jennifer Aschoff, Ira Bradford, Rachel Couch, Dayna Druke, Dominic Druke, Stephanie Furgal, Jennifer Garrison, Frank Graf, Kyle Graff, Emily Haney, Breanna Hennessy, J. R. Hennessey, Cody Holbrook, Kevin Hon, Lela Hunnicutt Mack, Daniel Loera, David Mercer, Keith Shannon, David Shelley, Kyle Shipley, Brent Waidmann, and Amy Weislogel. We also acknowledge insights and contributions of colleagues Amy Brock-Hon, Brenda Buck, Mark Fischer, Andrew Hanson, Sam Hudson, Constantin Platon, Adam Smith, and Francisco Vega.

We thank the following people for their insightful contributions to our regional understanding of La Popa Basin area: Dick Buffler, Samuel Eguiluz-Antuñano, Bob Goldhammer, Rod Graham, Gary Gray, Bill Hart, Thomas Hearon, Chris Johnson, Robert Laudon, Jim McKee, Hector Millán, Jasper Peijs, Robin Pilcher, Bob Ratliff, Tim Seeley, Kristian Soegaard, Bruno Vendeville, Ian Watson, James Lee Wilson, and Cindy Yeilding. We acknowledge the donors to the American Chemical Society Petroleum Research Fund for partial support of this research (Grant ACS-PRF 33339-AC8). Mexico Small Grants Program and Mini-grant RC95 073 from New Mexico State University provided additional support. A review by Michael Hudec improved a previous version of this monograph. We also gratefully acknowledge the administrative expertise and assistance of Lee Hubbard, Administrative Secretary of the NMSU Geological Sciences Department, and Nila Matsler, Administrative Assistant of the Institute of Tectonic Studies.

Sincere thanks go to past sponsors of the La Popa Basin Joint Industry Research Consortium (Amoco, Anadarko, BHP-Billiton, BP, Chevron, Cobalt, ConocoPhillips, Devon, ENI, ExxonMobil, Hess, Kerr-McGee, Marathon, Maxus, Nexen, Samson, Shell, Texaco, and Unocal) for their support of our La Popa Basin research. The Bureau of Economic Geology at the University of Texas at Austin provided facilities for the final stages in the preparation of this guidebook.

Contents

Chapter 1
General Information

1.1 Opening Statement

Excellent exposures of salt diapirs and flanking strata in La Popa basin, northeastern Mexico, contain world-class examples of salt-sediment interaction that provided the basis for the concept of halokinetic sequences. The basin also contains one of the first secondary salt welds described in outcrop. Two one-day excursions described in this monograph provide an easily accessible overview of salt-sediment relations within a short distance of Monterrey, Nuevo León, Mexico. Excursion 1 constitutes an introduction to basin stratigraphy, an introduction to halokinetic sequences at El Papalote diapir, and a visit to a salt-cored detachment fold near the community of Hidalgo, Nuevo León. Excursion 2 is a visit to La Popa salt weld, where stops at several parts of the weld permit comparison of different structural styles developed along the weld. Each excursion begins and ends at the Marriott Courtyard Aeropuerto Hotel, near the Monterrey International Airport.

1.2 General Access and Logistics

Each of the two excursions described here is accessed from the Monterrey International Airport on the north side of Monterrey, Nuevo León, Mexico, which is an hour and a half flight from Houston, Texas. The starting point for the road logs is the Marriott Courtyard Aeropuerto Hotel (km 7, Miguel Alemán 23, La Victoria, Provivienda Guadalupe, 66600 Apodaca, Nuevo León, Mexico. Phone: + 52 81 8196 7900). Each excursion follows Highway 1610, a toll road or periferico, west toward Saltillo, exits at Mexico Highway 53 to Monclova, and then proceeds north to kilometer post 50 on Mexico Highway 53, 26.8 km north of the community of Hidalgo, Nuevo León. Distances between decision points are detailed in each excursion.

T. Lawton et al., *La Popa Basin, Nuevo León and Coahuila, Mexico*, Springer Geology,
https://doi.org/10.1007/978-3-030-79397-5_1

1.3 Safety Instructions

The excursions involve driving on two-lane Mexican highways, stops along dirt roads, and walking on rough terrane in desert country. Driving on Mexican Highway 53 is perhaps the most hazardous part of the trip. While most drivers are extremely courteous, speed limits are observed in a rather haphazard manner, and it is not uncommon to suddenly have a vehicle filling your rear-view mirror that was not evident seconds before. It is a common expectation that you will move to the road shoulder to permit a vehicle to pass and it is not uncommon to suddenly encounter an oncoming vehicle in your lane. You are expected to move right, but keep in mind that road shoulders are typically absent, whereas pedestrians are abundant. A blinking left-turn signal on the highway means different things: It can indicate that it is safe to pass the vehicle in question on the open road (a right blinker similarly indicates "don't pass"), but gypsum haul trucks also signal a left when they intend to leave the highway. Interpret the blinker with caution, and be aware how a driver behind you interprets your left turn signal if you are making a left off the highway. Sometimes, if you have unknown vehicles following closely, it is best to continue along the highway to find a place where you can pull off on the right and turn around. Be sure to obey the speed limits in Hidalgo and Mina, especially when children are present in school zones. Heavy truck traffic is now common on the dirt road to El Papalote diapir. Pull off the road at stops, and use caution in exiting your vehicle. Army checkpoints on the highway are not uncommon; they just want to know where you're going and may also ask where you started.

Flat tires are inevitable occurrences on the dirt roads. Always carry a spare tire and functional equipment to change the tire. Check the jack at the rental agency and before departing in the morning. There are numerous places to have tires fixed ("Vulcanizadores, Vulka") along the excursion routes, including Mina and the road junction to San Jose de La Popa (Excursion 2).

1.3.1 Driving at Night in Mexico is not Advisable

The outcrops you will visit are in the eastern Chihuahuan Desert, where it can be hot and dry. The base elevation is about 650 m. El Papalote diapir has an upper elevation of 980 m, and the high point of the weld traverse is 1100 m. Sun exposure is extreme and the air is dry; both factors lead, sometimes imperceptibly, to rapid dehydration. Wear long clothing and sunscreen as sun protection; carry and drink adequate water, even if it doesn't seem hot.

Irregular terrane, loose rocks, and spiny plants constitute the most common hazards of the walking traverses. A long-sleeved shirt and stout trousers are the best protection from plants and tumbles against rocks, and sturdy boots are required for the walks—you do not want to fall because if you do, you will put your hand (or more) down on painful cactus. Rattlesnakes are present but uncommon during the

day, and are usually only out and about in the spring and fall, particularly after rain. Always check the underside of a rock for scorpions or spiders when you pick it up.

1.4 Emergency Contacts

1. Hospital San José Tec de Monterrey. Emergency Phone: **(81) 8347–1011.** Avenida Morones Prieto #3000 Pte, Col. Los Doctores. CP 64710.
2. Red Cross Ambulance: **8375–1212**
3. Private Ambulance: **8317–1211** (English Spoken)
4. Federal Highway Police: **8343–2576**

Chapter 2
Introduction

The principal motivation for understanding salt diapirism and tectonics (e.g., Hudec and Jackson 2007) derives historically from the abundance of hydrocarbon resources in salt basins of the world. Moreover, bodies of evaporite such as diapirs, salt walls, and salt canopies form important trapping mechanisms for migrating hydrocarbons in those sedimentary basins. With advances in seismic data acquisition and processing, many subsurface salt structures are exquisitely imaged which, when combined with analog and numerical modeling, has resulted in advanced understanding of salt-body geometries and evolution.

Despite the quality of models and subsurface data, no experience with salt basins can substitute for seeing and studying well-exposed salt structures in the field. Many hydrocarbon traps are three-way truncations against salt, and neither models nor seismic data can resolve or predict the structural and stratigraphic details encountered in near-diapir wells. As a result of field studies of exposed salt-tectonic relations in northeastern Mexico beginning in the final years of the Twentieth Century, La Popa salt basin emerged as a geological laboratory of global significance for understanding the interaction of mobile salt with depositional processes and adjacent sedimentary stratal geometries. Despite excellent seismic imaging of subsurface salt bodies, the processes of salt-sediment interaction during passive diapirism were first documented through study of high-quality outcrop exposures in La Popa basin (Lawton and Giles 1997a; Giles and Lawton 2002). In addition, detailed observation of La Popa outcrops resulted in a general structural model for passive diapirism, diapir-flank deformation, the first description of a salt weld, and models for stratigraphic cyclicity adjacent to mobile salt bodies (Giles and Lawton 1999; Rowan et al. 2003; Giles and Rowan 2012; Rowan et al. 2012). Moreover, the proximity of La Popa basin and its record of diapirism to the Cretaceous-Paleogene Mexican fold and thrust belt, where deformation was the result of shortening of strata on a salt substrate, provides an ideal opportunity to compare and contrast the geologic record of salt diapirism with that of salt-detached fold and thrust tectonics. A rising worldwide awareness of how salt basins are incorporated into fold and thrust belts (e.g., Rowan and Vendeville 2006; Granado et al. 2018; Fernández, et al. 2020) ensures that the region described

T. Lawton et al., *La Popa Basin, Nuevo León and Coahuila, Mexico*, Springer Geology,
https://doi.org/10.1007/978-3-030-79397-5_2

Fig. 2.1 Location map of Mexico, showing tectonic elements of Mexican orogen pertinent to this field trip guidebook. Barbed lines indicate important structural trends of structural fronts, not necessarily thrust faults. Structural provinces of Mexican orogen: BB, Bisbee basin; CT Chihuahua trough/Chihuahua tectonic belt; MS, Monterrey salient of Sierra Madre Oriental fold-thrust belt. Massifs or structural blocks where Jurassic through Lower Cretaceous strata are thin to absent: AP, Aldama platform; BS, Burro-Salado arch; CoP, Cordoba platform; CP, Coahuila platform; DP, Diablo platform; VSP, Valles-San Luis Potosi platform. Late Cretaceous-Paleogene basins: LP, La Popa basin; PB, Parras basin; SB, Sabinas basin; TMV, Tampico-Misantla-Veracruz foreland basin. Cities: C, Chihuahua; CV, Cuidad Victoria; G, Galeana; L, Linares; M, Monterrey; S, Sabinas; Sa, Saltillo; T, Torreón; TA, Tampico; VC, Veracruz. U.S. states: AZ, Arizona; LA, Louisiana; NM, New Mexico; TX, Texas. Mexican states: CHI, Chihuahua; COA, Coahuila; NL, Nuevo León; SON, Sonora; TAM, Tamaulipas. Sources cited in text

herein will continue to enjoy importance and prominence in the evolution of geologic thinking about salt tectonics.

La Popa basin is an onshore salt basin in the Mexican states of Coahuila and Nuevo León. The basin is broadly analogous to the interior salt basins of Texas and Louisiana that flank the Gulf Coast salt basin, and strikingly similar to adjoining salt basins of onshore northeastern Mexico (Fig. 2.1). La Popa basin provided one of the first examples of an exposed salt weld (Giles and Lawton 1999), previously interpreted as a reverse fault with entrained evaporite. Studies of strata surrounding several diapirs in La Popa basin likewise provided the first reported examples of distinctive conglomerate and finer-grained deposits derived directly from diapirs that were periodically exposed on the seafloor, or as ridges in subaerial depositional settings. In the

following sections we summarize the regional tectonic setting, the relevant tectonic provinces, the timing of deformation, the stratigraphy of La Popa basin, and the concepts of halokinetic sequences and composite halokinetic sequences. Halokinetic sequences were first recognized and interpreted on the basis of exceptional exposures in La Popa basin (Giles and Lawton 2002), but have subsequently been described from salt basins worldwide that contain passively rising salt diapirs (Giles and Rowan 2012). The primary historical motivation for understanding diapiric structure and the geometry of flanking strata has been exploration for, and improved understanding of, hydrocarbon reservoirs. In addition, diapirs are associated with important mineral deposits in many parts of the world. Onshore salt domes along the U.S coast of the Gulf of Mexico have been important sources of mineral resources, such as sulfur and gypsum. Zinc and lead deposits are associated with diapiric breccia in Neoproterozoic strata of South Australia (Cowley and Preiss 1997; Groves et al. 2003). The Central African Copperbelt of Zambia and the Democratic Republic of Congo, the world's largest sedimentary copper province, contains deposits associated with salt diapirs of the Neoproterozoic Katangan Supergroup (Hitzman et al. 2012). Moreover, diapirs and strata that flank salt structures increasingly will be exploited as sites for sequestration of carbon dioxide and other greenhouse gases as science and technology seek solutions to ongoing global change. The field study of salt-related stratal geometries and faults, near-salt fluid flow, as well as microfabrics and deformational textures of rocks flanking salt structures will provide important perspectives and insight into processes and reservoirs that must otherwise be inferred from subsurface data such as well logs and seismic-reflection data. Field study of the geologic phenomena of La Popa basin and environs, with results disseminated by excursions to the localities detailed here, will contribute to evolving scientific thought and changing societal requirements for the foreseeable future.

2.1 Regional Tectonic Setting

Late Cretaceous-Paleogene crustal shortening superimposed on sedimentary basins and structures formed during Jurassic extension created the varied regional structural domains of northern and eastern Mexico. The Mexican orogen consists of uplifts and basins that form a relatively continuous belt of deformation paralleling the Rio Grande through northeastern Chihuahua and central Coahuila and continuing through Nuevo León and Tamaulipas along the eastern coastline of Mexico (Fig. 2.1). In the United States, Cretaceous-Paleogene deformation of this approximate age range is termed Laramide, and the term is widely used in the Mexican geologic literature. Although the deformation in northeastern Mexico is of roughly similar age, the precise age of shortening was formerly not well constrained. For this reason, Guzman and de Cserna (1963) introduced the term "Hidalgoan" to refer to structures of the Sierra Madre and its foreland, but the term has not been used commonly in subsequent literature. More recent work indicates that shortening deformation in the mobile belt of Mexico ranges from ~ 100–43.5 Ma (early Late Cretaceous–Middle

Eocene; Fitz-Díaz et al. 2014; Juárez-Arriaga et al. 2019a, b) and thus demonstrates temporal overlap with the Sevier and Laramide deformational events farther north in North America. Several factors demonstrate the utility of a different name for Mesozoic-Paleogene orogenic shortening in Mexico: (1) deformation timing did not conform well with timing of Laramide deformation in the United States; (2) continental-margin arc magmatism was continuous during the interval of shortening in Mexico whereas it was interrupted during the Late Cretaceous along part of the western U.S. continental margin; (3) the deformed belt of Mexico displays diverse structural styles, described below. Therefore, we refer to deformation pertaining to Late Cretaceous-Paleogene shortening as the Mexican orogeny, as defined by Fitz-Díaz et al. (2018).

Both thin-skinned fold-and-thrust belts and thick-skinned inverted rift basins characterize deformation in the Mexican orogen of northern Mexico. In Chihuahua and the southwestern United States, the orogen consists of inverted sedimentary basins of Late Jurassic and Early Cretaceous age that are thrust outward over adjacent structural blocks with thinner Mesozoic stratigraphic sections, such as the Aldama and Diablo platforms, with inversion taking place along or near steep, basement-involved former normal faults (Hennings 1994; Lawton 2000). No significant foreland basin lies adjacent to the inverted Chihuahua trough or Bisbee basin; rather, synorogenic deposits are localized in intermontane basins adjacent to the uplifts (Seager and Mack 1986; Lawton and Clemons 1992). Apparently, loading of cratonal North America along the high-angle fault trends was insufficient to bend the thick lithosphere.

Southeast of the Chihuahua trough, the Sabinas basin is occupied by northwest-trending periclinal (doubly-plunging) folds of the Coahuila marginal fold belt (Wall et al. 1961). Farther south and southeast, sedimentary basins of Late Cretaceous and Paleogene age lie adjacent to a prominent fold-and-thrust belt that forms a system of ranges collectively known as the Sierra Madre Oriental. The Parras basin lies adjacent to the east–west-trending part of the Sierra Madre fold belt, and the Tampico-Misantla basin is adjacent to the part of the orogen that trends north-northwest (Fig. 2.1). As in the basins to the northwest, the Upper Cretaceous successions were folded and somewhat uplifted by late Mesozoic and early Cenozoic deformation, but they were also important sites of deposition coeval with ongoing deformation in the Sierra Madre Oriental (e.g., Guzman and de Cserna 1963; McBride et al. 1974; Ye 1997; Juárez-Arriaga et al. 2019a).

2.2 Tectonic Provinces

Four principal structural provinces of the Mexican orogen have historically been distinguished in the region that encompasses central and southern Coahuila and southern Nuevo León (Fig. 2.2). These provinces include: (1) The Sierra Madre Oriental, or Sierra Madre fold belt, which includes east-trending structures between Torreón and Saltillo as well as the northern part of the Monterrey salient (Figs. 2.1 and 2.2); (2) the Parras basin; (3) the Coahuila fold belt, Sabinas basin, and La Popa

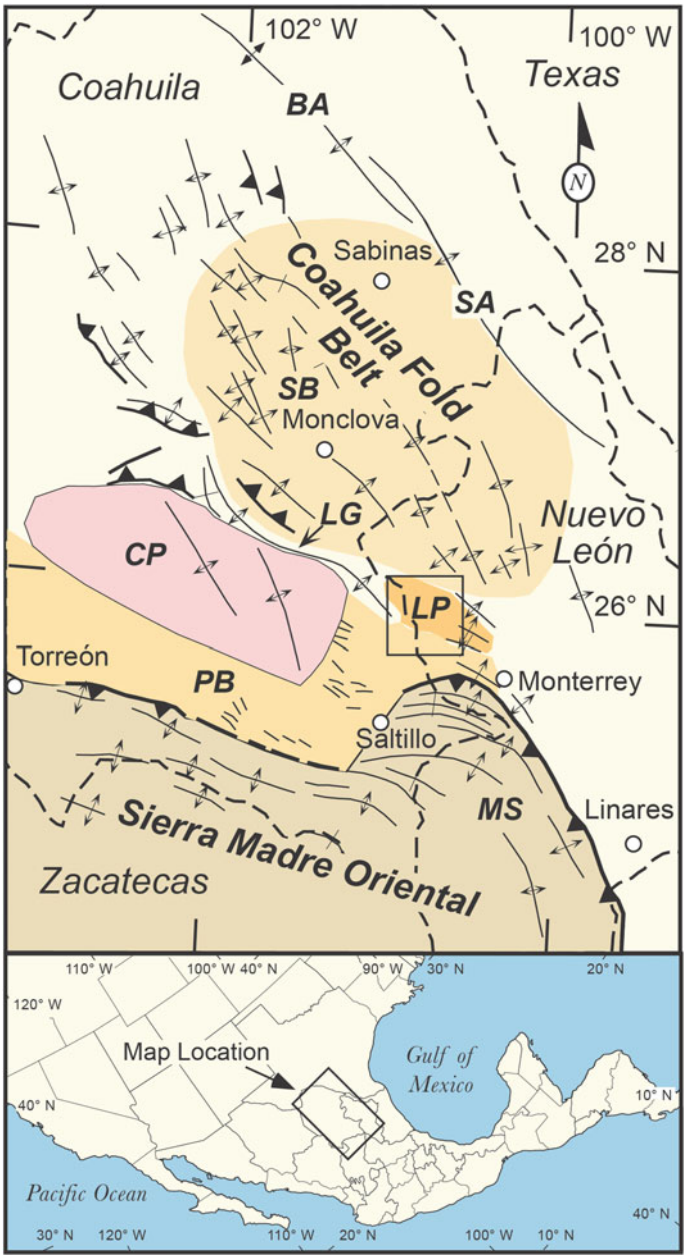

Fig. 2.2 Geologic elements of Coahuila and Nuevo León, Mexico. Tectonic features of the Mexican orogen: BA, Burro arch; Coahuila fold belt; CP, Coahuila platform; LG, La Gavia anticline, separating La Popa (LP) and Parras (PB) basins; MS, Monterrey salient of Sierra Madre Oriental fold belt; SA, Salado arch. The Sierra Madre Oriental includes east-southeast-trending structures between Torreón and Monterrey. Sedimentary basins of foreland region include: LP, La Popa basin; PB, Parras basin; SB, Sabinas basin

basin; (4) the Coahuila platform. These tectonic provinces were largely controlled by the distribution of Jurassic evaporite strata that were deposited in distinct salt basins of onshore Mexico (Lawton et al. 2001; Rowan et al. 2003; Hudec et al. 2013). The geologic characteristics of each of these provinces are described in the following sections.

2.2.1 Onshore Salt Basins

Jurassic evaporites of varying thickness were deposited in northeastern Mexico in discrete salt basins (Fig. 2.3). A series of basement arches, the Tamaulipas, Burro, and Salado arches, separated the onshore salt basins from the Louann salt basin of the Gulf of Mexico. An evaporite section estimated at ~2000 m thick was deposited in La Popa salt basin. Flanking La Popa basin to the north, the Sabinas basin also locally contains a thick evaporite section. The thick salt sections in La Popa basin led to mobile salt and the formation of diapirs, salt walls, and salt-withdrawal minibasins, the topic of this

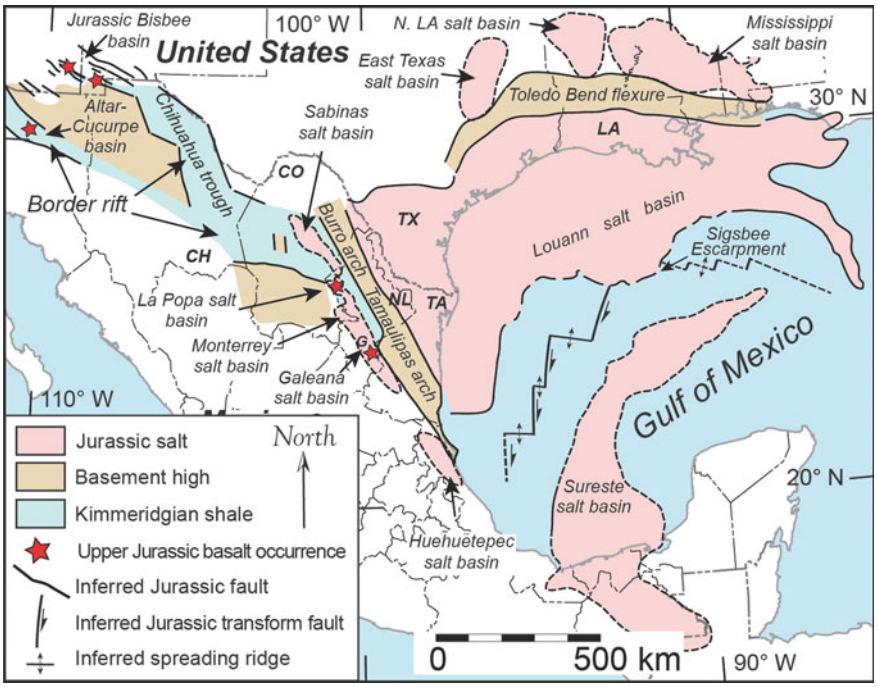

Fig. 2.3 Paleogeographic map of Gulf of Mexico salt basins and onshore salt basins flanking the Gulf, and including the Late Jurassic basins of the border rift system (Lawton and McMillan 1999). Adapted from Hudec et al. 2013; Lawton and Amato (2017). Locations of spreading centers and transform segments in Gulf of Mexico after Sandwell et al. (2014)

field guide. The Sabinas basin also contains examples of salt-induced deformation that include elongate periclinal detachment folds and a long, north-trending salt wall that was subsequently welded during shortening, paired with a large salt withdrawal basin, termed the San Antonio syncline (e.g., Vega et al. 2007). To the south in the fold belt, folds of the Monterrey salient are detached on a thinner evaporite section of the Monterrey salt basin (Hudec et al. 2013). The thinner evaporite section in the Monterrey salt basin was less mobile than in the basins to the north, and is characterized by parallel trains of detachment folds formed during the Cretaceous and Paleogene, described below. The evaporite section evidently thickens south of the Monterrey salient in the vicinity of Galeana, Nuevo León, attaining a thickness of at least 900 m (Cross 2012; Amezcua et al. 2020) in what is termed here the Galeana salt basin (Fig. 2.3).

2.2.2 Sierra Madre Oriental

The Sierra Madre Oriental is a fold and thrust belt of Late Cretaceous to Paleogene age that represents a southern extension of the western North American Cordillera (de Cserna 1956; Suter 1984; Campa-Uranga 1985; Drewes 1988; Aranda-García 1991). Isoclinal box folds of the Sierra Madre Oriental are detached from underlying basement and sedimentary rocks at a major decollement in Jurassic evaporites (Servais et al. 1986; Tardy et al. 1986 1994; Ye 1997; Marrett and Aranda-García 1999; Eguiluz-Antuñano et al. 2000).

The northern segment of the Sierra Madre Oriental exhibits a markedly arcuate map plan, known as the Monterrey salient, between Saltillo and Ciudad Victoria (Figs. 2.1 and 2.2). The salient consists of large-amplitude detachment folds with strikes that are broadly concordant with the arcuate front of the orogen (de Cserna 1956; Marrett and Aranda-García 1999). The folds are composed predominantly of Jurassic evaporites, carbonates, and siliciclastic sedimentary rocks and Lower Cretaceous marine carbonates (de Cserna 1956; Longoria 1984; Padilla y Sanchez 1985; Quintero-Legorreta and Aranda-García 1985; Campa-Uranga 1985; Suter 1984, 1987). The oldest rock exposed in the cores of isoclinal folds is gypsum of the Jurassic Minas Viejas Formation, indicating a detachment at the Jurassic evaporite level. Upper Cretaceous strata have generally been eroded from the folds, although the Parras Shale is widespread in tight synclines near the front of the orogen. The principal thrusts have displacements of tens of kilometers and bound nappes affected by faults of lesser displacement (Suter 1984, 1987; Padilla y Sanchez 1985; Quintero-Logorreta and Aranda-García 1985).

The structural style of the Sierra Madre Oriental fold belt and adjacent foreland depends to a great extent on the lithology and geometry of strata involved in the deformation (Ye 1997; Eguiluz de Antuñano et al. 2000; Fitz-Díaz et al. 2018). Two of the most striking lithology-controlled structural styles occur where the Upper Jurassic evaporite units significantly thicken. In the external thrust sheets (e.g., the Monterrey salient), upright isoclinal folds and the thrusts are detached on the salt (Gray and

Johnson 1995; Marrett and Aranda-García 1999; Eguiluz de Antuñano et al. 2000). In the Sabinas and La Popa salt basins thick evaporites led to the development of salt diapirs, elongate salt walls, and salt-withdrawal minibasins (Mc Bride et al. 1974; Laudon 1984; 1996; Lawton and Giles 1997a; Giles and Lawton 1999; Vega et al. 2007) that influenced subsequent shortening deformation (Rowan et al. 2003, 2012).

Where evaporite is thin or absent, such as southwest of Saltillo (Quintero-Legorreta and Aranda-García 1985) and near the mountain front of the eastern Sierra Madre west of Linares (Padilla y Sanchez 1982), low-angle thrusts become dominant over folds in accommodating shortening. Along-strike variation in structural style in the northern Sierra Madre Oriental is probably due to lack of evaporite units in the west and presence of thick evaporite deposits in the east, which pinch out abruptly near the present mountain front (Padilla y Sanchez 1982; Gray and Johnson 1995; Marrett and Aranda-García 1999), or differences in the thickness of evaporite and the pre-folding overburden (Gray and Johnson 1995).

2.2.3 Parras Basin

The frontal part of the Sierra Madre Oriental is flanked by foreland basins of Late Cretaceous to Paleogene age known as the Parras basin to the north and the Tampico-Misantla and Veracruz basins to the southeast (Fig. 2.1). The Parras basin lies north of the east-trending segments of the arcuate Sierra Madre Oriental orogenic belt, including the Torreón-Saltillo sector and the western part of the Monterrey salient (Fig. 2.2). The southern flank of the Parras basin is the abrupt thrust front of the Sierra Madre Oriental, where Upper Cretaceous strata have been eroded from folds of resistant Lower Cretaceous carbonate rocks (Imlay 1937; de Cserna 1956). The Parras basin is bounded by the Coahuila platform in the north and west, La Gavia anticline on the north and northeast, and the lateral edge of the salt-detached folds of the Monterrey salient in the east (Fig. 2.2).

2.2.4 La Popa Basin, Sabinas Basin, Coahuila Fold Belt

The Coahuila fold belt, or Coahuila marginal folded belt (Wall et al. 1961), is a southern extension of the northwest-trending Chihuahua fold-and-thrust belt (Charleston 1981; Fig. 2.1). The Coahuila fold belt is developed in the central part of the Sabinas basin (Smith 1981) and represents the northeasternmost part of the Mexican orogenic belt (Guzman and de Cserna 1963). The province is characterized by numerous NW–SE-trending folds with tight interlimb angles that involve Middle Jurassic through Upper Cretaceous rocks and are separated by wide synclines. Many of the anticlines are breached and demonstrate the presence of Jurassic evaporites in their cores.

La Popa basin lies on the southern edge of the Coahuila fold belt, and the structural style of northwest-trending folds that deform the basin indicates a greater structural affinity with the adjacent Sabinas basin than with the Parras basin. Northwest-trending detachment folds of La Popa basin are part of the Coahuila fold belt but generally below the level of surrounding structures. Aeromagnetic data (Eguiluz de Antuñano 1989) and depth to detachment calculations (Millán-Garrido 2004) indicate that basement is ~1500–2000 m deeper beneath La Popa basin than surrounding regions. The increased depth to basement provides a minimum original thickness for the evaporite in the basin. Much of that evaporite was evacuated during diapirism and the formation of salt-evacuation minibasins. Bordering the southwestern margin of the Coahuila fold belt are various anticlines (e.g., San Marcos and Sierra Madera anticlines) and thrusts, also of NW–SE bearing and with southwest vergence. With the notable exception of a long salt weld and San Antonio syncline in the Sabinas basin, mentioned above, La Popa basin is distinguished from the Sabinas basin by the presence of several diapirs and preservation of the youngest stratigraphic units in the region. The Parras and La Popa basins are separated by an anticline that forms the southeastern extension of the Sierra La Gavia, an anticlinal range that lies at the southwesternmost extreme of the Coahuila fold belt (Fig. 2.2).

2.2.5 Coahuila Platform

The Coahuila platform is a broad, southeast-plunging anticlinal arch of predominantly Cretaceous carbonate rocks resting on basement that includes Grenville metamorphic and granitic rocks, peri-Gondwanan accretionary complexes and Permo-Triassic granitic and sedimentary rocks (Charleston 1981; McKee et al. 1988; Goldhammer et al. 1991; Wilson and Ward 1993; Lopez et al. 2001). During the Late Jurassic and Early Cretaceous (Berriasian-Barremian ages), the Coahuila platform was exposed and served as a source for clastic strata on the southwest side of the Sabinas basin (Krutak 1967; Smith 1981; McKee et al. 1984 1988; Lawton and Molina- Garza 2014). The northeastern flank of the block was a high-angle extensional or transcurrent fault in Middle to Late Jurassic time (McKee et al. 1984, 1988; Chavez-Cabello et al. 2005). Seismic data likewise suggest that the northeastern boundary of the Coahuila platform and the Parras basin is a normal fault (Eguiluz de Antuñano 1989). La Gavia anticline is likely a fault-tip anticline that resulted from reactivation of a Jurassic normal fault. The Coahuila platform is deformed by open NW–SE-trending folds, indicating that folding here is basement-involved.

2.3 Timing of Deformation in the Mexican Foreland

The foreland of the Mexican orogenic belt experienced two major episodes of deformation since the middle Mesozoic. During Late Triassic to Late Jurassic time,

basement of the foreland was cut by high-angle structures that probably included both extensional and strike-slip faults (McKee et al. 1988; Eguiluz de Antuñano 1989). These faults created footwall uplifts, such as the Coahuila platform, with thin and onlapping sedimentary sections, and basins, such as La Popa basin, with thick Jurassic-Lower Cretaceous clastic and evaporite sections. Extension probably took place from Late Triassic through Late Jurassic (Kimmeridgian) time during the breakup of Pangea and development of the Gulf of Mexico (e.g., Pindell 1985; Marton and Buffler 1994; Dickinson and Lawton 2001).

The second major deformation event was the Mexican orogeny. The time of folding and thrusting in the Sierra Madre Oriental is defined on the basis of the ages of the foreland basin fill, which suggests an age range of Late Cretaceous (Cenomanian) to post-middle Eocene (e.g., McBride et al. 1974; Vega and Perrilliat 1989; Ye 1997; Martini et al. 2012) and direct $^{40}Ar/^{39}Ar$ ages on newly-formed illite that crystallized during folding (Fitz-Díaz et al. 2014, 2018). Fold timing is also locally defined from growth strata in the Parras and La Popa basins. In the Parras basin, estuarine growth strata of early Paleocene age onlap fold flanks (Couch 2005). Stratigraphic relations in La Popa basin indicate that folding began in Late Cretaceous (middle Maastrichtian) time and continued at least into the early Eocene (Gray and Lawton 2011). The onset is marked by the transition from prekinematic to growth (synkinematic) strata in areas lacking salt evacuation (Weislogel and Lawton 2000; Hon 2001; Druke 2005). Because of deep Oligocene–Miocene erosion of the Parras and La Popa basins (Gray et al. 2001, 2020), no post-tectonic overlap assemblage constrains the cessation of deformation.

The long-lived growth of diapirs and associated minibasins in La Popa basin represents an important exception to the regional pattern of two major deformation events. The nature and age of the onset of salt movement is not well understood, but diapirs rose passively throughout the 80 m.y. time interval represented by exposed strata (Aptian to early Eocene) in the basin.

2.4 La Popa Basin Stratigraphy

La Popa basin contains, in addition to the evaporite within the diapirs, a section of exposed sedimentary strata that ranges in age from Early Cretaceous (Aptian) to Eocene (Figs. 2.3, 2.4, 2.5, 2.6 and 2.7; Vega and Perilliat 1989; Vega-Vera et al. 1989; Lawton et al. 2001). The Lower Cretaceous part of the stratigraphic section is exposed principally in halokinetic growth strata that are upturned and exposed adjacent to the La Popa weld (Lawton et al. 2001; Rowan et al. 2012). In addition, something of the Jurassic history of the basin is known from carbonate strata and metaigneous blocks found encased in the gypsum caprock of exposed diapirs. Blocks of hydrothermally metamorphosed biotite diorite and monzonite in El Papalote diapir have isotopic and trace-element characteristics consistent with emplacement in a rift environment and $^{40}Ar/^{39}Ar$ cooling ages of 145.6 and 146.5 Ma (Garrison and McMillan 1999). Initial

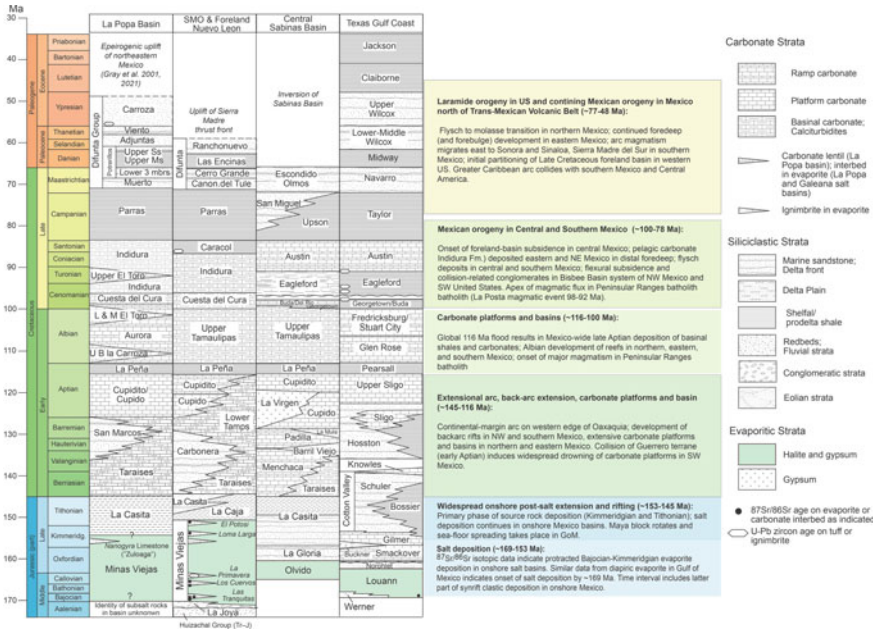

Fig. 2.4 Correlation chart for northeastern Mexico and Texas Gulf Coast, modified after Lawton et al. (2020). Tectonic episodes pertinent to northern Mexico indicated at right. Phrases in hiatal intervals indicate interpretation of hiatus origin. References for columns: La Popa basin, Sierra Madre: Eguiluz de Antuñano (1989); Fortunato and Ward (1982); Goldhammer (1999); Vega-Vera et al. (1989); Lawton et al. (2001); Vega and Lawton (2011). Sabinas basin: Cuevas-Leree (1985); González-García (1984); Götte and Michalzik (1992); Lehman et al. (1998); Zwanziger (1992). Texas Gulf Coast: Goldhammer (1999); Imlay and Herman (1984); Scott (1984); Eldrett et al. (2014). Age of salt in onshore Mexico salt basins primarily from Amezcua et al. (2020). Geologic Time Scale: Cohen et al. (2013; updated). Zircon symbols indicate ages of dated tuffs

metamorphism was probably the result of hydrothermal activity at the base of the evaporite section rather than deep burial before the end of the Jurassic.

2.4.1 Age of Evaporite Succession

The age of salt deposits in La Popa basin, as well as in the Gulf of Mexico and other onshore salt basins of eastern Mexico, remains a topic of active study and debate. Our stratigraphic correlation chart (Fig. 2.4) summarizes published biostratigraphic and geochronologic data for Jurassic to Eocene strata of northeastern Mexico. In addition, it incorporates age interpretations derived from the following datasets: $^{87}Sr/^{86}Sr$ isotopic data from diapiric evaporite sampled from various parts of the Gulf Coast onshore salt basins and Gulf of Mexico (Pulham et al. 2019; Snedden and Galloway 2019; Pindell et al. 2020), but depicted only on the Texas Gulf Coast column of

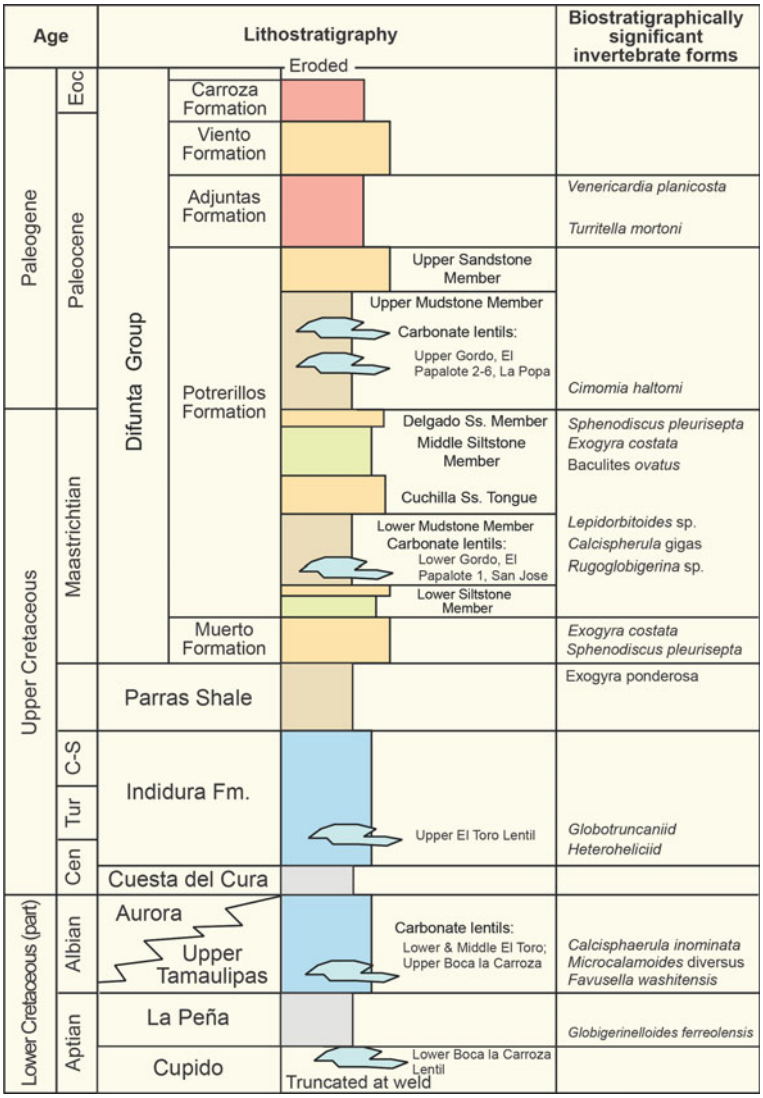

Fig. 2.5 Stratigraphic section exposed in La Popa basin (modified from Lawton et al. 2001). Carroza Formation is uppermost exposed unit of Difunta Group. AAPG© 2001, reprinted by permission of the AAPG, whose permission is required for further use

Fig. 2.4; carbonate strata interbedded with gypsum of the complexly deformed Minas Viejas Formation in the onshore Galeana salt basin (Fig. 2.4; Amezcua et al. 2020); and inferences regarding ages of allochthonous igneous blocks in diapirs of the Louisiana gulf coast (Stern et al. 2010) and La Popa basin (Lawton and Amato

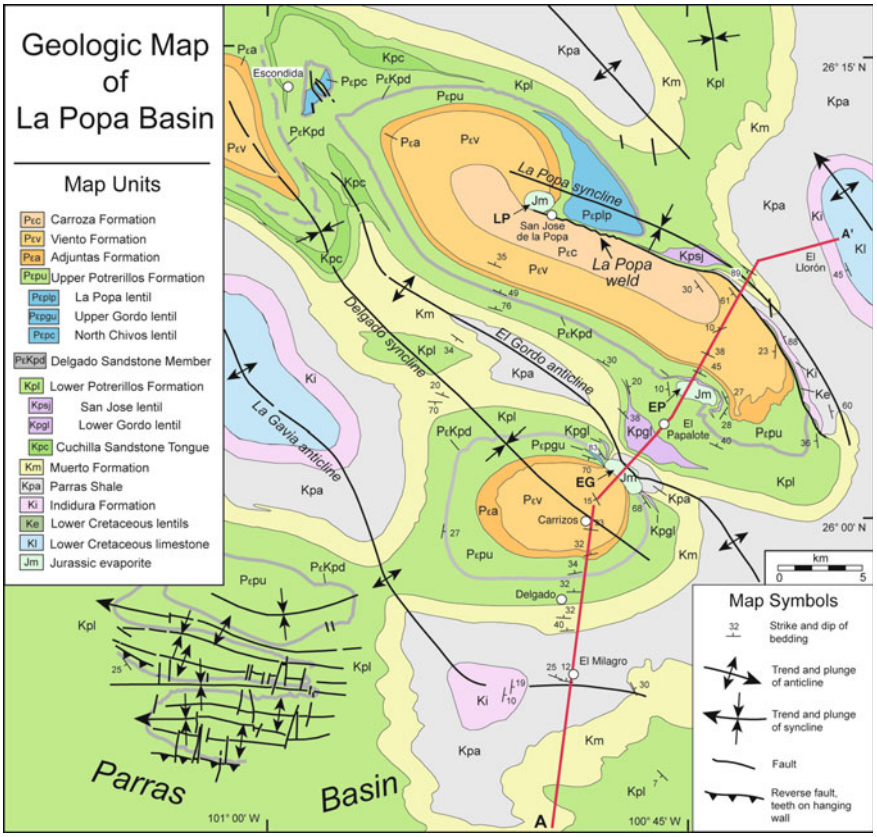

Fig. 2.6 Geologic map of La Popa Basin. Cross section line of Fig. 2.7 indicated. From Lawton et al. (2001). AAPG© 2001, reprinted by permission of the AAPG, whose permission is required for further use

2017). Strontium isotopic ratios in evaporite are more susceptible to diagenetic alteration than comparable isotopic ratios in carbonate rocks, although consistency of interpreted ages from evaporite samples around the Gulf of Mexico suggests that salt ranges as old as Bajocian (~170–169.5 Ma; Pulham et al. 2019; Snedden and Galloway 2019; Pindell et al. 2020). Although the Minas Viejas Formation of the Galeana salt basin experienced complex deformation due to tectonic shortening, $^{87}Sr/^{86}Sr$ ratios (Amezcua et al. 2020) are consistent with the inferred stratigraphic succession there (Cross 2012) and biostratigraphic ages of the sampled carbonate strata. The complete range of salt age is not yet known from La Popa salt basin, but limestone blocks within El Papalote diapir are Late Jurassic (Kimmeridgian), and thus correlative with the Zuloaga Formation (Vega and Lawton 2011). The younger evaporite age in La Popa basin is somewhat older than an age of 151 Ma (early Tithonian) interpreted for the top of the Minas Viejas Formation of the Galeana salt basin (Amezcua et al. 2020), but the presence of numerous thin carbonate beds in La Popa

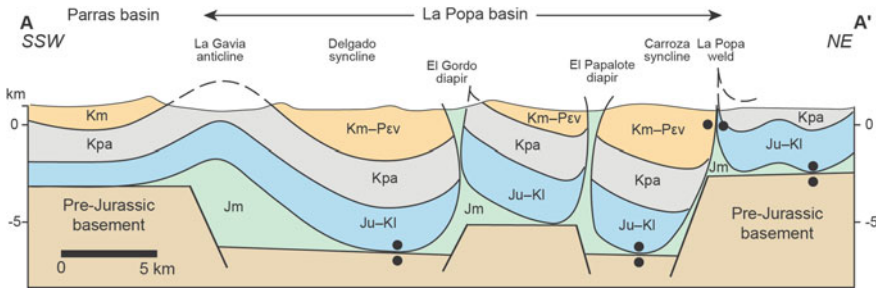

Fig. 2.7 Geologic cross-section of La Popa basin. Line of section indicated in Fig. 2.6. The Parras Shale in La Popa basin is structurally lower than its regional elevation in the Parras basin and at the northeast end of the section, indicating subsidence due to salt evacuation and an inferred depositional evaporite section in excess of 2 km thick. Map units of Fig. 2.6 generalized: Jm, Minas Viejas evaporite; Ju–Kl, undifferentiated Upper Jurassic and Lower Cretaceous formations from Zuloaga Limestone to Indidura Formation; Kpa, Parras Shale; Km–Pgv, Muerto through Viento Formations. Black dots indicate salt welds

diapirs suggests a gradational contact with originally suprajacent limestone strata, and the potential for a younger, possibly Tithonian, age for the top of the evaporite there. Indeed, the adjacent Gulf of Mexico basin has beds of anhydrite and other indicators of hypersaline conditions through most of the Oxfordian section (Rowan, in press).

Stratigraphic associations of evaporite in the Galeana and La Popa salt basins with subordinate interbedded lithologies indicates a shallow marine to supratidal depositional environment (Kroeger and Stinnesbeck 2003; Cross 2012; Lawton and Amato 2017). Several carbonate blocks in gypsum quarries at El Papalote diapir contain stratigraphic successions on the order of 5 m thick that consist of laminated limestone and displacive evaporites characteristic of a sabkha setting. Interbeds of fossiliferous carbonate strata in the evaporite section imply periodic flooding by marine transgressions. The younger $^{40}Ar/^{39}Ar$ ages of igneous blocks in El Papalote diapir in La Popa basin likely record basement cooling at the end of rifting near the Jurassic-Cretaceous boundary (Garrison and McMillan 1999).

2.4.2 Post-evaporite Stratigraphic Succession

All exposed post-salt formations in La Popa basin were deposited coevally with diapirism, which influenced stratal thicknesses and structure adjacent to the mobile evaporite bodies (Laudon 1984 1996; Lawton and Giles 1997a, b; Giles and Lawton 1999). Local exposures of limestone along the southeastern segment of La Popa weld (Fig. 2.6) contain the oldest post-salt rocks exposed in the basin, which contain Early Cretaceous (late Aptian and early Albian) forams (Lawton et al. 2001) indicating equivalence with the Cupido, La Peña, Upper Tamaulipas and Aurora formations of

the surrounding region. In La Popa basin, these limestone exposures represent lentils (locally developed formation members) deposited on bathymetric highs induced by passive diapiric growth; lentils are substantially thinner and of different facies than their regional correlatives (Giles and Lawton 1999). Limestone beds of the Indidura Formation, which overlies the Aurora Formation, yielded Late Cretaceous (Turonian) forams (Lawton et al. 2001).

The Parras Shale and Difunta Group (Campanian to Paleogene age) overlie the Indidura Formation in La Popa basin. Their outcrop thicknesses are less than in the Parras basin, partly as a result of southward thickening of the entire stratigraphic section toward the orogenic belt (e.g., Soegaard et al. 2003), but also due to thinning of strata adjacent to salt structures in the basin. Nevertheless, in the centers of minibasins in La Popa basin, particularly in the Delgado and Carroza synclines, the post-salt stratigraphic section achieves thicknesses of ~5000 m (Figs. 2.6 and 2.7). The thick Paleogene Difunta Group succession in La Popa basin (Vega and Perilliat 1989; Vega-Vera et al. 1989) is equivalent to the Wilcox Group of Texas (Fig. 2.4). The Cretaceous-Paleocene contact is marked by an intraformational conglomerate that contains impact ejecta derived from the Chicxulub impact crater (Aschoff et al. 2001; Shipley 2004; Lawton et al. 2005).

2.5 Halokinetic Sequences and Composite Halokinetic Sequences

Strata adjacent to passively rising diapirs thin and upturn toward the diapir to form stratigraphic packages bounded locally by angular unconformities that become conformable with distance from the diapir. These stratigraphic packages are termed *halokinetic sequences* (Giles and Lawton 2002). Two types of halokinetic sequence of distinctive geometry are recognized, hook and wedge halokinetic sequences (Fig. 2.8). In the case of hook halokinetic sequences, folding occurs within 200 m of the diapir, and the beds may be folded to interlimb angles of as much as 90° in individual hooks. Deposits of sediment-gravity flows are locally common in marine strata that contain hook halokinetic sequences. The discordance of the overlying angular unconformity similarly may be up to 90°, and slumps/debrites are common just above the unconformities in hook halokinetic sequences. In the case of wedge halokinetic sequences, the folding extends to as much as 1 km from the diapir, such that thinning and folding are gradual, the unconformity discordance does not exceed 30°, and deposits of sediment-gravity flows are rare.

Figure 2.10. Genetic model for the formation of tabular composite halokinetic sequence: (a) inflate diapir with folded thin roof (Hook HS 1); (b) failure of roof forming angular unconformity overlain by debrites (brown) and onlapping/overlapping strata; (c) inflation of the diapir and drape folding; (d) failure & repeat of deposition to form Hook HS 3; and (e) failure of Hook HS 3 roof. From Giles and Rowan (2012).

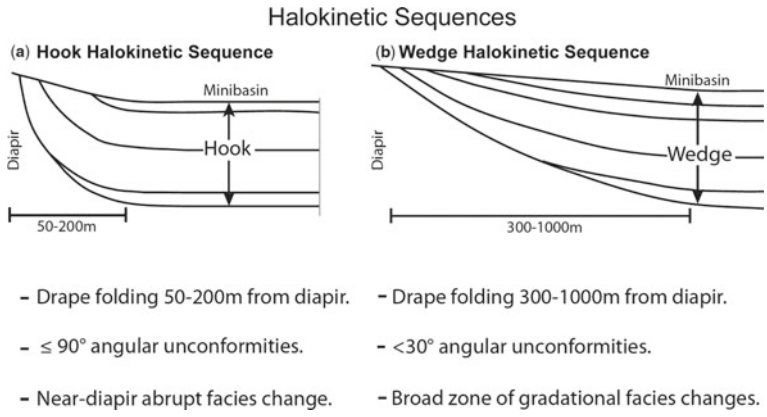

Fig. 2.8 Two end-member types of halokinetic sequences (HS): **a** hook halokinetic sequence and **b** wedge halokinetic sequence. From Giles and Rowan (2012). Geological Society of London© 2012, reprinted by permission of the Geological Society of London, whose permission is required for further use

Halokinetic sequences in La Popa basin are thin (usually 40–80 m) and correlate to 4th—or 5th—order depositional sequences (Giles and Lawton 2002). Individual halokinetic sequences are unlikely to be visible on deep seismic data, but they can stack to form successions within larger-scale, unconformity-bounded packages termed *composite halokinetic sequences* (CHS; Giles and Rowan 2012) that are more likely to be imaged on seismic data. Hook halokinetic sequences stack to form tabular CHS (Fig. 9a), where all folding and thinning takes place within 200 m of the diapir, so that the upper and lower boundaries of the CHS are essentially parallel. Wedge halokinetic sequences stack to form tapered CHS (Fig. 9b), where deformation and thinning occur over a distance of as much as 1 km, resulting in an unconformity-bounded stratal succession with gradually converging upper and lower surfaces. Shallower wedge halokinetic sequences have only minor upturn and stratigraphic truncation at the bounding unconformity, whereas the deeper wedges fold up to 90° and have significant structural relief.

It is the thickness of the strata deposited on the diapir, termed the roof, and thus the corresponding width of the zone of monoclinal drape folding that provides the dominant control on geometric style of halokinetic sequences and composite halokinetic sequences (Rowan et al. 2003; Giles and Rowan 2012). Roof thickness is usually dependent on the interplay between salt-rise rate and sediment-accumulation rate. In cases where sediment-accumulation rate is low relative to salt rise rate, the roof is thin, resulting in a narrow drape fold and tabular CHS development (Fig. 2.10a). The narrow drape fold corresponds to steep topographic relief over the diapir edge and increased propensity for slumping (Fig. 2.10b). In cases where deposition outpaces diapir rise, the roof tends to thicken and topographic relief is minor, resulting in a wide drape fold and tapered CHS development with rare redeposited material (Fig. 2.11).

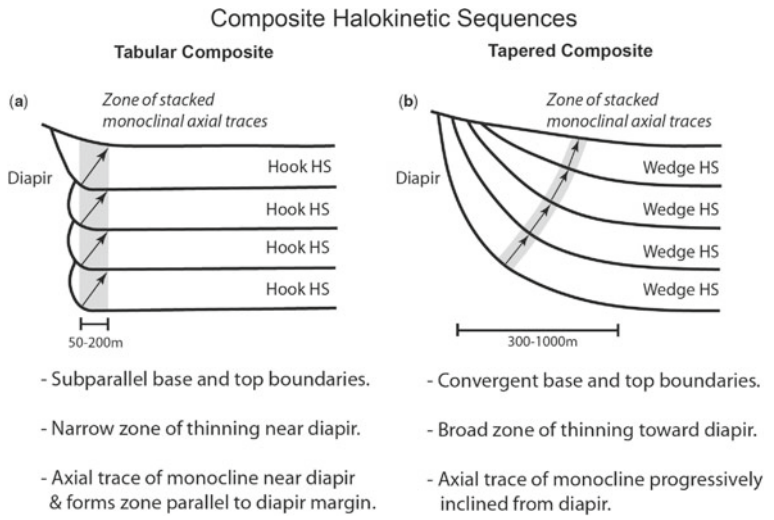

Fig. 2.9 Two end-member types of composite halokinetic sequences (CHS): **a** tabular CHS and **b** tapered CHS. From Giles and Rowan (2012). Geological Society of London© 2012, reprinted by permission of the Geological Society of London, whose permission is required for further use

2.6 Application to Deepwater Salt Provinces

The depositional setting of La Popa basin, described in the pages that follow, includes siliciclastic environments that range from shelfal, through delta front and shoreface, to continental, the latter including fluvial red beds. Topographically elevated sites on and adjacent to salt diapirs permitted deposition of platformal carbonates that accumulated in clear marine waters. In this regard, the basin differs substantially from deep-water salt basins dominated by turbidites and debrites. In addition, the basin lacks allochthonous salt sheets and canopies. Although the carbonate strata can be expected to be absent in deep-water settings, the overall aspects of the halokinetic sequences are similar in these shelfal settings and deep-water environments, both in geometry and scale (e.g., Rowan et al. 2020). The principles of comparative rates of sediment accumulation and salt rise rate that control the form and radial extent of halokinetic sequences and composite halokinetic sequences are also applicable in both types of depositional setting (Giles and Rowan 2012; Hearon et al. 2015). And in both settings, topography developed adjacent to rising diapirs, particularly in marine strata, leads to failure in flanking strata, which creates halokinetic sequence boundaries and suprajacent debrites. Therefore, with prudence, the concepts so beautifully displayed in La Popa basin can be, and have been, applied to salt basins elsewhere (see Rowan et al. 2020, for references).

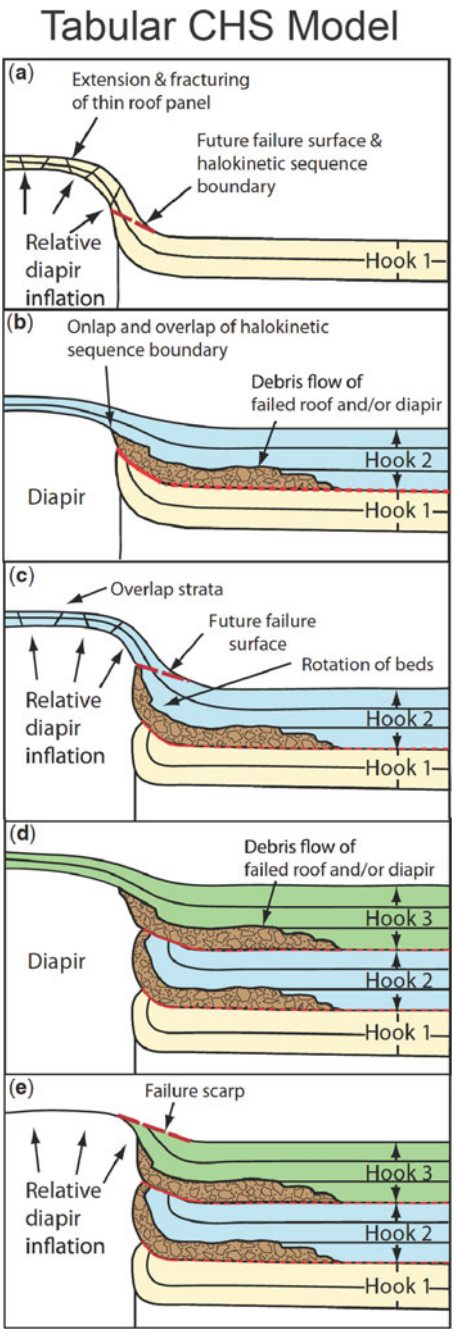

Fig. 2.10 Genetic model for the formation of tabular composite halokinetic sequence: **a** inflate diapir with folded thin roof (Hook HS 1); **b** failure of roof forming angular unconformity overlain by debrites (brown) and onlapping/overlapping strata; **c** inflation of the diapir and drape folding; **d** failure and repeat of deposition to form Hook HS 3; and **e** failure of Hook HS 3 roof. From Giles and Rowan (2012). Geological Society of London© 2012, reprinted by permission of the Geological Society of London, whose permission is required for further use

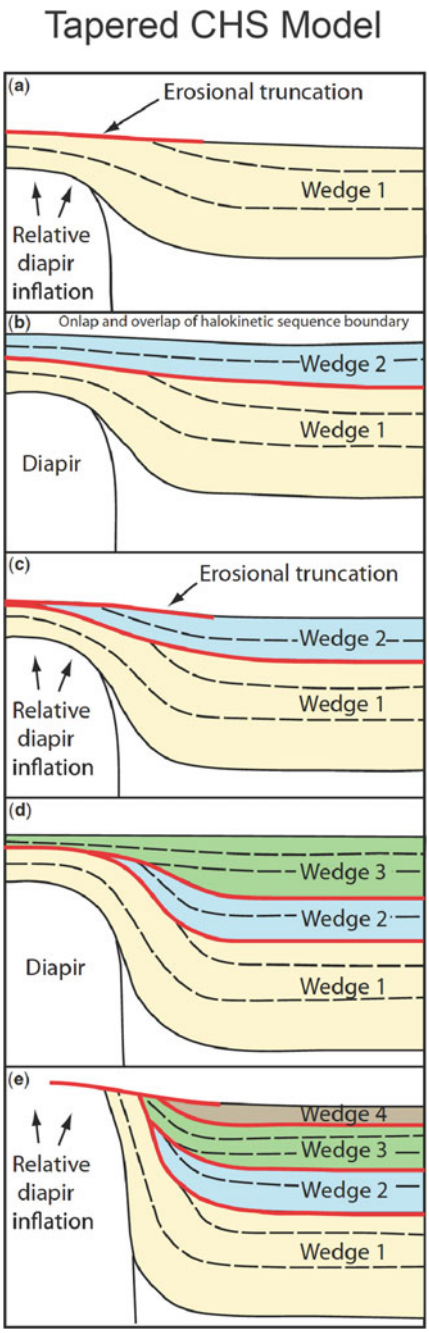

Fig. 2.11 Genetic model for the formation of tapered composite halokinetic sequence: **a** inflate diapir with minor erosional truncation of folded thick roof (Wedge HS 1); **b** overlap of Wedge HS 1 by Wedge HS 2; **c** inflation and erosional truncation of Wedge HS 2; **d** onlap and overlap of Wedge HS 3; and **e** erosional truncation of Wedge HS 3 and onlap of Wedge HS 4. From Giles and Rowan (2012). Geological Society of London© 2012, reprinted by permission of the Geological Society of London, whose permission is required for further use

Chapter 3
Excursion 1: EL Papalote Diapir and Potrero Chico

The excursion for each day is shown in Fig. 3.1. Excursion 1 consists of a visit to El Papalote diapir in La Popa basin and return via Potrero Chico near Hidalgo to compare diapiric and detachment structures. Excursion 2 is a tour of La Popa weld to observe the structural and stratigraphic variability of that feature. Both excursions, especially Excursion 2, contain ambitious itineraries polished during many trips by the authors; a newcomer to these itineraries might consider allotting additional time to visit all of the stops described here.

The objectives of Excursion 1 are:

1. To examine the lithologic character, sedimentologic origin, and structural deformation of growth strata in the lower mudstone, upper siltstone and upper mudstone members of the Potrerillos Formation, all of which underlie a salt overhang on the east side of El Papalote diapir.
2. To relate progressive structural deformation to stratigraphy within the concept of halokinetic sequences and to review possible models for halokinetic sequence generation adjacent to passive diapirs.
3. To evaluate how repeated and missing stratigraphic sections might be generated under a salt overhang in the context of the structural deformation observed.
4. To consider the observed variability of stratal and structural geometry adjacent to a single diapir in terms of diapiric evolution, basin paleogeography, and petroleum systems in three-way truncation traps against diapirs.
5. To observe the structural and stratigraphic nature of Jurassic and Lower Cretaceous beds deformed by tectonic shortening and detached on the Jurassic Minas Viejas salt horizon at Potrero Chico.

3.1 Geologic Setting of El Papalote Diapir

El Papalote diapir is one of several exposed evaporite bodies hosted by Upper Cretaceous and Paleogene strata of the Difunta Group (McBride et al. 1974; Laudon 1984).

T. Lawton et al., *La Popa Basin, Nuevo León and Coahuila, Mexico*, Springer Geology,
https://doi.org/10.1007/978-3-030-79397-5_3

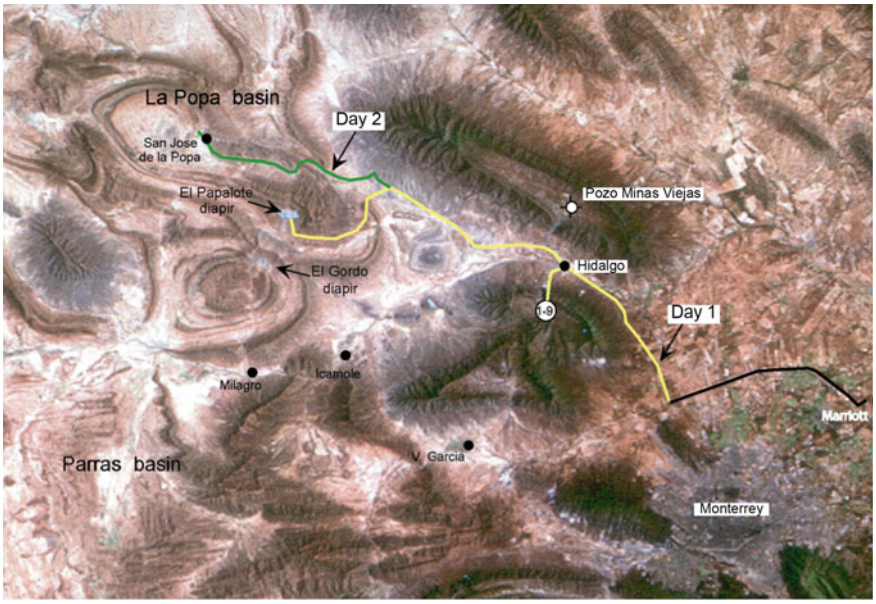

Fig. 3.1 Daily routes for the field trip. North to top of figure. A more detailed trip route, including trip stops, is found in each day of the field trip guide, except for stops outside of La Popa basin, indicated here

Syndiapiric stratigraphic units exposed adjacent to El Papalote diapir are Upper Cretaceous (Maastrichtian) through Paleocene strata of the Potrerillos Formation (Figs. 3.2 and 2.3). Depositional facies and structural deformation of the Potrerillos Formation record progressive diapiric growth, fluctuating topographic relief and episodic failure of the diapir and its roof, and folding of adjacent strata during rise and lateral expansion of the evaporite mass. Integration of the stratigraphy and structural features of the Potrerillos Formation therefore offers an opportunity to interpret the history of the diapir and to understand the geometry of strata adjacent to and beneath a flaring passive diapir.

In plan view, El Papalote diapir has an elliptical shape, elongate in a WNW-ESE direction (Fig. 3.2). Its exposed area is about 4.5 km^2. The exposed diapir consists of gypsum and anhydrite caprock that presumably overlies halite derived from Jurassic evaporite beds (Minas Viejas Formation) that lie an estimated 5000 m beneath the Potrerillos Formation (Laudon 1984). The caprock contains blocks of greenschist facies meta-igneous rocks (Garrison and McMillan 1999) whose protoliths include basalt, diabase, diorite, and andesite. These blocks are most common around the edges of the diapir. Uncommon but large blocks of Upper Jurassic limestone are also present (Laudon 1984) and represent carbonates originally interbedded with the upper part of the layered evaporite sequence (Vega and Lawton 2011). Clasts and blocks of meta-igneous rocks derived exclusively from the diapir are present in carbonate beds in the upper mudstone member of the Potrerillos Formation around

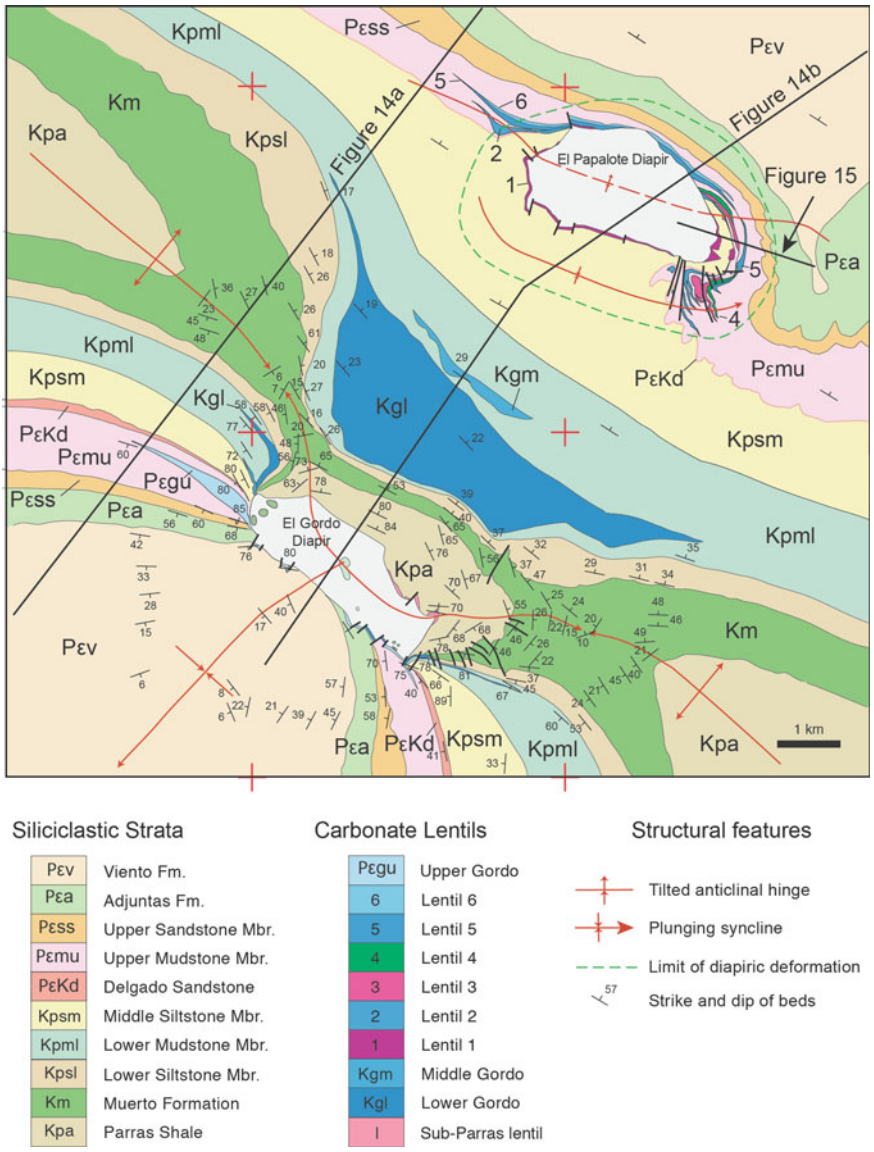

Fig. 3.2 Geologic map of El Papalote and El Gordo diapirs. El Gordo diapir is situated in the core of a detachment anticline indicated by black attitude symbols and fold hinge; in contrast, El Papalote diapir is located on a northeast-dipping fold limb, with black attitude symbols beyond the green dashed line representing the regional, "background" structure. The area within the green dashed line is the area of diapir-related deformation, which affects both the siliciclastic strata and the lentils (brighter shades). There is a syncline along the southwestern margin where regional dips reverse as the strata approach the diapir and a minor anticlinal flexure extending away from the diapir to the WNW and ESE. Cross sections are shown in Figs. 3.3 and 3.4 as indicated. Adapted from Rowan et al. (2003). AAPG© 2003, reprinted by permission of the AAPG, whose permission is required for further use

the periphery of the diapir and provide unequivocal evidence for exposure and erosion of the diapir, likely in both subaerial and submarine settings.

Carbonate strata, termed lentils by McBride et al. (1974) and Laudon (1984), are laterally-restricted beds of limestone present only near the margins of the diapir. They display facies relations indicative of deposition on a surface of some topographic relief (Giles et al. 2008). All lentils associated with El Papalote diapir are genetically related to the stratigraphic section and are part of the Potrerillos Formation; they do not represent exotic or allochthonous lithologies as previously asserted (Laudon 1984, 1996). Five lines of evidence support this inference: (1) Lentils can be traced laterally away from the diapirs into the surrounding Upper Cretaceous and Paleogene strata; (2) lentils contain Upper Cretaceous and Paleogene invertebrate faunas (Lawton et al. 2001); (3) interbedded siliciclastic strata thin toward the diapirs and display internal onlap relations, also in the direction of the evaporite exposures; (4) depositional facies within individual lentils record shallowing toward the diapir; and (5) meta-igneous clasts eroded from the diapir are present in the lentils and interbedded siliciclastic strata. These observations document long-lived passive diapirism that influenced sea-floor relief.

In general, the carbonate lentils can be divided into two depofacies: (1) meta-igneous clast bearing, oyster-rich debris flows and (2) oyster- and red algal-dominated wackestone-packstone (Hunnicutt 1998). As many as six stratigraphically discrete lentils are present on the east side of El Papalote diapir, whereas only three are well developed near the northwest corner (Figs. 3.2 and 3.3). The lowermost lentil lies stratigraphically beneath the Delgado Tongue of the Potrerillos Formation and is therefore Cretaceous in age; the other lentils are stratigraphically above the Delgado Tongue and are Paleocene in age (Vega-Vera et al. 1989; Vega and Mitre-Salazar 1997).

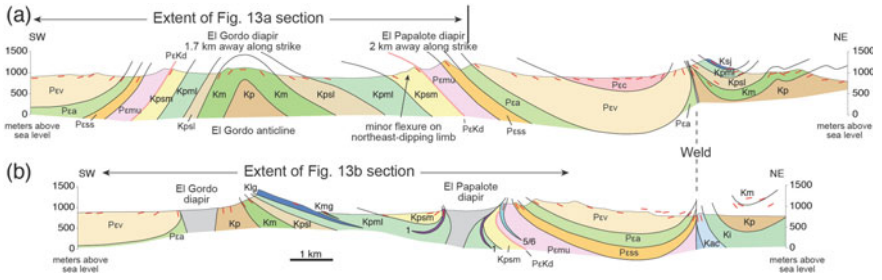

Fig. 3.3 Cross sections of El Papalote and El Gordo diapirs and vicinity. Section northwest of the diapirs crosses a major detachment fold, El Gordo anticline, and extends northwest beyond a minor anticlinal flexure on the northeast-dipping limb of the anticline. The axial trace of the flexure dips to the SW, essentially perpendicular to the dip of the major fold limb, which has an approximately vertical axial surface. The southwest section, which crosses the diapirs, displays a halo of deformation near the diapirs and lacks the flexure on the NE limb of the fold. Section locations indicated in Fig. 3.3; note that both sections continue NE to La Popa weld (Fig. 2.5). Adapted from Rowan et al. (2003). AAPG© 2003, reprinted by permission of the AAPG, whose permission is required for further use

Adjacent to the east flank of the diapir are at least six halokinetic sequences (Figs. 3.2 and 3.4; Giles and Lawton 2002; Rowan et al. 2003; Giles and Rowan 2012). Angular unconformities separate halokinetic sequences and have annular trends subparallel to the contact of the evaporite and Potrerillos Formation. The halokinetic sequences thin depositionally and erosionally toward the diapir and are overlain by conglomeratic strata rich in carbonate and meta-igneous clasts and fossils derived from erosion of the diapir and sediment that mantled it. The angular unconformities record uplift and deformation of adjacent strata during rise of the diapir, concomitant subsidence of an adjacent minibasin, and attendant erosion and beveling of uplifted strata toward the diapir. Internal thinning of halokinetic sequences resulted from this erosion, and also from depositional onlap of strata toward the diapir and incremental, upsection decreases in dip angle within sequences. These fanning dips within the stratal packages represent growth strata deposited during passive rise of the diapir.

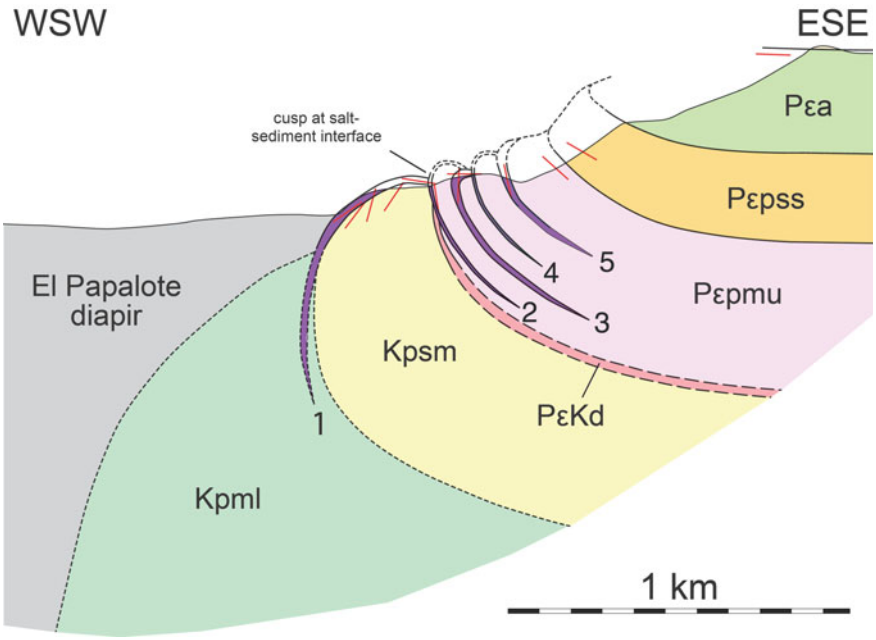

Fig. 3.4 Structural geometry of deformation halo on the east end of El Papalote diapir. Each halokinetic sequence (Giles and Lawton 2001) has as its base a carbonate lentil numbered 1–5. Adjacent to the diapir, the sequences are separated by angular unconformities that pass into correlative conformities away from the diapir. Siliciclastic beds within each sequence thin and onlap toward the diapir. The sequences are folded past vertical to overturned attitudes, which requires sliding to take place along the unconformities at the bases of the sequences. The resulting geometry requires the presence of cusps in the edge of the diapir at each unconformity. Location indicated in Fig. 3.2. Adapted from Rowan et al. (2003). AAPG© 2003, reprinted by permission of the AAPG, whose permission is required for further use

The western margin of the diapir lacks the dramatic overturning of flanking strata found near the eastern margin of the diapir, with strata attaining only near-vertical attitudes. Siliciclastic strata of the upper siltstone member of the Potrerillos Formation flatten rapidly away from vertical strata of the lowermost carbonate lentil directly adjacent to El Papalote diapir. In combination with the asymmetric distribution of lentils about the diapir, these observations indicate that the rising near-surface diapir flared to the east and southeast, in a basinward direction. Sediment supplied from the west (McBride et al. 1974) created a basinal slope to the east, favorable for diapiric expansion, and was deflected around the diapir to create a clear-water, sediment-shadow zone that favored local carbonate production (Hunnicutt 1998; Giles et al. 2008).

Ongoing diapiric rise and periodic breaching of the diapir crest preceded and accompanied the regional folding that affected La Popa basin. The lowermost carbonate lentil forms an almost continuous belt of exposures around the diapir, the limestone being absent only near the northeast corner of the diapir. This lentil is linear and separated into fault-bounded blocks on the south side of the evaporite mass, but folded about near-vertical axes along the west side. The elongate shape of the diapir, the folding of the lower lentil on the west side, and a gentle flexure of strata on the northwest and southeast flanks are consistent with NE-SW shortening of the sedimentary section during Mexican deformation.

The relative timing of diapirism and regional folding is also recorded by cleavage-bedding relationships on the flank of the diapir. A strong, subvertical east–west cleavage is present in the fine-grained siliciclastic strata of the Potrerillos Formation on both east and west flanks of the diapir. The cleavage cuts the axial surfaces of overturned folds adjacent to the diapir and therefore post-dates diapiric folding. We infer that the cleavage is an axial-planar cleavage related to the east–west fold trend of the Monterrey salient of the Sierra Madre Oriental to the south. Its relationship to the diapiric folds corroborates the inference that the culmination of Mexican shortening post-dated early diapirism.

3.2 Excursion 1 Itinerary and Road Log

The road log begins at the parking lot of the Marriott Courtyard Hotel located near the Monterrey Airport on the northeast side of Monterrey (Apodaca, Nuevo León). The route follows the toll road (*periferico*) toward Saltillo, exits at Mexico Highway 53 to Monclova, and then proceeds north to kilometer post 50 on Mexico Highway 53, 26.8 km north of the community of Hidalgo, Nuevo León. Bold numbers in the road log are cumulative kilometers (CK) and plain numbers are interval kilometers (IK) since the previous description.

CK IK.

0.0 0.0 *Marriott Courtyard Aeropuerto Hotel, Monterrey, Mexico. The route* (Fig. 3.1) *follows the toll road toward Saltillo, exiting the toll road at Mexico Highway*

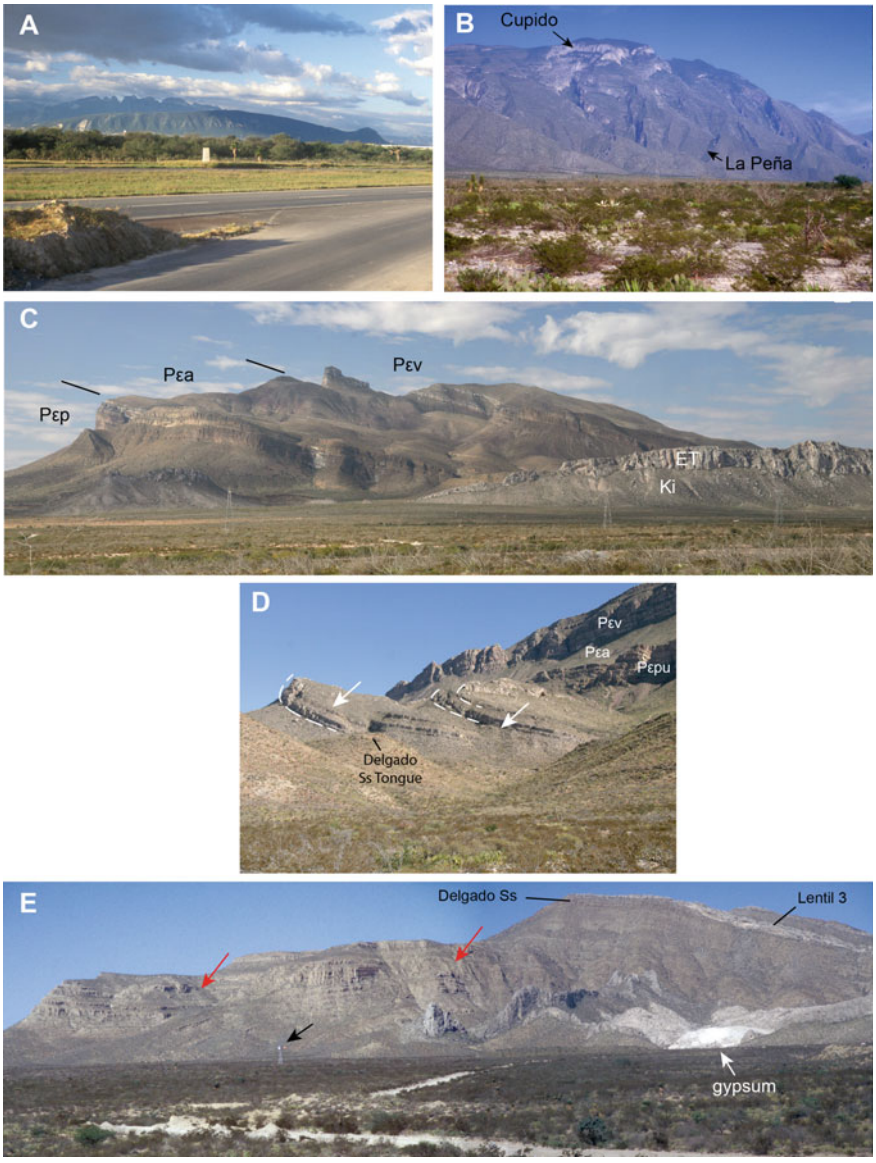

53 (sign to Monclova). On clear days the detachment folds west of Monterrey are visible from the toll road (Fig. 3.5a).

62.0 62.0 *km Post 50, HWY 53 (26.083741°/-100.632837°). Turn left (west) onto dirt road. Be cautious in signaling your left turn; a left blinker in Mexico can be*

◀**Fig. 3.5** Geologic features en route to El Papalote diapir. **a** Periclinal detachment folds northwest of Monterrey. Popo Chico anticline in foreground has a reefal buildup on its northwest (right-hand) end. The rugged skyline of the Las Mitras anticline is in the background. The Lower Cretaceous Cupido Limestone defines these folds. View southwest. **b** Sierra Potrero Grande (Sierra Minas Viejas). View west from road to El Papalote diapir. Thick-bedded Cupido Limestone forms skyline; Aurora Limestone forms steep flanks. **c** Panorama of Paleogene strata of Carroza minibasin (background) and Cretaceous strata on upthrown block of La Popa weld (foreground) viewed from east. Cretaceous strata include El Toro Lentil (ET), and Indidura Formation (Ki). Lentil is subvertical with top toward viewer. North-dipping beds in background are upper sandstone member of Potrerillos Formation (Pgp), Adjuntas Formation (Pga), and Viento Formation (Pgv). **d** Lentil 3 (white arrows) on southeast flank of El Papalote diapir. Resistant ledges dipping to right in middle foreground are fault-repeated exposures of the lentil. A facies change from thickly bedded diapir-flank oyster-foram packstone to thinner-bedded carbonate debris flows is visible in the left-hand lentil. The strata fold abruptly to vertical and overturned, indicated by dashed lines, toward the diapir, which lies out of sight on the other side of the hills. Delgado Sandstone Tongue of Potrerillos Formation marks K-Pg boundary. Background is upper sandstone member of Potrerillos Formation (Pgpu), Adjuntas Formation (Pga) and Viento Formation (Pgv). **e** View west of the minor syncline SW of El Papalote diapir and the anticlinal flexure adjacent to the diapir in upper siltstone member of Potrerillos Formation. Note thickening and divergence of strata between red arrows and windmill for scale (black arrow)

interpreted as an invitation to the following driver that it is safe to pass. Pull well away from highway onto dirt road headed west for stop 1–1 (Fig. 3.6).

STOP 1–1 Overview of stratigraphy and geography of La Popa basin. (26.082758°/ -100.638176)

Directly to the east is Sierra Potrero Grande or Sierra Minas Viejas, which is a periclinal detachment fold (Fig. 3.5b). The visible western limb is composed of vertical beds of Cupido and Aurora limestones of Aptian-Albian age (Fig. 2.4). Reefal biohermal Cupido Limestone caps the anticline, and backreef (?) beds onlap the reef from the northwest. The core of the anticline contains exposures of folded, but autochthonous gypsum of the Jurassic Minas Viejas Formation. A Pemex well in the core of the fold penetrated 3600 m of gypsum and of halite (Lopez-Ramos 1982) described in more detail at today's final stop at Potrero Chico.

To the west are exposures of the Parras Shale and Difunta Group of La Popa basin (refer to photo Fig. 3.5c for identification of key units in the area). Parras Shale and older Cretaceous siliciclastic units underlie the valley in the foreground. The ridge in the middle ground is composed of vertical, Lower Cretaceous El Toro carbonate lentils, with tops toward the observer, within the Lower Cretaceous siliciclastic succession. This ridge is separated from the main range by La Popa salt weld, which juxtaposes Lower Cretaceous limestone against Upper Cretaceous to Eocene formations in the background (the weld will be examined on Day 2). The younger units dip approximately 40° to the northeast in the northeastern limb of El Gordo anticline. The Potrerillos Formation underlies the southern third of the range. The upper siltstone and upper mudstone members of the Potrerillos underlie the lower slopes on the south. The upper sandstone member of the Potrerillos forms the prominent cliff above the lower slope. The middle elevations are dominated by reddish-brown to

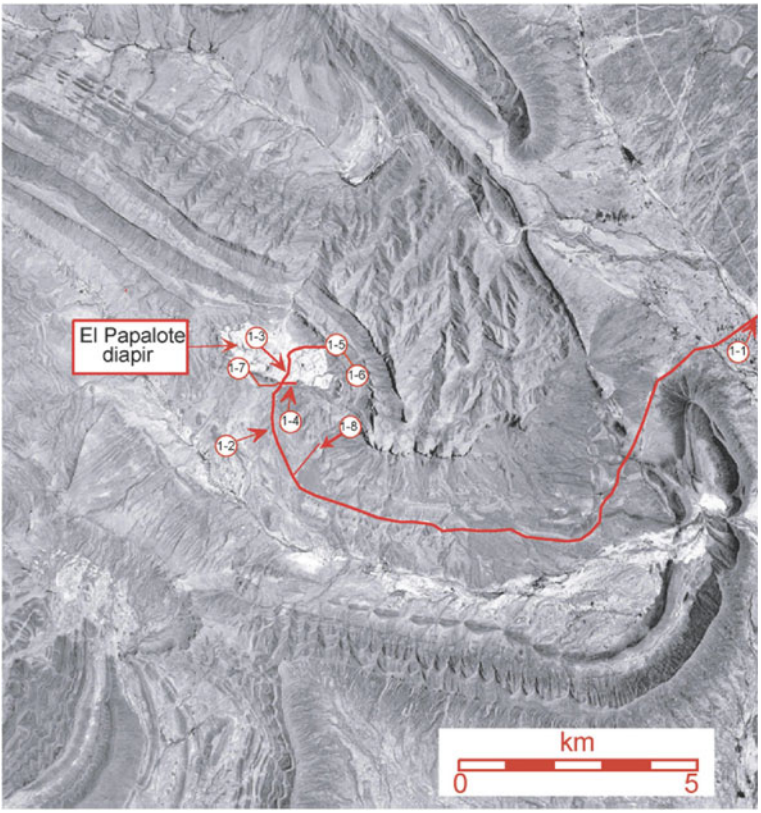

Fig. 3.6 Excursion 1 route. Excursion stops are indicated by circles. North is to top of figure

olive green-gray mudstone slopes of the Paleogene Adjuntas Formation. The upper cliffs and ledges are underlain by the Paleogene Viento.

Formation, which forms the highest promontory on the skyline. To the northwest (to the right of the photo in Fig. 3.5c) and off in the distance, the limestone massif of La Popa lentil, which is in the upper siltstone member of the Potrerillos Formation, lies in the up-thrown block of La Popa weld and records the diapiric phase of the structure.

Estimated travel time: From the Marriott Courtyard Aeropuerto Hotel to Stop 1.1 is 1 h by vehicle

Estimated stop Time: 15 min

Proceed west on dirt road.

64.6 2.6 *Hill at 9:00 (south) underlain by Parras Shale on lower slope, capped by sandstone ledges of the Muerto Formation. Muerto beds define the hinge of La Popa syncline, which lies in the upthrown block of the weld and parallels the weld.*

66.9 2.3 *Vertical beds of El Toro Lentil on right (west). To the left, folded and faulted beds of Parras Shale and Muerto Formation (Campanian–Maastrichtian) mark the SE end of La Popa weld, which dies out southward in a plunging anticline recorded in Upper Cretaceous strata. See Day 2 description for details about this area.*

69.3 2.4 *Long strike ridge of Muerto Formation forms southern skyline.*

71.9 2.6 *Ledges of very fine grained sandstone of the upper siltstone member of Potrerillos Formation exposed at 3:00 (north). These oyster-rich, upward-coarsening deposits probably represent deposits of hyperpycnal flows delivered to shelfal depths by storm surges.*

75.7 3.8 *Carbonate lentils and growth strata in low ledges to north of road.*

STOP 1.2 Carbonate lentils and growth strata, southeast flank of El Papalote diapir. (26.050868°/ -100.739658°)

Growth stratal wedges of carbonate and siliciclastic strata within halokinetic sequences on eastern flank of El Papalote diapir (Fig. 3.5d) dip southeast, away from the diapir, and are folded to just past vertical adjacent to the diapir, which is just behind the ridge in the middle distance. Note that the two carbonate outcrops are the same lentil offset by a fault that is hidden from view. The ridge in the foreground is the Delgado Tongue of the Potrerillos Formation, an important siliciclastic marker horizon in La Popa basin. The Cretaceous-Paleogene boundary, determined by the first occurrence of Paleocene nautiloids and marked by an ejecta-bearing sandstone, lies near the top of the Delgado Sandstone Tongue (Vega-Vera et al. 1989; Vega and Mitre-Salazar 1997; Lawton et al. 2005). The upper sandstone member of the Potrerillos Formation forms imposing cliffs to northeast, overlain by slopes of the Adjuntas Formation and succeeding cliffs of the Viento Formation.

To the northwest, beds within the syncline on the western margin of El Papalote diapir fan and thicken away from vertical beds of the lowermost exposed carbonate lentil (Fig. 3.5e). The gentle folding represents a minor flexure that flanks the slightly squeezed El Papalote diapir in the north limb of El Gordo anticline (Fig. 3.3a).

Estimated travel time from Stop 1.1 to 1.2 is 15 min

Estimated stop time: 15 min

78.58 2.88 *Bear right at a Y intersection marked by an explosives sign, proceeding northward to white exposures of diapir. This route passes a series of piles of gypsum on the road. The left fork goes to an active quarry in the southwestern corner of the diapir. The El Papalote diapir stops are shown in detail in* Fig. 3.7.

El Papalote diapir is currently the site of a large gypsum quarry. To visit the diapir, you must contact the quarry operator in advance (see contact information below). A letter of introduction from an academic institution has been requested of visitors in the recent past (September 2019).

The quarry operator is:

Yesera Monterrey, Serafín Peña 938 Sur, Centro, 64,000 Monterrey, N.L., Mexico.

Phone: +52 81 8345 1122.

http://www.yeseramonterrey.com/

79.06 0.48 *Crossing edge of diapir. Vertical beds of lowermost carbonate lentil (Kpl1) exposed on both sides of road. Continue driving up this road toward the*

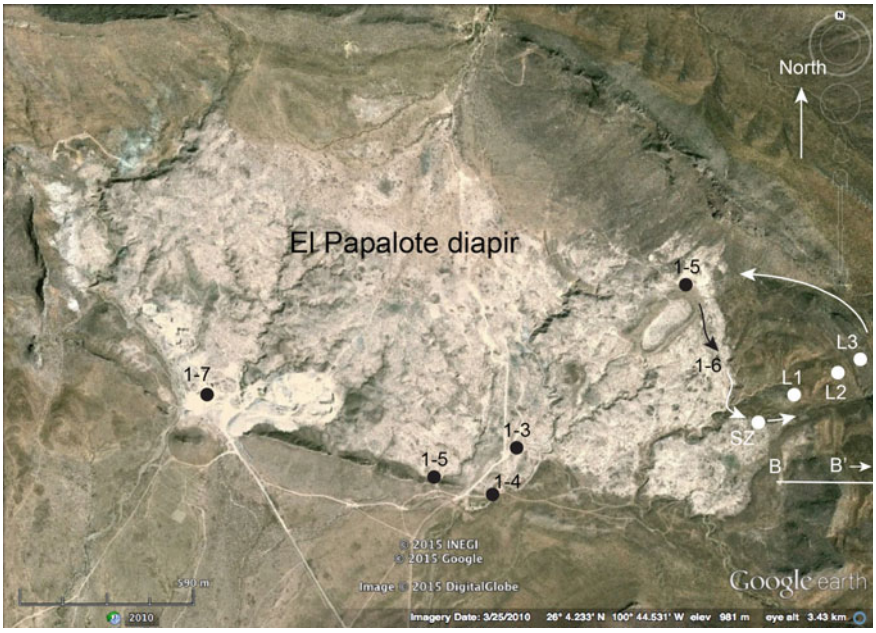

Fig. 3.7 Detail of field trip stops at El Papalote diapir. GPS locations of stops are in the text. Explanation: L1, L2, L3—Lentils 1, 2 and 3; SZ—Shear zone in diapir. Arrows indicate traverse of Stop 1–6. Section B-B' refers to trend of halokinetic sequence diagram in Fig. 3.17, but line reaches only to lentil 2 at east edge of photo. Image from Google Earth

abandoned cinder block building on the east side of the road. This road traverses the diapir.

79.54 0.48 *Park off to side of road.*

STOP 1.3 Non-evaporite blocks within El Papalote Diapir (Note: as of August 2015, this stop has been extensively obscured by quarry operations). (26.066894°/ -100.740155°)

Three primary lithologies (carbonate, meta-plutonic and meta-volcanic rocks) are present as blocks within El Papalote diapir. They represent stringers of competent rocks that were originally part of the layered evaporite sequence and subsequently broken up during diapirism, a common feature of salt provinces around the world, e.g., Paradox salt of Utah and Colorado (Lawton and Buck 2006); Zechstein salt of northern Europe (Becker and Bechstädt 2006), Keuper salt of the Spanish Pyrenees (Salvany and Bastida 2004), Hormuz salt of the Zagros Mountains of Iran (Alavi 2004), and Callanna salt of the Flinders Ranges of South Australia (Hearon et al. 2015). South of La Popa basin in the Sierra Madre Oriental, carbonates and volcanic layers are observed interbedded with gypsum in stratigraphically in-place Minas Viejas Formation (Kroeger and Stinnesbeck 2003). The largest carbonate block in El Papalote diapir (approximately 100 m across) has been identified as fossiliferous wacketone equivalent in age to the Jurassic Zuloaga Formation (Laudon 1984; Lawton et al. 2001) and was probably interbedded in the uppermost part of the evaporite section as normal marine conditions gradually prevailed (Vega and Lawton 2011). Other carbonate lithic types include micrite and recrystallized dolomite.

The igneous rocks are metamorphosed to greenschist facies and are divided into four general groups on the basis of petrology and geochemistry (Garrison and McMillan 1999): plutonic rocks, high Nb meta-volcanic rocks, intermediate Nb meta-volcanic rocks, and low Nb meta-volcanic rocks. The plutonic rocks have an equigranular texture and lack clear-cut evidence of chilled margins; nevertheless, preliminary U–Pb zircon analysis indicates that at least one block has a Paleogene age (Jeffrey Amato, NMSU, oral communication 2005) and thus may be related to Eocene intrusions near Monclova, north of La Popa basin. The meta-volcanic rocks are dominantly pale green meta-andesite, meta-diorite, and meta-diabase (Fig. 3.8a), with a variety of textures including vesicular, equigranular, and porphyritic. Phenocrysts in the meta-andesites range in size from several millimeters to 1 cm in length. Some outcrops of fine-grained igneous blocks have vesicles, which are filled with calcite, chlorite, and epidote. These rocks are most likely related to each other by partial melting of heterogeneous mantle (Fig. 3.9).

Metamorphism is dated at approximately 146 my based on $^{40}Ar/^{39}Ar$ ages on biotite and potassium in the meta-plutonic blocks (Fig. 3.10). This date is younger than the age of the Minas Viejas evaporite beds, suggesting that high heat flow from the basement continued into the latest Jurassic within the evaporite.

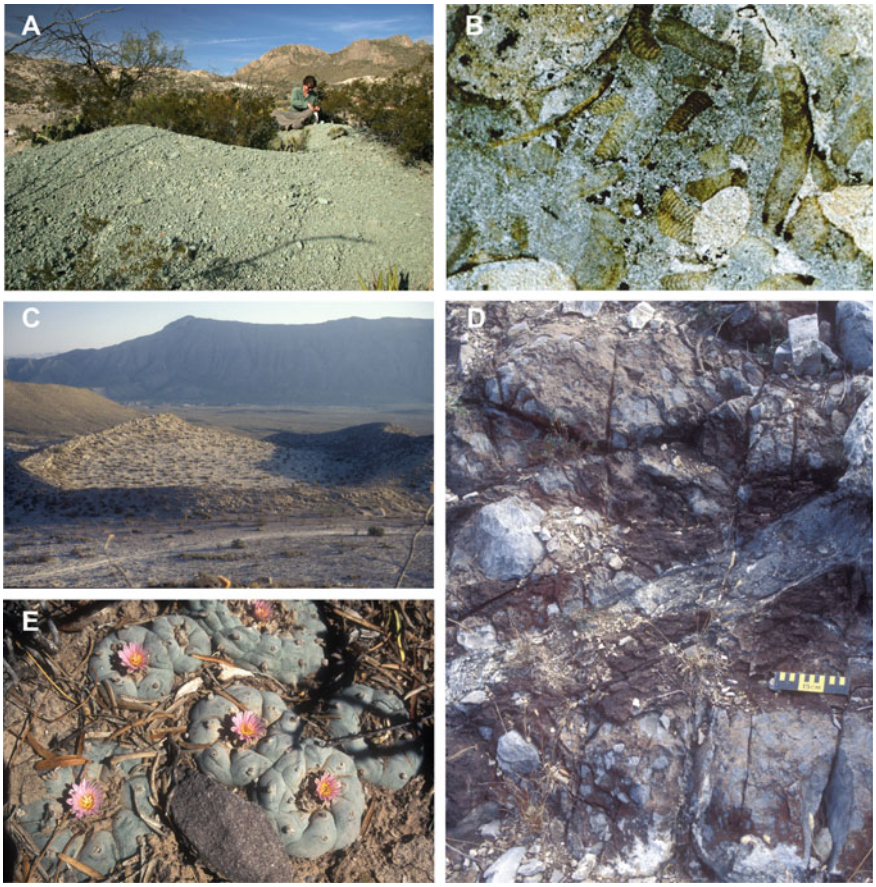

Fig. 3.8 Views of field trip stops at El Papalote diapir. **a** Typical exposure of mafic block that has been prospected at El Papalote diapir. Material in foreground consists of fragments of basalt altered to epidote and chlorite. **b** Photomicrograph of red algal packstone, Lentil 1. Red algal fragments, peloids, and micrite-filled bivalves in micrite. Field of view is 4 mm across. **c** Block of Upper Jurassic (Kimmeridgian) limestone in El Papalote diapir. Limestone exposure is about 150 m across from left to right. View south. **d** Debris-flow breccia exposed at base of Lentil 1. **e** Cactus typical of diapirs and their surroundings in La Popa basin

Estimated travel time from Stop 1.2 to 1.3 by vehicle is 5 min

Estimated stop time 25 min

79.86 0.32 *On foot, retrace route 0.32* km*to the south. Turn left (east) on dirt road. Road passes a small outcrop of stratified gypsum and basalt or diabase and enters a small arroyo.*

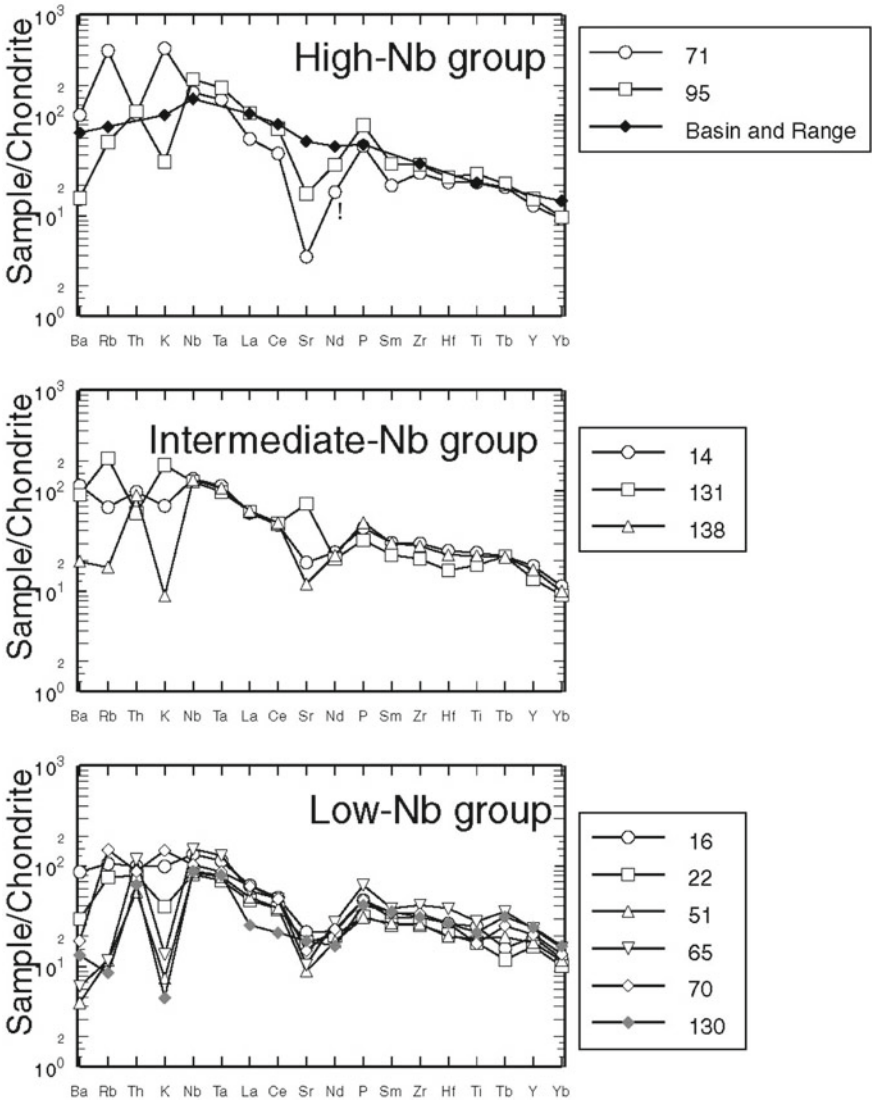

Fig. 3.9 Chondrite-normalized incompatible trace element diagrams (Thompson et al. 1984) for the low, intermediate and high Nb samples (Garrison and McMillan 1999)

STOP 1.4a Stratigraphy of Lentil 1 and contact with El Papalote diapir in arroyo (note as of October, 2019, runoff from the quarry and vegetation have partly obscured this outcrop). (26.065259°/ -100.740433°)

Vertical beds of Lentil 1 are exposed in the arroyo on the south side of the road in direct contact with gypsum caprock of the diapir. Lentil 1 is approximately 12 m

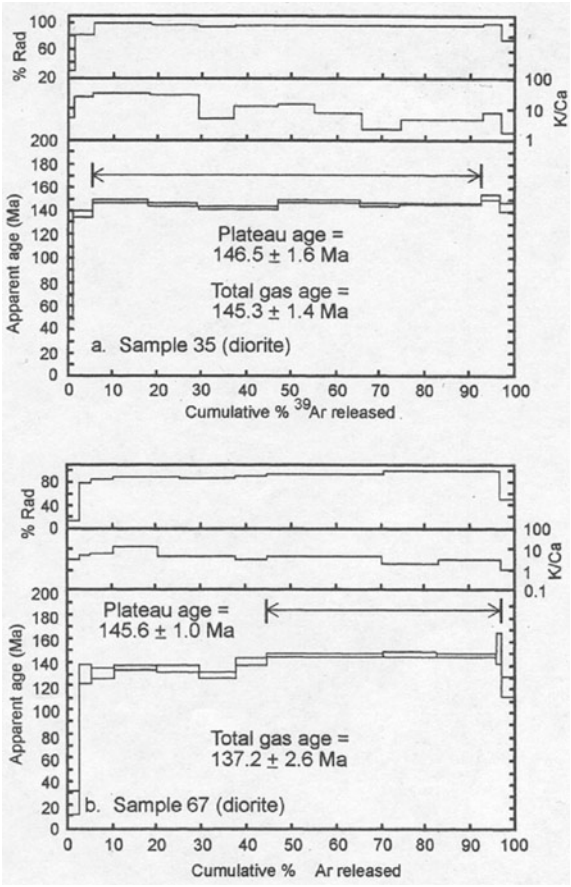

Fig. 3.10 Incremental heating $^{40}Ar/^{39}Ar$ spectra on biotite in two separate diorite blocks (Garrison and McMillan 1999)

thick here and stratigraphic up is to the south. The gypsum is poorly exposed but appears massive with local concentrations of shear fabric and small (pebble-cobble size) meta-igneous blocks.

The salt-sediment contact at the edge of the diapir is sharp and marked by a thin (<0.5 m) conglomerate horizon. The conglomerate contains abundant meta-igneous clasts derived from El Papalote diapir. The conglomerate is gradationally overlain by thick to massive beds of foram and red algal-dominated wackestone to packstone (Fig. 3.8b; Hunnicutt 1998). The lentil is capped by a distinctive red algal-foram packstone to grainstone horizon that contains abundant red algal coated grains. Locally red algae concentrically coat grains and achieve a large size (>1 cm), forming algal balls termed rhodoliths. This rhodolith marker horizon defines the uppermost beds of Lentil 1 and, in concert with sedimentary structures in interbedded sandstone, defines facing direction of the lentil in the more structurally complex areas. Locally the upper surface of Lentil 1 contains secondary fabrics indicative of karst

brecciation. Lentil 1 is interpreted as representing deposition in moderately deep-water conditions, but within fair weather wave base and the photic zone (lower-middle shoreface).

Note that although Lentil 1 contains calcite-filled fractures with a variety of orientations, there is no structural fabric parallel to the edge of the diapir, nor indication of a fault at the contact. This is also true of other diapirs in the basin; in other words, the diapirs are not fault-bounded and there are no shear or drag zones in strata adjacent to diapirs. The implication is that the relative motion of salt (up) and minibasin strata (down) was accommodated within the salt itself.

On foot, retrace walking route to main road and continue across it (west) to the first gap in lentil 1, where gypsum filled fractures are exposed in an arroyo at an offset in the lentil.

Estimated walking time from stop 1.3 is 1.4a is about 5 min

Estimated stop time: 20 min

STOP 1.4b Radial fractures in Lentil 1 (again, note that quarry runoff has partly obscured this outcrop). (26.065631°/ -100.742297°)

At this point, Lentil 1 consists of 2 discrete outcrops separated by a gap. The bedding is offset across the gap, suggesting the presence of a radial fault. At the gap, there are abundant radial calcite veins that accommodated subhorizontal extension parallel to the diapir edge (Fig. 3.11a). In addition there are several gypsum dikes with the same radial orientation (Fig. 3.11b) that formed by evaporite filling in gaps as Lentil 1 was pulled apart due to concentric extension caused by doming of the diapir roof during passive rise. Retrace walk to vehicles.

Estimated walking time from Stop 1.4a to 1.4b is 10 min

Estimated stop time: 10 min

Estimated walking time from stop 1.4b to vehicles at Stop 1. 3 is 5 min

80.18 0.32 *Return to car and proceed north along primary dirt road toward the northern end of the diapir, about 0.2 mile. Where the dirt road splits, follow the right (east) fork and take this poorly maintained road to the broad open flat space adjacent to limestone outcrops on the south side of the road. This will be our lunch stop for the day. (Note: In May, 2014, these roads were busy quarry haul roads, and stop 1–5 was accessed* via*foot across the east part of the diapir).*

STOP 1.5 Block of Jurassic Zuloaga-age limestone in El Papalote diapir. (26.071227°/ -100.734314°).

The limestone block exposed in the northeastern corner of the diapir (Fig. 3.8c) has long been considered Zuloaga Limestone (Laudon 1984). It is a large saucer-shaped exposure, 200 m in long dimension, of strata that are upright and dip inward toward

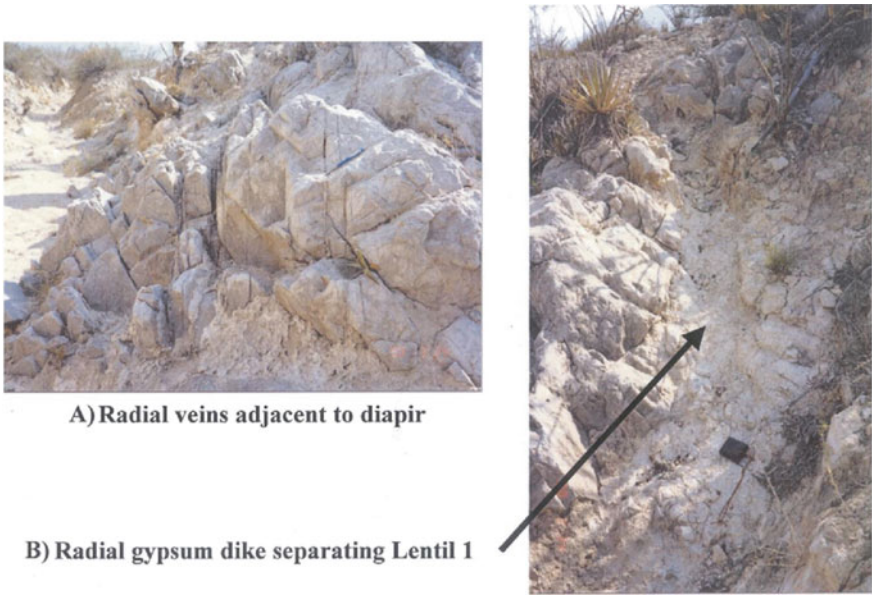

Fig. 3.11 Radial veins **a** and gypsum dike **b** in Lentil 1 that accommodated extension parallel to the diapir edge due to domal drape folding of roof strata. Views are from the diapir, and that in **a** is of the base of the vertical lentil at the contact with the diapir

the interior of the block. It consists of oyster wackestone with local beds of laminated mudstone deposited in shallow subtidal to intertidal environments consistent with a sabkha setting. It contains abundant *Nanogyra* cf. *N. virgula*, a Late Jurassic (Kimmeridgian) oyster, and yielded a specimen of *Cymatoceras* sp., a Late Jurassic nautiloid. We interpret this block as limestone deposited as part of the uppermost Minas Viejas Formation during periodic freshening of the evaporite brine and subsequently broken and carried upward with the diapir (Vega and Lawton 2011). Younger carbonate or siliciclastic rocks are not found as blocks in the diapir, indicating that suprasalt strata were not incorporated from the roof or walls of the diapir.

Estimated driving time from Stop 1.4 to Stop 1.5 is about 15 min, plus a short walk of 5 min. Estimated stop time: 45 min

STOP 1.6 Structure and stratigraphy of the eastern margin of El Papalote diapir. (26.071227°/ -100.734314°).

This walking traverse is a moderately rugged hike of approximately 1.5 km round trip. It begins at Stop 1.5 and ends at Stop 1.5 but key stops along the traverse are indicated on Fig. 3.5 and indicated by GPS coordinates in the following text. We will examine overturned stratigraphy and unconformities that are exposed on the east side of the diapir within the middle siltstone and upper mudstone members of the Potrerillos Formation (Fig. 2.5). Hazards of this walking stop include sharp-leafed,

ankle-high lechuguilla agave, steep slopes and loose rocks. Sturdy boots, a hat, and water are necessary and binoculars are useful.

Estimated walking time of Stop 1.6 traverse, including stops, round trip from Stop 1.5: 2.5 h

Proceed on foot southeast from the Zuloaga-age limestone block into the deep, steep walled arroyo cut into the diapir. Turn left into the first major side arroyo, which leads eastward out of the diapir and into the Potrerillos Formation.

Shear fabrics within diapiric gypsum (SZ in Fig. 3.7; 26.067536°/ -100.731929°).

There are two nearby stops in this drainage. The first is a shear zone (minimum 6–7 m wide within the diapir that dips approximately 60° west. It comprises anastomosing bands of massive gypsum, cataclasite with gypsum matrix and clasts of other lithologies, and gypsum veins. The cataclasites are green where coarser-grained and purple where finer-grained. The structural fabric indicates hanging wall up.

Outcrops are then covered until the second stop, which is just inside the diapir (within 10–20 m of the edge). Here, all you see is flow-banded (sheared?) gypsum with the fabric dipping about 32° west (similar to the dip of nearby Lentil 1).

Both outcrops are probably different expressions of a broad shear zone near the outer edge of, and within, the diapir that accommodated the relative movement between subsiding sediments and rising diapir. Viscous drag of the ductile salt against the brittle minibasin requires that the upward movement of the salt decrease in rate and magnitude toward the edge of the diapir. The difference in dip of the two fabrics may reflect a change in the dip of the diapir wall as it flares to the east, or it may just represent a larger-scale anastomosing fabric within a zone that is parallel to a straight (rather than curved) diapir margin.

Proceed east up the drainage and then up the small hill to the left (north) to a small saddle between a mound of green meta-igneous rock and the first limestone ledge outside the diapir.

Lentil 1 (L1 in Fig. 3.7; 26.068280°/ -100.730931°).

The saddle marks the edge of the diapir, with the meta-igneous clast just within the diapir. On the northeastern side of the saddle is an accumulation of carbonate and meta-igneous pebbles to boulders in a red sandstone matrix, which represents the northernmost identifiable exposure of Lentil 1 on this side of the diapir. At present levels of exposure, it is the oldest unit adjacent to the eastern flank of El Papalote diapir (Figs. 3.2, 3.4 and 3.12). Lentil 1 at this location dips approximately 35° WSW. Sedimentary structures in siliciclastic units indicate that the sandstone beds up the hill from Lentil 1 are overturned, as is the lentil. The basal 2 m of the limestone is a breccia of limestone, meta-igneous, and gypsum clasts (Fig. 3.8d). This breccia at the base of Lentil 1 is in contact with the evaporite of the diapir (Fig. 3.13a). The breccia represents a debris flow deposit at the base of halokinetic sequence I that was initiated by salt diapiric rise.

North from the saddle, two resistant ribs of sandstone on the hill are visible dipping west (to the right) on the other side of the small drainage (Fig. 3.13b). The sandstones dip toward the diapir and converge going uphill (this is effectively the view schematically drawn in Fig. 3.12). Again, these strata are overturned. If you

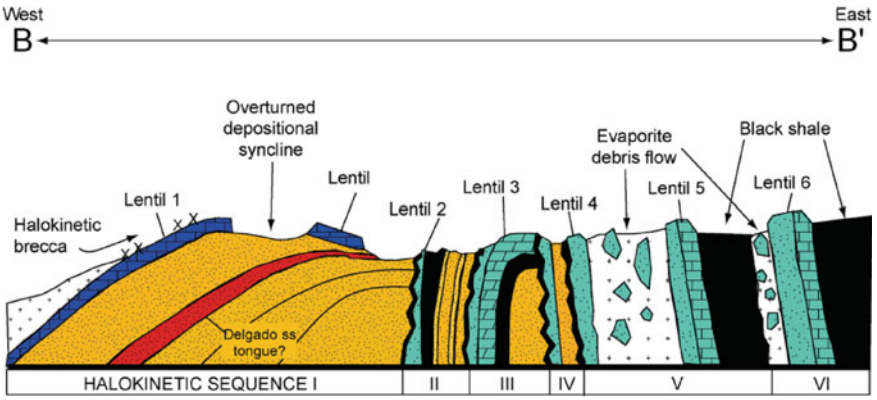

Fig. 3.12 Schematic cross section across growth strata on the east margin of the El Papalote diapir. Cross section line B-B' is indicated on Fig. 3.7. From Giles and Lawton (2002). AAPG© 2002, reprinted by permission of the AAPG, whose permission is required for further use

think about rotating them counterclockwise (in this view), back to a right-side-up orientation, you will see that the beds originally thinned toward the diapir and actually extended onto the top of the diapir.

Proceed up (between the two drainages) climbing over the upward-coarsening and thickening siliciclastic beds of Fig. 3.13b *to gain elevation and a vantage point. As you ascend the ridge note the significant change in dips from moderately southwestward to nearly horizontal. All of these strata are overturned! Continue until you reach an outcrop of thin, vertical limestone (Lentil 2).*

You have been climbing up through siliciclastic strata of the middle siltstone member of the Potrerillos Formation that are stratigraphically above, but structurally beneath, carbonate Lentil 1 and consist of olive green-gray siltstone and very fine-grained sandstone. Sandstone beds are 25–60 cm thick and typically coarsen upward from sharp bases with intraclasts of siltstone and shell fragments to burrowed tops with uncommon wave ripples. These strata comprise a series of lower shoreface parasequences that thin toward and onlap Lentil 1 just to the south of this traverse.

Across the large drainage to the south, Lentil 1 and strata immediately overlying it occupy a depositional syncline, now an antiformal syncline whose eastern limb is truncated at a near-vertical unconformity beneath carbonate Lentil 2 (Fig. 3.13c). Regional mapping suggests that the western (diapir proximal) limb steepens in the subsurface first to vertical and eventually to the moderate northeast dips of the northeastern limb of El Gordo anticline. In other words, this is a recumbent isoclinal fold, opening away from the diapir, whose upper limb is truncated by the unconformity at the base of Lentil 2 (Figs. 3.3 and 3.12). The axis of this fold is curved in plan view and parallels the contact between the diapir and Cretaceous rocks, indicating a genetic relationship between folding and diapirism. The strata between Lentil 1 and this unconformity form "Halokinetic Sequence I" (Fig. 3.14) (see definition below).

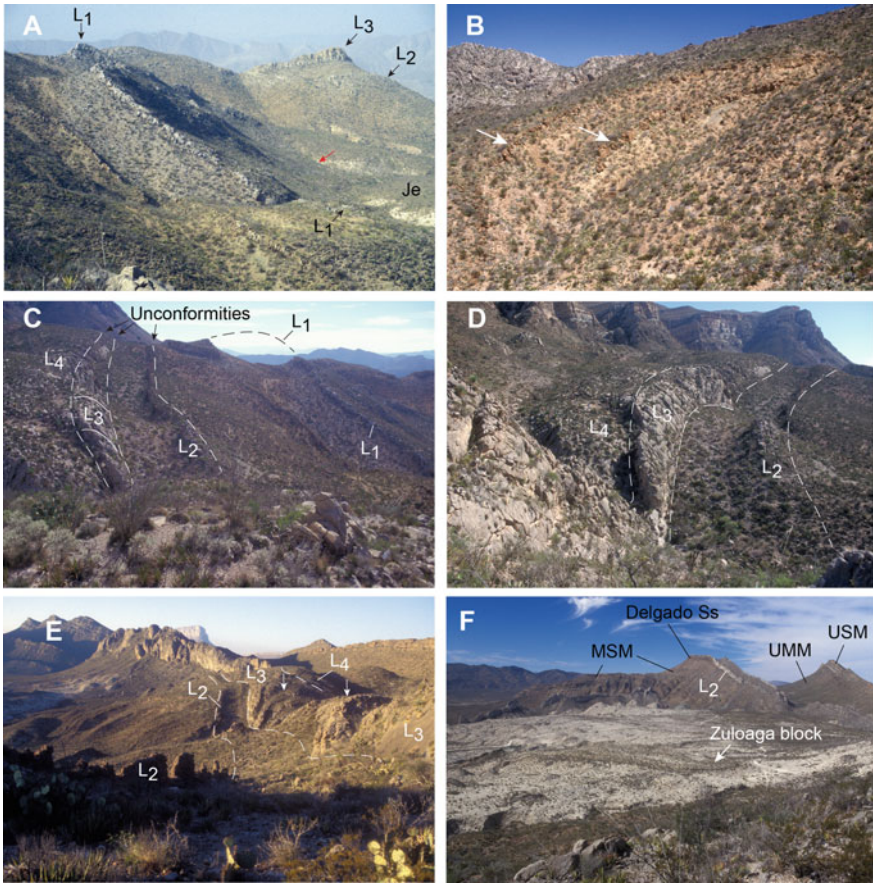

Fig. 3.13 Structural relations on east flank of El Papalote diapir. **a** Overturned limestone of Lentil 1 (L_1), view south. Contact with diapir (Je) indicated by red arrow; dip slope along base of overturned lentil is the edge of the flaring diapir. Lentils 2 and 3 in the upper right (south flank of diapir) dip away from the observer around a corner of the diapir. **b** Overturned sandstone beds stratigraphically above Lentil 1. View north. Arrows indicate bed bases. Note thinning and convergence of sandstone beds to right (east). Restoration of beds to upright by mentally flipping them over to the left indicates that stratigraphic thinning was toward the diapir. **c** View south of overhang structure on east flank of El Papalote diapir. Lentil 1 (L_1) and siliciclastic beds of Potrerillos Formation (both overturned) are truncated beneath Lentil 2 (L_2). Siliciclastic beds above Lentil 2 are truncated at an unconformity at the base of Lentil 3 (L_3). Lentil 3 is overturned (solid white lines show folding of base of bed) and truncated beneath Lentil 4 (L_4). **d** View to southeast of Lentils 2 and 3 (L_2, L_3). Lentil 3 is folded from a near-vertical attitude to subhorizontal and overturned at the easternmost part of its exposure (folded bed is the base of the lentil). **e** View to northwest of overturned syncline in Lentil 3 (L_3) at base of halokinetic sequence III. Synclinal fold hinge is indicated by arrows. Lentil 2 (L_2), at base of halokinetic sequence II, forms a broken wall in middle of foreground and middle distance. **f** View to the west across El Papalote diapir from Lentil 3 showing the minor anticlinal flexure extending away from the diapir. Delgado Sandstone Tongue of Potrerillos Formation (brown subhorizontal unit) thins toward diapir and is truncated beneath Lentil 2 (L_2) on ridge skyline. MSM = middle siltstone member, UMM = upper mudstone member, USM = upper sandstone member

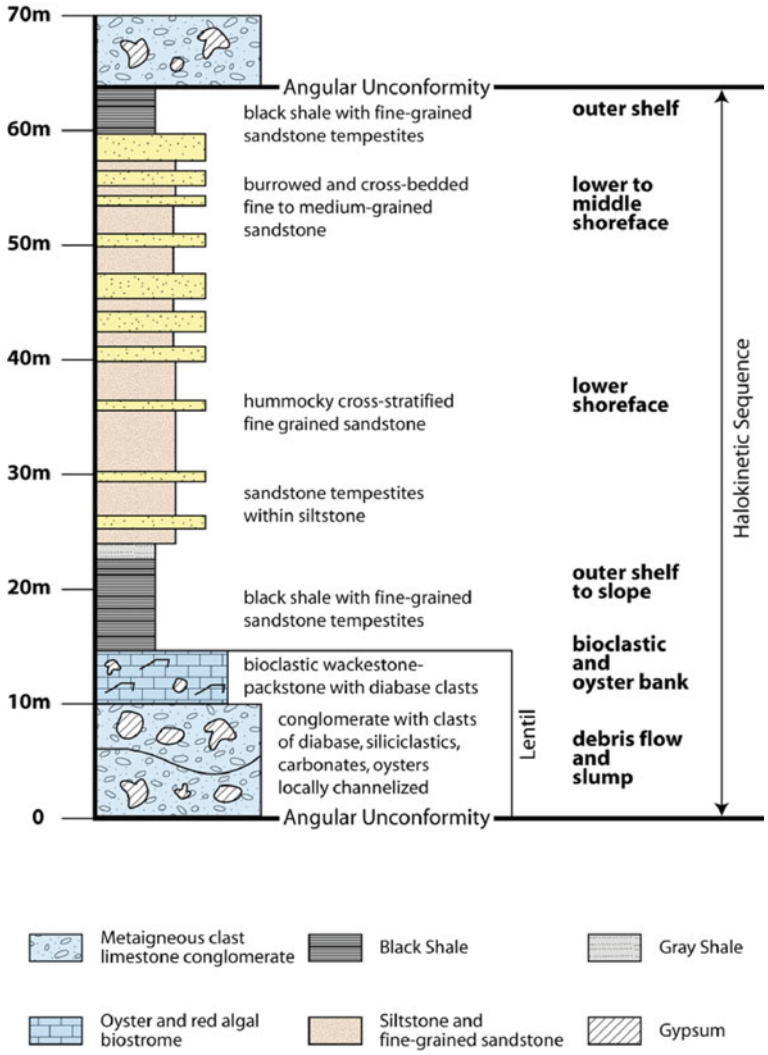

Fig. 3.14 Idealized halokinetic sequence facies progression adjacent to rising El Papalote diapir. From Giles and Lawton (2002). AAPG© 2002, reprinted by permission of the AAPG, whose permission is required for further use

Onlap and thinning of Halokinetic Sequence I beds toward the diapir (upon restoration of structure) and truncation of beds beneath younger lentils (Fig. 3.13c, d) further indicate that diapir-related folding was episodic during deposition of these strata and therefore of Late Cretaceous (latest Maastrichtian) and early Paleocene age.

Lentil 2 (L2 in Fig. 3.7; 26.068930°/ -100.729385°).

Halokinetic Sequence I is truncated at an angular unconformity overlain by a thin (<0.5 m) conglomerate bed that grades laterally to a calciclastic lentil (Fig. 3.13c;

Lentil 2) at the southeastern margin of the diapir. This is the vertical bed you are standing on. This conglomerate contains siltstone and sandstone clasts derived from the Potrerillos Formation, oyster shells, and meta-igneous clasts. The latter indicate that the diapir was exposed to subaerial or submarine erosion.

A thin, recessive, outer shelf to lower shoreface succession of siliciclastic strata overlies carbonate debris flow beds of Lentil 2 to form Halokinetic Sequence II (between the base of Lentil 2 and the base of the prominent limestone just up the hill). Halokinetic Sequence II has been correlated around the diapir. It can be shown to lie directly above the Delgado Sandstone Tongue and thus lies within the upper mudstone member of the Potrerillos Formation and above the Cretaceous-Paleogene boundary.

To the south, you will see a prominent curved limestone bed (Figs. 3.13c, d). This is the base of Lentil 3 that you can also see just uphill to the east of your present location.

Continue hiking up hill (east) toward and up onto the next limestone ridge (Lentil 3). There is an easy route up the face of the lentil just a bit to the left (north).

Lentil 3 (L3 in Fig. 3.7; 26.069257°/-100.728890°).

Lentil 3 (L3) forms a conspicuous limestone wall at the head of the slope. This limestone exposure is formed by the base of a single bed that is upturned and folded from a vertical attitude to a nearly horizontal overturned one over a short distance (Fig. 3.13c–e). The basal bedding plane contains a heterogeneous collection of abundant debris, including meta-igneous and siltstone clasts, shark teeth, bored molluscs, and echinoderm and sponge skeletal debris. This unit is interpreted to represent a transgressive lag deposit and forms the lowermost unit of Halokinetic Sequence lII (Fig. 3.13c).

The view from Lentil 3 across the diapir to the west displays many of the key features of the stratigraphy and structure associated with the diapir (Fig. 3.13f).

Halokinetic sequences, visible at this stop, are relatively conformable successions of strata genetically influenced by near-surface salt movement and are locally bounded at the top and base by angular unconformities that become disconformable to conformable with distance from the diapir (Giles and Lawton 2002). Halokinetic sequences represent growth strata associated with the dominantly passive rise of diapirs and display depositional thinning, abrupt lateral facies changes, and intense local deformation toward the diapir. Adjacent to El Papalote diapir the idealized halokinetic sequence facies succession (Fig. 3.14) in ascending order is:

Facies 1: Basal conglomerate containing clasts derived exclusively from the diapir (i.e., clasts of meta-igneous rocks, Jurassic carbonate, and gypsum) and from material that mantled the diapir (Fig. 3.15a), collectively referred to as diapir-derived detritus (Lawton and Buck 2006).

Facies 2: Oyster, foram and red algal bioclastic wackestone to packstone (Fig. 3.15b).

Facies 3: Upward-shallowing and -coarsening slope turbidites and/or lower to middle shoreface siliciclastic strata that generally lack diapir-derived detritus (Fig. 3.15c).

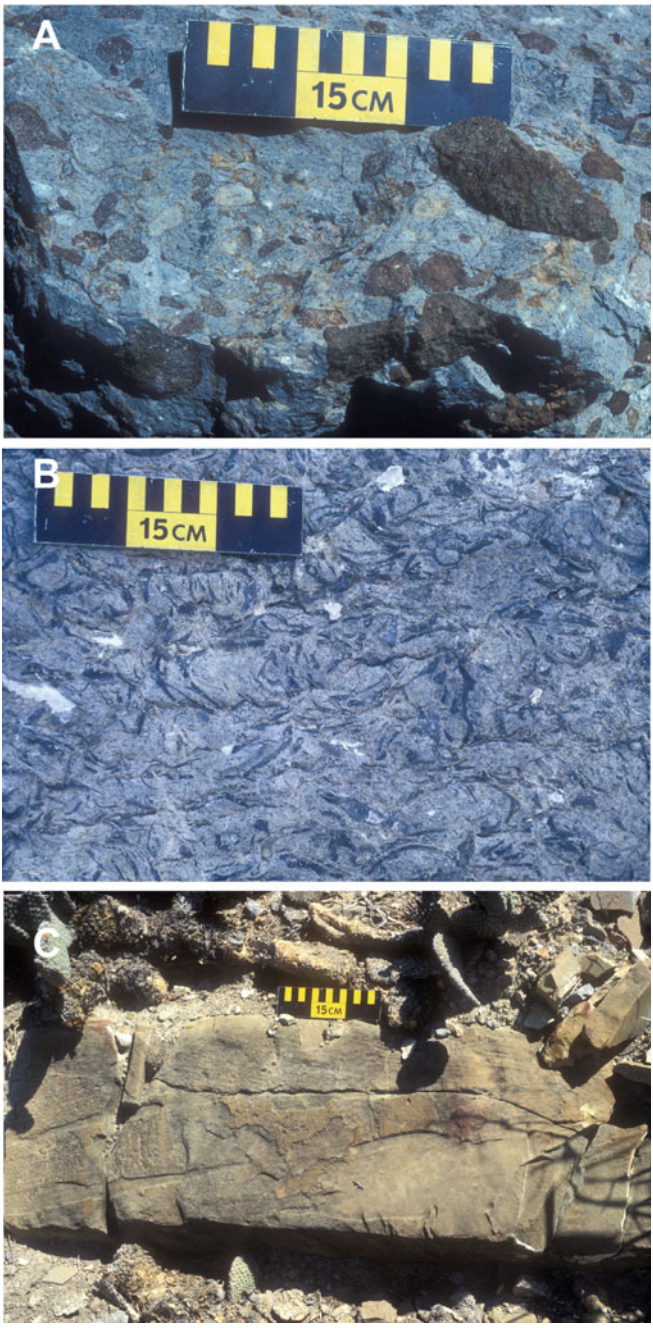

Fig. 3.15 Lithofacies of halokinetic sequence. **a** Diabase clasts (brown) and wackestone clasts (gray) in Lentil 2, northwest corner of diapir. Debris-flow facies. **b** Bioclastic oyster wackestone-packstone in upper part of Lentil 6. **c** Hummocky cross stratification in very fine grained sandstone, Delgado Sandstone Member of Potrerillos Formation. West of El Papalote diapir, directly beneath Lentil 2

Facies 1 and 2 are commonly interbedded, but one or the other may be absent from a particular sequence. These two facies together form the carbonate lentils. Individual carbonate lentils are typically thickest (~17 m) and coarsest (cobble to boulder clasts) directly adjacent to the diapir. Lentils decline in importance in the sequence with distance from the diapir and generally do not extend beyond 1 km from the diapir. Diapir distal facies comprise carbonate turbidites overlain by outer shelf black shale and siltstone.

We interpret halokinetic sequences to form as a result of a repetitive progression of processes responding to variations in net diapiric rise rates relative to local sedimentation rates (Fig. 3.16):

Phase 1 (Fig. 3.16a): Salt rise rate exceeds sediment accumulation rate. This results in inflation of the roof, drape folding of the strata to steeper attitudes, and an increase in topographic relief.

Phase 2 (Fig. 3.16b): With increasing relief, the salt edifice develops steep unstable margins. Strata steepened by drape folding locally fail, forming slump scars (angular unconformity surface) that are overlain by debris flows and slumped material derived from the diapir and its roof. Biostromal carbonate facies nucleated on the diapiric dome, which was topographically above turbid bottom waters. Slumping and formation of debris flows may have continued throughout this phase to form intercalated debris flow and biostrome beds.

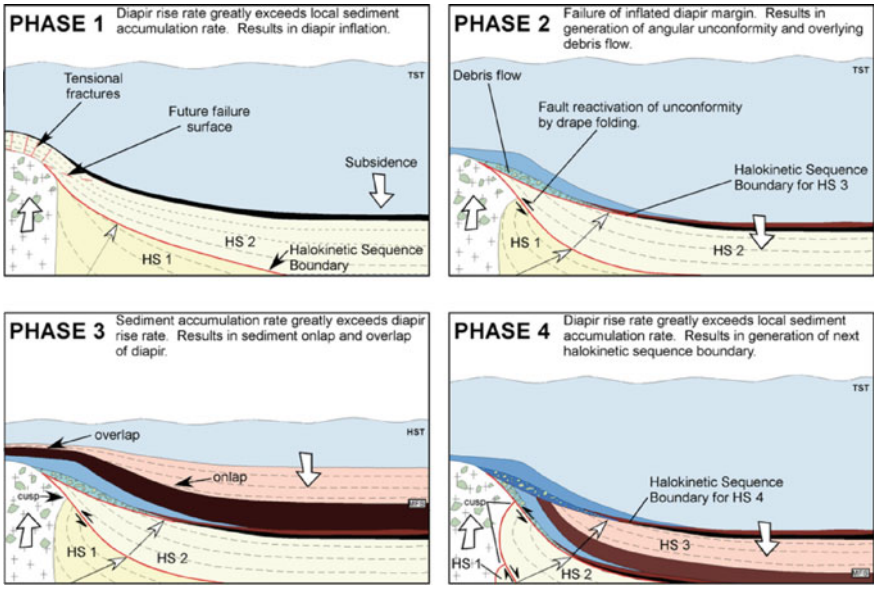

Fig. 3.16 Depositional model for the formation of halokinetic sequences. Adapted from Giles and Lawton (2002). AAPG© 2002, reprinted by permission of the AAPG, whose permission is required for further use

Phase 3 (Fig. 3.16c): Regional siliciclastic influx increased, bringing coarser detritus to the area at relatively higher sediment accumulation rates. The siliciclastics onlapped the diapir and its roof and decreased the diapir-related topography. During this phase the diapir was not exposed at the surface and did not shed clasts into the surrounding sediments.

Phase 4: Repeat of the processes in Phases 1–3 to begin a new halokinetic growth sequence.

Passive rise of the diapir results in rotation of the thinned flaps of strata onlapping the diapir. Bed rotation results in flexural slip along the converging bedding planes and along the unconformities between halokinetic sequences (Rowan et al. 2003). Sliding along the unconformity accentuates the angle of truncation at the contact, and in some cases results in a perpendicular truncation that greatly exceeds the original angle of erosional truncation (Fig. 3.17). Structural evidence for shearing along the unconformity at the base of Halokinetic Sequence II (with the correct sense of shear) has been observed in an arroyo south of the field trip traverse (Figs. 3.18 and 3.19).

What about small-scale fracturing associated with passive diapirism? You've seen the edge of the diapir and walked through flanking stratigraphy. Fracturing is not excessive or pervasive. We find that small-scale faults and fractures fit into several categories: (1) those due to halokinetic folding; (2) those due to doming of the roof during drape folding (the radial veins of Fig. 3.11); and (3) others that are probably related to the late shortening. In other words, there are few, if any, faults and fractures that formed due to any kind of shearing of the strata during salt rise. The shear zones accommodating relative upward movement of salt and concomitant subsidence of the minibasin are within the weaker evaporites (as seen on the traverse up the eastern side of the diapir).

Controls on halokinetic processes may be either autogenic (variation in rate of diapir rise) or allogenic (variation in sedimentation rate or eustatic sea level) or some combination of the two. Our observations at El Papalote diapir suggest that local sedimentation rate tied to sea level cycles corresponds well with development of halokinetic sequences on the east and southern margin of the diapir. In addition, the sedimentation rate during diapiric rise, and hence the thickness of the roof, influences the thickness of the halokinetic sequences and the width of the folded zone adjacent to the diapir (Figs. 3.20 and 3.21; Rowan et al. 2003).

Uphill from Lentil 3 is another angular unconformity marked by a very thin carbonate conglomerate horizon generally covered by talus and sediment.

Halokinetic Sequence lII is truncated beneath another conglomerate that forms an angular unconformity at the base of Halokinetic Sequence IV. Above this point, the section consists of conglomerate beds, discontinuous oyster-bearing sandstones, dark gray to olive green shale, and evaporite horizons that display apparently concordant dips for the rest of the exposure of the upper mudstone member of the Potrerillos Formation (Fig. 3.13c, d). However, we define three halokinetic sequences within these strata that are delineated on the basis of intercalated gypsum horizons. Although the diagnostic angular unconformity is not displayed at this position in the stratigraphy, we infer that it was present directly adjacent to the diapir and has been subsequently removed by modern erosion of the strata closest to the diapir (Fig. 3.4). We

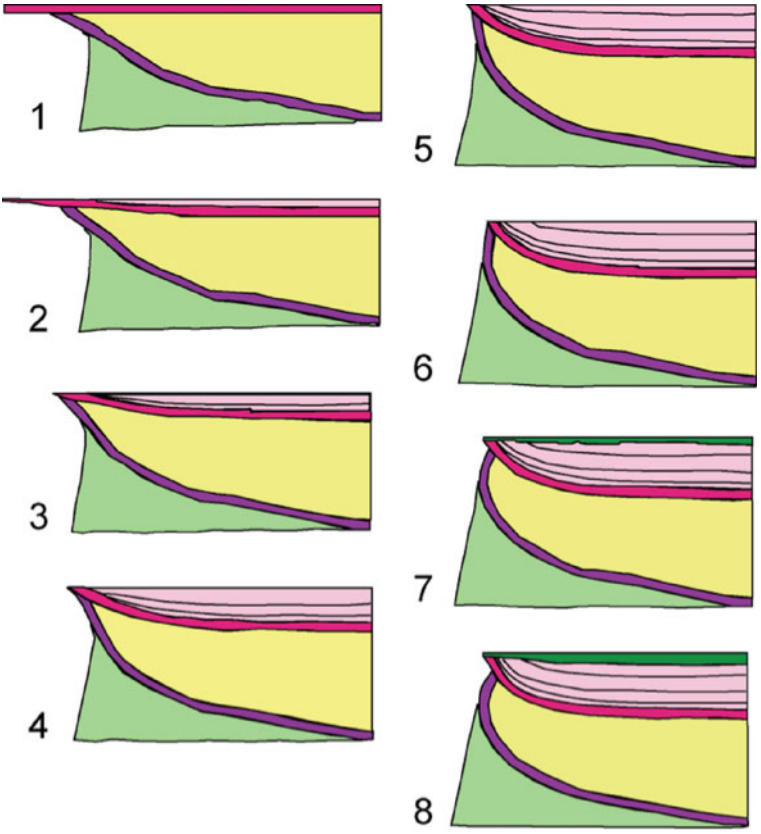

Fig. 3.17 Kinematic model for development of a halokinetic sequence by passive rotation of strata adjacent to a rising diapir (Rowan et al. 2003). As the upper (red) lentil is folded, the lower (purple) lentil slides incrementally away from the diapir along the unconformity, creating an increasingly angular relationship between the sequences and a salt-edge cusp at the edge of the diapir. Topographic relief is not indicated but is a key component of the deformation. AAPG© 2003, reprinted by permission of the AAPG, whose permission is required for further use

interpret the gypsum horizons to represent gypsum debris flows derived from failure of the exposed "domed" gypsum cap in similar fashion to the carbonate debris flows in Lentils 1, 2, and 3. An alternative interpretation is that they are salt glaciers (namakiers), whereby the gypsum layer is left as a residual deposit intercalated with the minibasin stratigraphy.

Halokinetic Sequences V and VI were initiated by gypsum caprock failure. The gypsum beds locally contain meta-igneous clast conglomerate beds and display "bedding" or lamination marked by thin dark gray to black horizons within the white gypsum. We interpret this apparent bedding to represent a post-depositional pressure-solution residue (dark gray laminae) caused by differential compaction of the gypsum during burial. The basal debris flow beds of Halokinetic Sequence VI

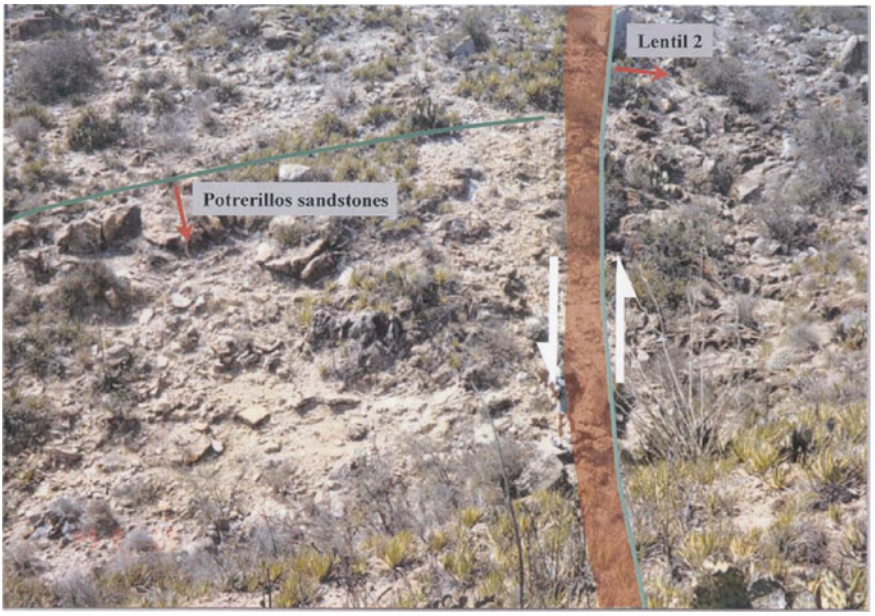

Fig. 3.18 Unconformity at the base of Lentil 2, where Potrerillos clastics are truncated at an angle of about 80°. The unconformity is a shear zone with a width ranging from 10 to 40 cm. From Rowan et al. (2003). AAPG© 2003, reprinted by permission of the AAPG, whose permission is required for further use

contain a series of stacked channelized, conglomeratic debris flow beds. Conglomerates contain blocks of meta-igneous debris as much as 20 m in length. Locally blocks contain crackle breccias (Yarnold 1993; Blair and McPherson 1994) with fractures near their bases that are injected with siltstone derived from the underlying bed. These blocks are interpreted as components of subaqueous rock avalanches or debris flows suggestive of catastrophic depositional events.

Halokinetic sequences V and VI are capped by black shale representing the regional sedimentation found in the upper mudstone member of the Potrerillos Formation. Although both the upper mudstone and upper sandstone members of the Potrerillos Formation thin over the diapir (Figs. 3.2 and 3.4), diapiric growth no longer created an environment suitable for development of carbonate lentils in this area.

The return route to the carbonate block in the diapir and the vehicles is via*a trail in a strike valley northeast of Lentil 5.*

82.18 2.5 *km Retrace route, turning left off spur road, descending steep grade, passing cinder block building, and passing south edge of diapir. Take first right 0.4* km *south of diapir. Travel west 1.2* km*and re-cross edge of diapir and pass mine buildings, continuing straight to abandoned quarry near west edge of diapir.* ***Note: Permission must be secured from the quarry foreman for this stop****. From 2000–2010, the active quarry was northeast of the buildings.*

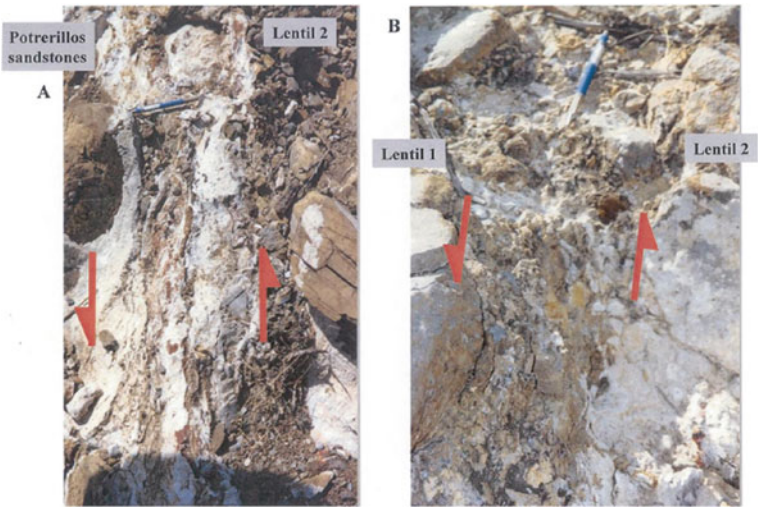

Fig. 3.19 **a** Cataclastic shear zone along the unconformity, consisting of a breccia with clasts of the underlying siliciclastics in a matrix of fine-grained crushed rock and caliche-like carbonate. Shear lozenges within the zone indicate a sense of shear that is compatible with older rocks down (as in the model of Fig. 3.17). **b** The same unconformity, but where Lentil 1 is truncated against Lentil 2, with the same fabric and shear sense. Note that brecciation is entirely expected: as underlying beds slide along the unconformity, the angular relationship increases and the ends of the beds get more offset just as the edge of a pack of cards gets irregular as the deck is folded. These offsets are ground off during movement, with the clasts forming the breccia. From Rowan et al. (2003). AAPG© 2003, reprinted by permission of the AAPG, whose permission is required for further use

STOP 1.7 El Papalote Gypsum Quarry. Plastic deformation and carbonate-gypsum blocks in Minas Viejas Formation of El Papalote Diapir. (26.070074°/ -100.751085°)

Hazards at the stop include steep unstable quarry walls and possible unexploded dynamite in drill holes. A hard hat is necessary. The gypsum quarry exposes fresh gypsum and numerous limestone blocks, some of which appear to be in stratigraphic continuity with sedimentary gypsum. The foreman has said that this part of the gypsum quarry was abandoned because of the high percentage of exotic blocks. The gypsum at this locality preserves both plastic structural deformation features and apparently primary sedimentary features. Deformation includes recumbent, isoclinal folds expressed in gypsum with thin beds of insoluble material (Fig. 3.22a). Some of this folding took place around the ends of limestone boudins that experienced brittle extension and fracturing.

A Jurassic carbonate block in stratigraphic continuity with nodular gypsum with chicken-wire or enterolithic structure (Fig. 3.22b, c) indicates that some of the gypsum within the diapir lacks the penetrative deformation indicated by the folds. This undeformed gypsum can thus be considered to constitute yet another type of block in the diapir. The nodular gypsum becomes more pervasively deformed

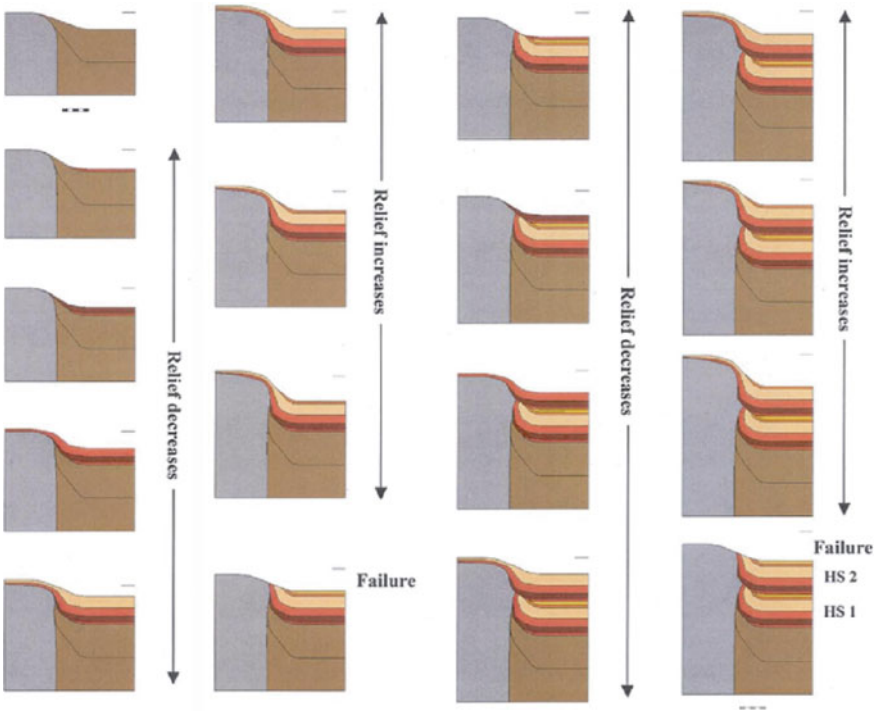

Fig. 3.20 Halokinetic sequences formed in the case of a thick diapiric roof likely caused by a relatively high sedimentation rate compared to salt-rise rate. Starting from the upper left, bathymetric relief first decreases as relatively rapid sedimentation fills in the basin, reduces topographic relief, and buries the diapir. But then a slowdown in sedimentation leads to increasing relief and eventual gravitational failure. This failure erodes the folded strata and exposes the diapir at the sea floor (bottom of second column). The cycle is repeated, thereby creating two halokinetic sequences, each containing thinned, rotated strata that are bounded by angular unconformities adjacent to the diapir that pass into conformities away from the diapir. From Rowan et al. (2003). AAPG© 2003, reprinted by permission of the AAPG, whose permission is required for further use. Further work led to these being identified as wedge halokinetic sequences and tapered CHS (Giles and Rowan 2012)

(Fig. 3.22d) over a distance of several m from the limestone, showing the effects of viscous drag. The limestone blocks are of variable restricted shallow marine depositional environments. Lithologies are dominantly lime mudstone containing quartz silt and bivalve fragments. Rare echinoderm fragments indicate normal marine salinities were locally present. Recrystallized peloidal-mollusc-ostracode wackestone to packstone suggest very shallow, highly restricted, peritidal conditions, consistent with a sabkha-type environment. The associated gypsum consists of centimeter-scale microcrystalline nodules in a selvage of dark gray micrite. The association of shallow-marine carbonate and supratidal gypsum suggests that the waning phases of deposition of the Minas Viejas Formation took place in a sabkha setting prior to deposition of the Zuloaga-age limestone, which contains abundant oysters. The

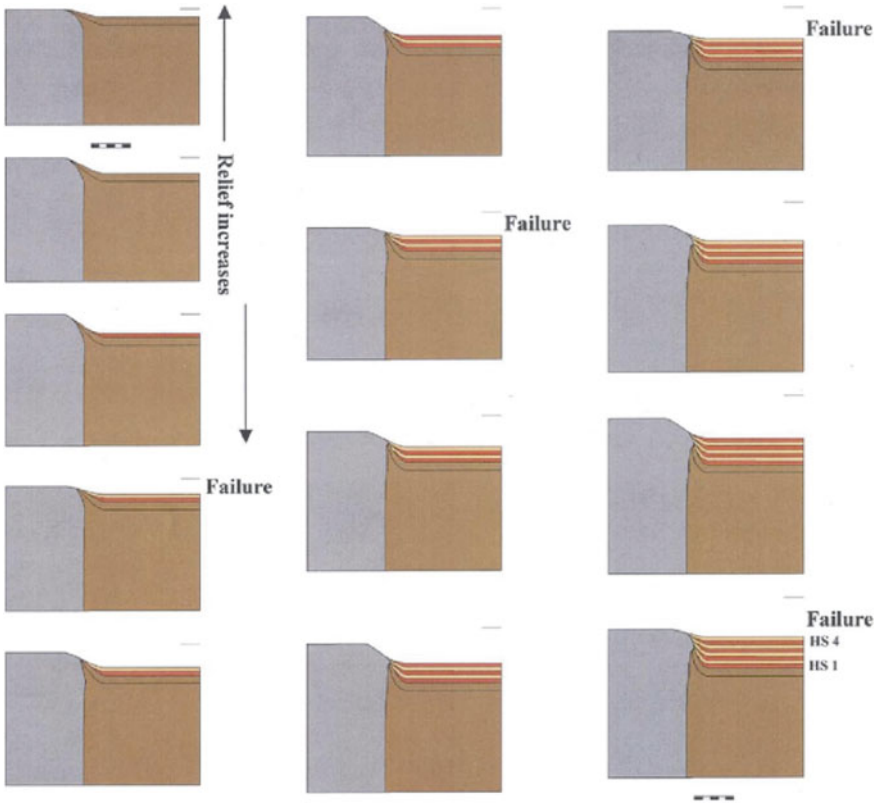

Fig. 3.21 Halokinetic sequences formed in the case of a thin diapiric roof likely caused by a relatively low sedimentation rate compared to salt-rise rate. Due to relatively slow deposition, relief never decreases by infill and onlap, but only by erosional truncation. Starting from the upper left, bathymetric relief gradually increases even though some sediment is added, leading to failure and truncation. More cycles produce a pattern that varies significantly from that produced in the previous model. Halokinetic sequences are thinner and have a narrower zone of deformation with less folding and at most minor erosional truncation. From Rowan et al. (2003). AAPG© 2003, reprinted by permission of the AAPG, whose permission is required for further use. Further work led to these being identified as hook halokinetic sequences and tabular CHS (Giles and Rowan 2012)

shallow setting of the facies at El Papalote diapir poses an interesting paleogeographic problem, because the nearest exposures of Zuloaga Limestone at Potreros Chico and Garcia appear to record basinal deposition as calciturbidites.

Estimated driving time from Stop 1.5, which is the termination of Stop 1.6 traverse: 15 min. Estimated stop time: 30 min

Retrace route toward Mexico Highway 53. A faint dirt road intersects the gypsum haul road on the north at km marker sign 13 (26.044760°/ -100.732340°). Walk or

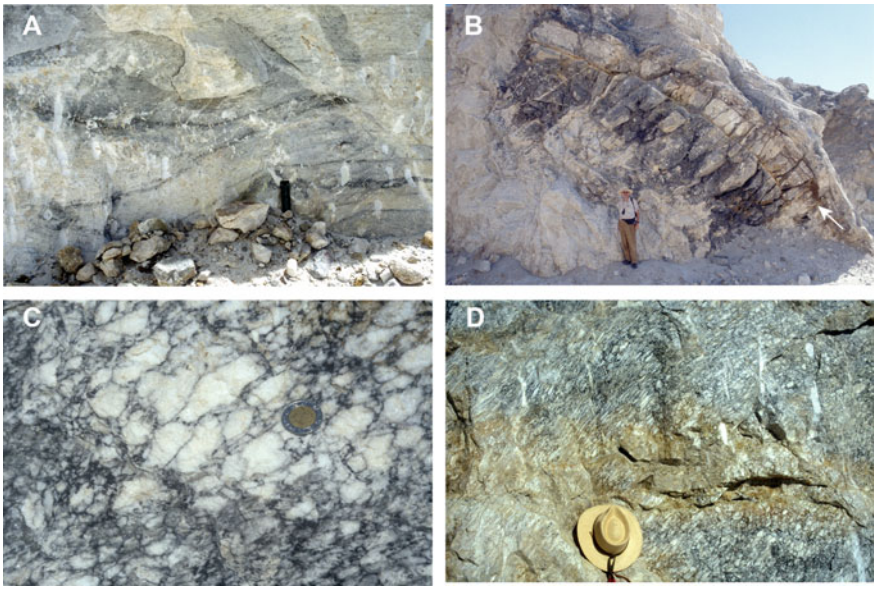

Fig. 3.22 Gypsum caprock in El Papalote gypsum quarry, southwest corner of El Papalote diapir. **a** Recumbent isoclinal folds in gypsum and micrite. Scale bar is 20 cm long. **b** Carbonate-gypsum stringer that formed by boudinage during diapirism. Peloidal packstone and nodular gypsum are in apparent stratigraphic continuity here, with contact indicated by arrow. Stratigraphic facing direction is uncertain. Bottom edge of carbonate is fractured and intruded by gypsum, indicating block erosion and volume reduction by stoping. **c** Nodular gypsum in selvages of micrite. This is a displacive, enterolithic fabric resulting from growth of gypsum nodules in unlithified supratidal mud. This lithology is in stratigraphic contact with peritidal carbonate. Coin is 1.5 cm across. **d** Nodular gypsum with with planar structural fabric due to increasing shear away from the competent carbonate. Vertical marks are drill holes. Hat size is 7–1/4 (59 cm)

drive north along the dirt road to the point where it enters Rock Canyon. The road widens at this point and provides a turn around point for vehicles.

90.3 7.3 *Parking area at entrance to Rock Canyon.* (26.052202°/ -100.733907°).

STOP 1.8 Delgado Sandstone and K-Pg boundary tsunamite (26.052202°/ -100.733907°)

From the parking area walk north along the dirt track into Rock Canyon. Exposures of the K-Pg boundary beds are 230 m*north, just to the east of where the track climbs out of the canyon. (26.054202°/ -100.732651°).*

The walls of the canyon consist of fine- to medium-grained sandstone beds of the Delgado Sandstone Tongue of the Potrerillos Formation, which overlies the middle siltstone member. The Cretaceous-Paleogene boundary lies near the top of the Delgado Sandstone and is overlain by coarse-grained deposits that we interpret as a tsunami event bed related to the Chicxulub meteorite impact on the Yucatán Peninsula, 1200 km SE of this location.

The Delgado Sandstone Member was deposited in a complex, wave-dominated, eastward prograding deltaic depositional system coeval with passive diapiric rise (Aschoff and Giles 2005). Typical parasequences comprise offshore shale overlain by lower to upper shoreface sandstone (Fig. 3.23; Aschoff 2003; Aschoff and Giles 2005). The Delgado contains two parasequence sets; the lowermost parasequence set exhibits a progradational stacking pattern, whereas the uppermost set exhibits a retrogradational pattern. The lowermost parasequence set is part of a highstand systems tract developed in the middle siltstone member of the Potrerillos Formation,

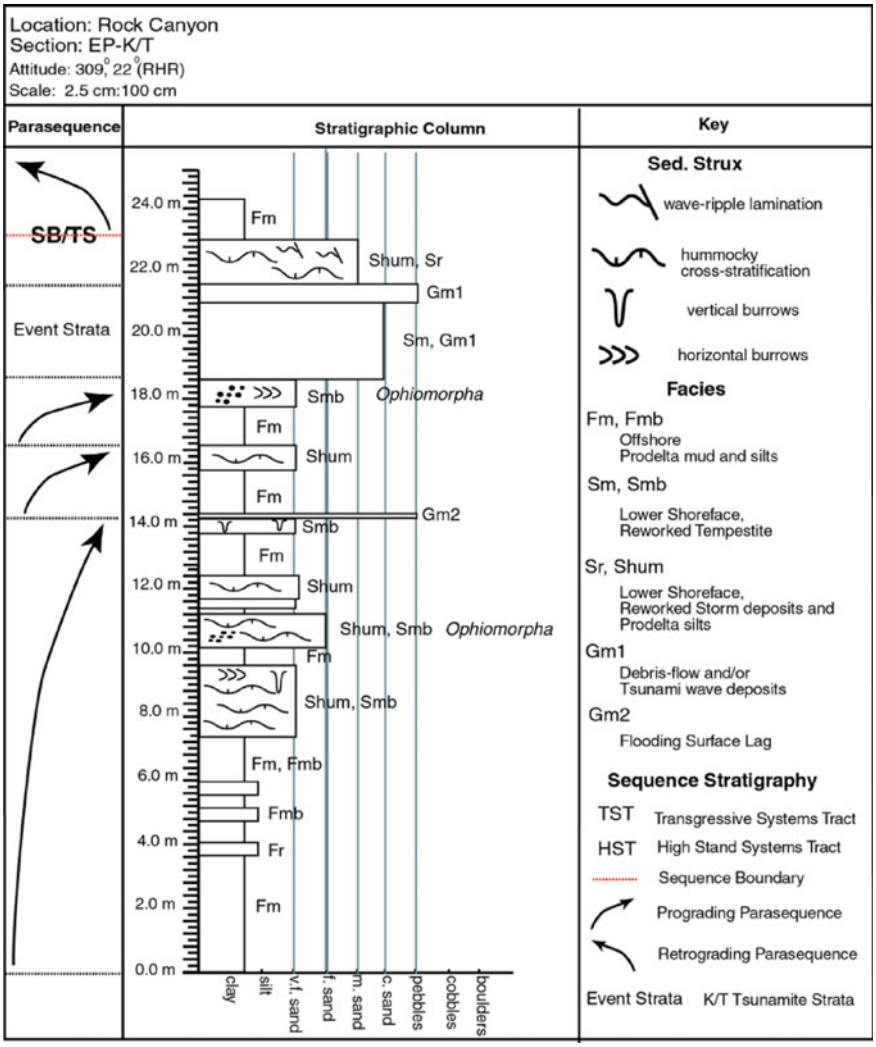

Fig. 3.23 Measured stratigraphic section of the Delgado Sandstone Member near Rock Canyon (Aschoff 2003)

while the uppermost parasequence set is part of a transgressive systems tract of the overlying upper mudstone member. The highstand and transgressive systems tracts are separated by an erosional sequence boundary that incises into underlying strata as much as 10 m and preserves pebble and boulder conglomerate within lowstand systems tract incised valleys.

Sequence stratigraphic correlation of 30 detailed, measured stratigraphic sections indicates that: (1) strata proximal to El Gordo diapir to the south and La Popa salt wall to the north show depositional thinning within a 1 km radius, higher energy, shallower water lithofacies and a difference in stratal stacking patterns toward the diapirs; and (2) strata proximal to El Papalote salt diapir exhibit very little thinning until within a 0.3 km radius of the diapir, no change in lithofacies nearing diapir bathymetry and similar stacking patterns on either side of the diapir. These data suggest that the diapirs had different bathymetric expressions during deposition of the Delgado Sandstone Member and may have had different uplift styles and/or rates.

A unique, 0.25–10 m thick, massive, matrix-supported, boulder to cobble, heterolithic conglomerate containing subordinate, ripple cross-laminated sandstone lenses fills both broad (>20 m wide, 5 m deep) and narrow, deeply incised (<10 m wide, 10 m deep), valley-form features within the upper 5–15 m of the Delgado Sandstone Tongue. Boulder conglomerates (MPS = 20–70 cm) are preserved exclusively in narrow, deeply scoured valley-forms; conversely, cobble and pebble conglomerates are preserved in broad, shallow valley-forms. Although clast size varies with the depth of valley-forms, the sedimentologic character and heterolithic clast lithology (presence of intra- and extrabasinal clast/grain types) are laterally and stratigraphically persistent.

Field observations and petrographic analysis of the valley-fill deposits provide evidence for origin of the valley-fill succession as tsunami-related deposits (Aschoff et al. 2001; Shipley 2004; Lawton et al. 2005). Primary evidence for an impact-related origin includes: (1) stratigraphic position at the K-Pg boundary; (2) absence of bioturbation, which is abundant in the underlying sandstone, indicating the beds were deposited in rapid succession; (3) parasequences continue to prograde above the conglomerate suggesting the regular progradational regime was simply "interrupted" and not part of a standard basinward shift; (4) the conglomerate and associated coarse-grained sand and granule bed (Fig. 3.24a, b) contain heterolithic grain types including abundant and diverse whole fossils and microspherules that are not present in the Delgado above or below this unit; (5) presence of microspherules composed of granular calcite and devitrified silicate glass (Fig. 3.24c, d; Shipley 2004); (6) widespread large-scale convolute lamination stratigraphically below the event bed, interpreted as liquefaction structures indicative of rapid event loading.

Analysis of the sedimentology of the valley-fill succession indicates that tsunami backflow, rather than run-up, deposited the conglomeratic strata. Bedsets in the valley-fill deposit contain crudely graded intraclastic conglomerate and ejecta-rich sandstone with a mixed, transported fauna that includes coastal forms. Shipley (2004) and Lawton et al. (2005) interpret these beds as upper-flow regime deposits of tsunami backflow that entrained and carried shallow-water organisms significant distances into deeper-water depositional settings.

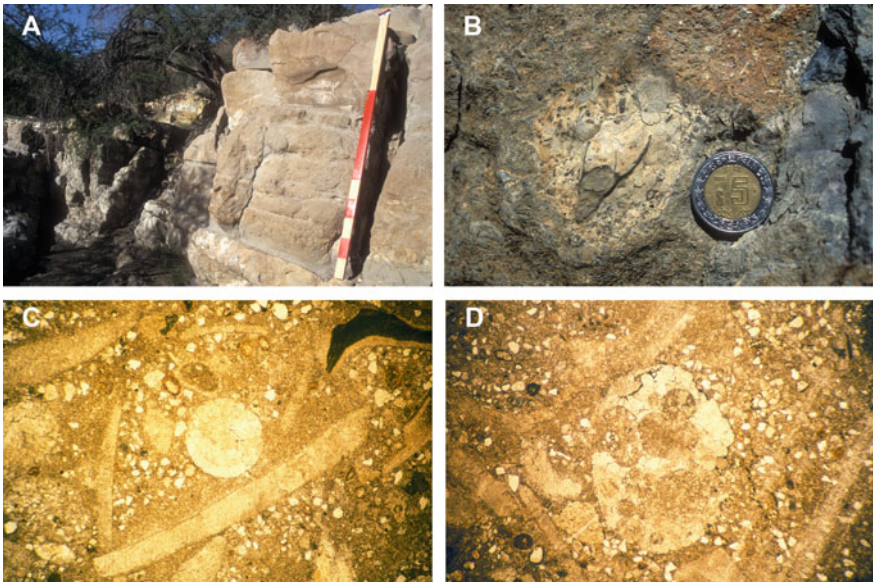

Fig. 3.24 Images of terminal Cretaceous event bed. **a** Outcrop photo of tsunami backflow beds that occupy a broad valley fill eroded into the Delgado Sandstone Member. Outcrop southeast of El Papalote diapir. **b** Siltstone intraclast containing shallow-water gastropod in fossil-rich matrix of boundary event bed. Coin is 2 cm across. **c** Thin section photomicrograph of granular calcite microspherule (tektite) and unusual skeletal debris not found in the underlying or overlying Delgado Sandstone. Spherule is 1 mm in diameter. **d** Thin section photomicrograph showing elongate shape and vesicular character of a calcite microspherule, which is 3 mm in long dimension

Estimated driving time from Stop 1.7 to Stop 1.8: 15 min; walking time to outcrop is about 10 min

Estimated stop time: 20 min

Retrace route to Highway 53 and turn right, toward Monterrey. Proceed south on Highway 53 approximately 18.5 km*to the town of Hidalgo.*

41.8 19.3*Turn off right (west) from Highway 53, just south of the river bridge at the base of the grade north of Hidalgo (25.982292°/ -100.451677°). Make your way west through town, following the signs to Potrero Chico. Drive into the narrow canyon and past the picnic area on the right. Continue through gate and up grade along gravel road to a concrete structure (a water well) on the right side of the road. Park near the well to view the evaporite and stratigraphy in the core of the fold (25.935233°/, -100.478589°).*

To best see the vertical strata of the Cupido Limestone and La Peña Formation, retrace the route to the picnic area and park on the shoulder of the road opposite the picnic area (25.949045°/ -100.476354°).

STOP 1.9 Potrero Chico (25.935233°/ -100.478589°)

The approach to Potrero Chico from the town of Hidalgo passes through near-vertical beds of Aurora Limestone (Albian) and Cupido Limestone (Aptian). The Cupido makes up the resistant wall of the potrero and defines the structure exposed at the surface (Fig. 3.25a, b). The recessive La Peña Formation is well expressed on the outer flank of the potrero wall. Wall et al. (1961) assigned strata above La Peña to the Aurora (Figs. 3.26 and 3.27), a convention accepted by Goldhammer et al. (1991), although the latter authors assigned cyclic carbonates directly beneath La Peña to an informal "Cupidito" unit. The Potrero Chico pericline trends northwest and adjoins the Potrero Garcia anticline to the southwest along an elevated saddle formed by the Arista and Escobedo synclines, which also trend northwest (Wall et al. 1961).

Recessive formations forming the interiors of both potreros consist of a Jurassic through Lower Cretaceous section that includes Minas Viejas Formaton evaporite, Zuloaga Limestone, La Casita Formation, and Taraises Formation (Figs. 3.26, 3.27 and 3.28). The resistant beds of the Cupido Limestone form the walls of the potreros (Figs. 3.25a–d and 3.28). Massive reef facies occupy the fold crests of Potrero Chico (Fig. 3.25e) and the Minas Viejas anticline (Fig. 3.1); these thick carbonate bodies were likely important in determining crestal width, and thus influenced fold geometry.

In the core of Potrero Chico is an exposure about 1 km^2 of gypsum (Figs. 3.25f and 3.26) assigned to the Minas Viejas Formation (Wall et al. 1961; Longoria 1984). The Minas Viejas Formation consists of thick-bedded, light gray gypsum with thin beds of dark gray carbonate. Bedding is continuous only on a scale of meters and locally convolute. Abundant shear planes are present in the gypsum, indicating mobilization of evaporite in the fold hinge during folding (Fig. 3.29). Adjacent to the gypsum, apparently on a steep contact, are vertical beds of dark gray carbonate mudstone with small sparry grains (echinoid fragments) and convolute gray shaly beds. This is the Zuloaga Limestone or lower La Casita/La Gloria Formation. On the hillside above these beds is an exposure of Minas Viejas that overlies a gently sloping surface, apparently formed by lateral flow of the gypsum above the younger strata within the core of the anticline (Fig. 3.25f).

Stratigraphically above the mudstone-shale succession is an interval of laminated gypsiferous siltstone with uncommon carbonate mudstone beds similar to those described previously. Beds are vertical, face northeast and strike 300°–305°. Subhorizonal, discontinuous bedding-normal fractures are pervasive in the gypsiferous siltstone. The fractures are 2–3 mm thick and filled with gypsum. With the exception of the gypsiferous siltstone, the facies present adjacent to the Minas Viejas are similar to facies in the type La Casita Formation southwest of Saltillo on the flank of the Sierra Madre orogen. Carbonate mudstone beds probably represent deep-water debris flow deposits interbedded with basinal black shale.

The anticlines at Potreros Chico and Garcia have been interpreted alternatively as diapirs or salt-cored detachment folds. Penetration of gypsum into the Zuloaga and La Casita formations and lineated fabrics in the gypsum at Potrero Chico led Wall et al. (1961) to interpret the evaporite as diapiric (Figs. 3.26 and 3.27). Citing the deformed fabric of the gypsum and apparently missing Zuloaga Formation, those

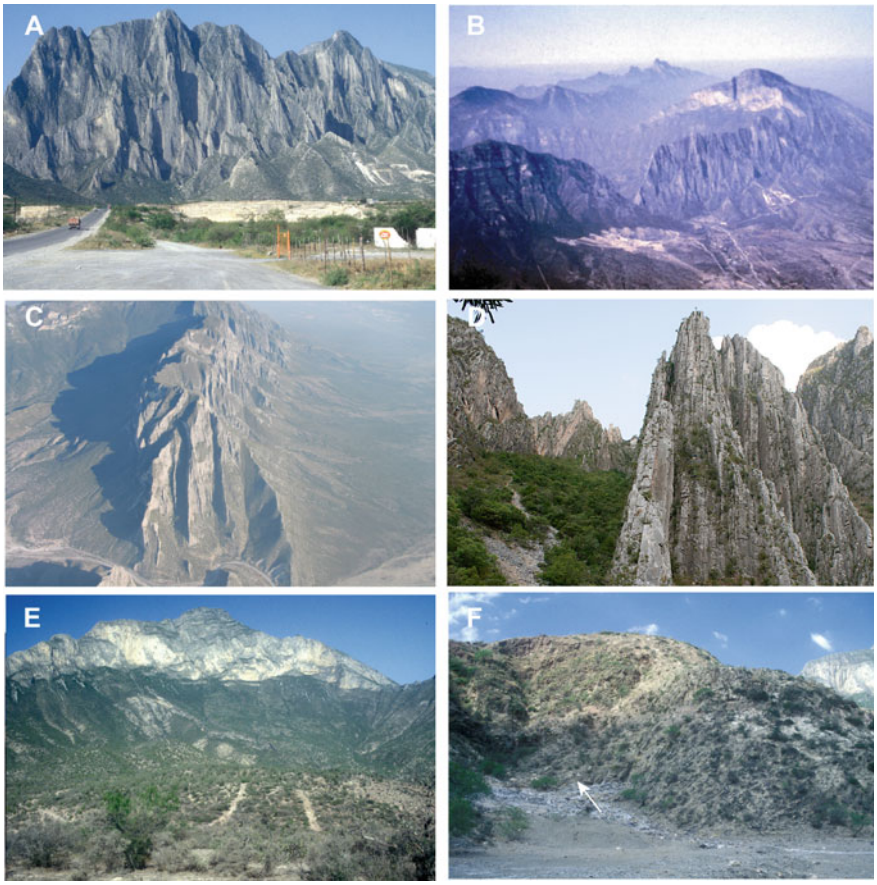

Fig. 3.25 Characteristics of detachment folds south of La Popa basin. **a** Flatirons at entrance to Potrero Chico. Southwestward view is of upper bedding surfaces in vertically-dipping Cupido Limestone on northeast wall of the potrero. Vertical relief is approximately 1 km or 3000 ft. **b** Aerial view of entrance to Potrero Chico. The white cliffs at the northwest end of the periclinal fold are rudistid reef facies of the Lower Cretaceous (Aptian) Cupido Limestone. Photo by Bob Goldhammer. **c** Vertical Lower Cretaceous strata on the south flank of Potrero Garcia, between sections A-A' and B-B' of Fig. 3.26. View east. Main body of ridge is Cupido Limestone, recessive arroyo on right is underlain by La Peña Formation, and slopes at right base of ridge are underlain by Tamaulipas Superior, a deep water equivalent of the Aurora Limestone. All beds are vertical and lack intraformational unconformities, indicating that these strata were deposited before development of the anticline. Photo by Bob Goldhammer. **d** Vertical beds in Cupido Limestone in northeastern limb of Potrero Chico anticline. Middle cliff is about 150 m high. View to south. **e** Cupido reef margin facies exposed in northwest-plunging nose of Potrero Chico anticline. Exposure is same as upper right exposure in Fig. 3.25b. **f** Gypsum (light tan outcrop) in hinge of anticline at Potrero Chico (Cerro Blanco in Fig. 3.26). Gypsum has flowed laterally above thin-bedded carbonate mudstone of Zuloaga Limestone (gray exposures in lower half of photo; contact at arrow)

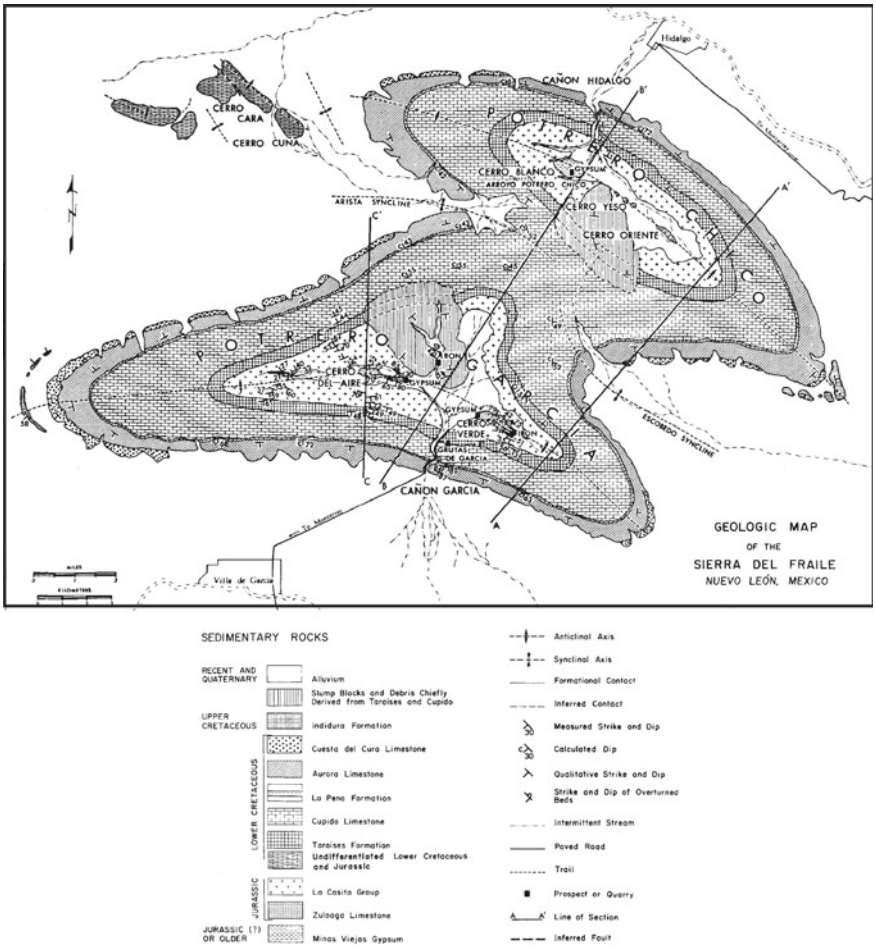

Fig. 3.26 Geologic map of Potrero Chico and Potrero Garcia (From Wall et al. 1961). AAPG© 1961, reprinted by permission of the AAPG, whose permission is required for further use

authors concluded that the gypsum was intrusive into the younger beds, but that the primary impetus for diapirism was crustal shortening. However, we consider the lateral flow to have been a recent phenomenon due to erosional unroofing of the evaporite. We interpret the anticline at Potrero Chico to have originated as a detachment fold with a decollement in the Minas Viejas evaporite section, but with no diapiric component, so that the pericline at Potrero Chico is part of the family of northwest-trending detachment folds that comprise the Coahuila fold belt of the La Popa and Sabinas basins. Observations that suggest a detachment origin include:

(1) The geometry of the fold in cross section and map view are similar in scale and form to detachment folds of the Monterrey salient and the Sabinas basin (e.g., Gray et al. 1997; Marrett and Aranda-García 1999).

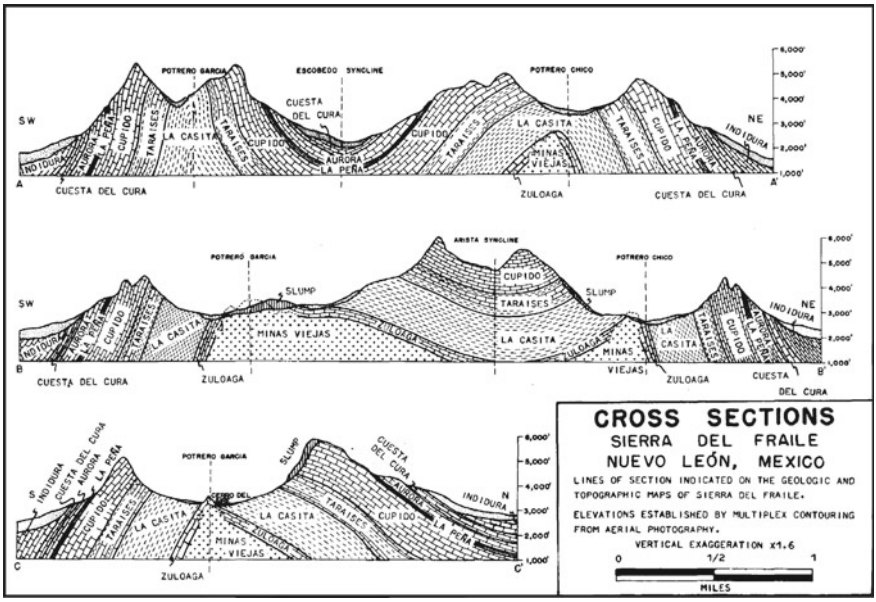

Fig. 3.27 Geologic cross sections of Potrero Garcia and Potrero Chico (From Wall et al. 1961). AAPG© 1961, reprinted by permission of the AAPG, whose permission is required for further use

(2) The strata of the fold limbs do not thin toward the fold crest, but instead continue over the salt to form an isopachous roof (Figs. 3.27 and 3.29; Wall et al. 1961; Gray et al. 1997). During this excursion, we have observed that such thick roofs are not present over diapiric structures. Moreover, models for late inception of diapirism after significant sedimentary overburden has developed require significant coeval extension of roof strata; the resultant diapirs have an extensive system of normal faults at their apices and on their flanks (Vendeville and Jackson 1992), features not observed at Potrero Chico. Normal faults at Potrero Garcia are due to erosion and/or dissolution of evaporite in the hinge region (Fig. 3.28).

(3) Disregarding the minor recent flow of gypsum, the overburden is stratigraphically conformable and structurally concordant with the top salt. A concordant stratigraphic relationship is expected to result from detachment folding but not diapirism.

The detachment level at Potrero Chico probably lies between −2000 and −3000 m elevation. The Minas Viejas #1 well, spudded in gypsum on the crest of the Minas Viejas anticline, 10 km northeast of Potrero Chico (Fig. 3.1), encountered a thick section of Minas Viejas evaporite (Lopez-Ramos 1982) and probably encountered the detachment there. The well penetrated 600 m (1967 ft) of gypsum, 900 m (2951 ft) of interbedded gypsum and halite, and 2100 m (6885 ft) of halite. The well then encountered several meters of mafic igneous rock interpreted as “basalto de

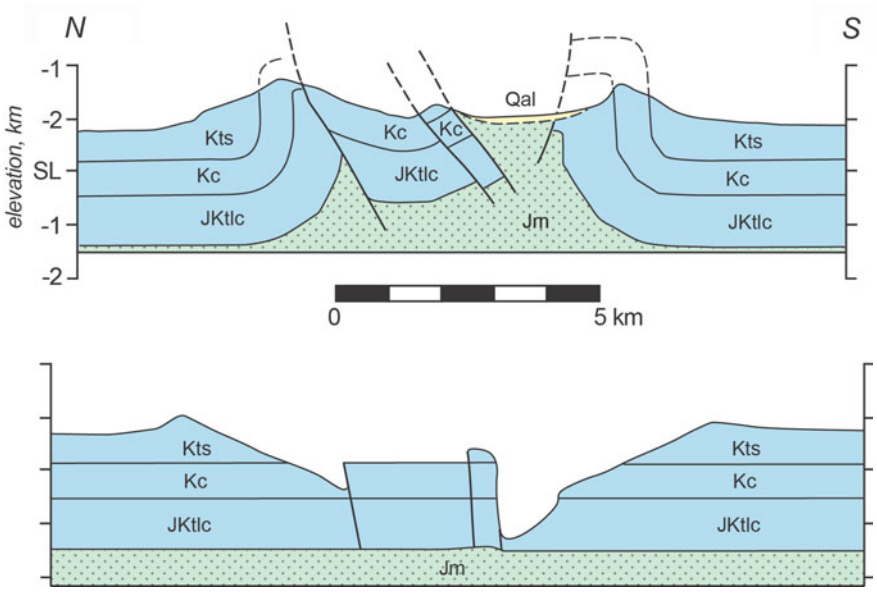

Fig. 3.28 (**a** Geologic cross section of Potrero Garcia showing the salt-supported core and a crestal collapse graben. **b** Restoration of the cross section using bedding-parallel shear (flexural slip). Formation abbreviations: Jm, Minas Viejas; JKtlc, Taraises, La Casita, Olvido, and Zuloaga; Kc, Cupido and Cupidito; Kts, Tamaulipas Superior and younger units; Qal, alluvium. Line of section is approximately C–C' in Fig. 3.26. From Gray et al. (1997). AAPG© 1997, reprinted by permission of the AAPG, whose permission is required for further use

olivino o dolerite," a rock type similar to the meta-igneous blocks of both vesicular basalt and phaneritic diabase at El Papalote diapir; therefore, both flows and sills are likely present in the Minas Viejas Formation at Minas Viejas anticline. Below the mafic rock, the well penetrated 520 m of interbedded halite and black carbonaceous limestone, followed by 370 m (1213 ft) of black carbonaceous limestone with Late Jurassic palynomorphs to a total depth of 4500 m (14,754 ft). Götte and Michalzik (1992) interpreted the limestone as Oxfordian Novillo Formation (equivalent to Olvido of Fig. 2.4), which underlies the Minas Viejas Formation in the Sierra Madre Oriental. Such an interpretation indicates that the detachment in the Minas Viejas section lies above the limestone, and likely above the interbedded limestone and salt. The elevation of the well in Minas Viejas anticline is ~700 m; therefore, the detachment elevation is probably above -2900 m (-9508 ft).

Estimated driving time to Stop 1.9 from Stop 1.8: 45 min.

Estimated stop time: 1 h (includes stop in vertical Cupido beds on return)

Return to Highway 53 at Hidalgo along the same route as used to enter Potrero Chico. Turn right (east) on Highway 53 toward Monterrey, and retrace the route of

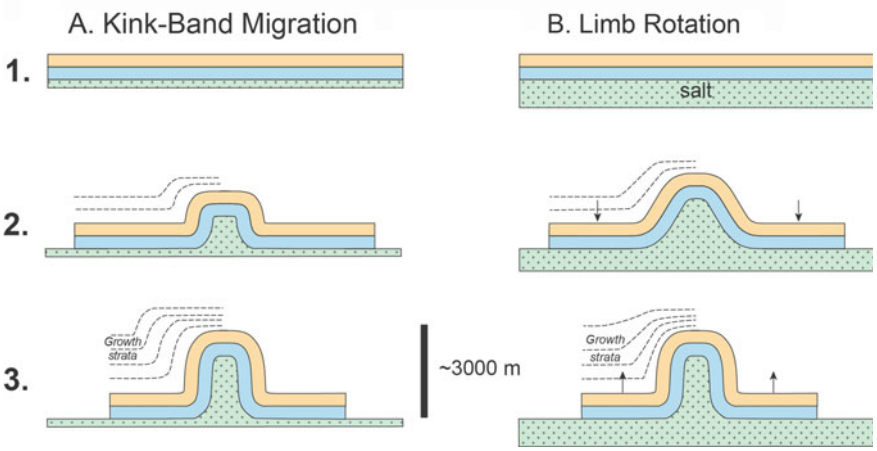

Fig. 3.29 **a** Two models for developing a detachment fold with a box-fold shape. **b** Kink-band or hinge-migration model, in which limb dip stays constant while limb length increases and, consequently, all parts of the fold limb pass through the 90-degree bend during fold growth. **b** Limb-rotation or buckling model, in which limbs of fixed length rotate to steeper dips over time. In model A, the two sets of hinges become farther apart with time, whereas in model B, the hinges maintain their spacing because the limb length is established at the onset of buckling. Vertical arrows in step 2 indicate that the adjacent synclines must initially descend because salt migrates into the fold core as the volume of the core increases during early fold growth; subsequently, in step 3, area balancing requires that the synclines rise as the cross sectional area of the hinge region decreases with continued limb rotation. However, tightening of the anticline in step 3 is more likely accompanied by migration of salt along the axial trend of the fold, resulting in elongation of the periclinal fold and requiring no uplift of the synclines. Growth strata accumulated during fold development permit discrimination of the two folding mechanisms (Suppe et al. 1997), but such relations have not been observed in outcrop in the region. Drawing Adapted from Gray et al. (1997)

the morning by taking the perifico toll road back to the Marriott Aeropuerto. Follow the signs to the airport.

Estimated driving time to hotel from Stop 1.9: One hour

Chapter 4
Excursion 2: La Popa Salt Weld

The excursion route is fshown in Fig. 3.1. The itinerary provides a detailed look at La Popa weld to observe the structural and stratigraphic variability of that feature. La Popa salt weld was the first weld described in detail from outcrop exposures (Giles and Lawton 1999).

The objectives of Excursion 2 are:

1. To observe the structural and stratigraphic nature of the early salt wall phase of La Popa weld.
2. To develop an understanding of composite halokinetic sequences, which are thick packages of stacked hook and wedge halokinetic sequences.
3. To examine, at both large- and small-scale, the geometry and lateral variability of a salt weld formed by shortening of a salt wall.

4.1 Geologic Setting of La Popa Weld

La Popa Weld is a 24 km long near-vertical structure with a prominent bend in strike of 30° approximately halfway along its length (Fig. 4.1). The weld is flanked by synclines (Carroza and La Popa) that roughly parallel the trend of the weld (Fig. 4.2). Halokinetic folding, local unconformities and diapir-derived detritus in flanking strata document a precursor salt wall in the position of the weld (Giles and Lawton 2002; Rowan et al. 2012). Shortening during the latest Cretaceous to Eocene Mexican orogeny squeezed the salt wall, causing evaporite evacuation to form the weld.

The weld consists of an upthrown block on its northern and northeastern flanks that constitutes the La Popa salt-evacuation minibasin and a downthrown block that constitutes the Carroza salt-evacuation minibasin (Figs. 4.1 and 4.3). All strata adjacent to the weld record interaction with rising evaporite, and many contain fragments of meta-igneous rocks derived from the former salt wall. Halokinetic sequences and

T. Lawton et al., *La Popa Basin, Nuevo León and Coahuila, Mexico*, Springer Geology,
https://doi.org/10.1007/978-3-030-79397-5_4

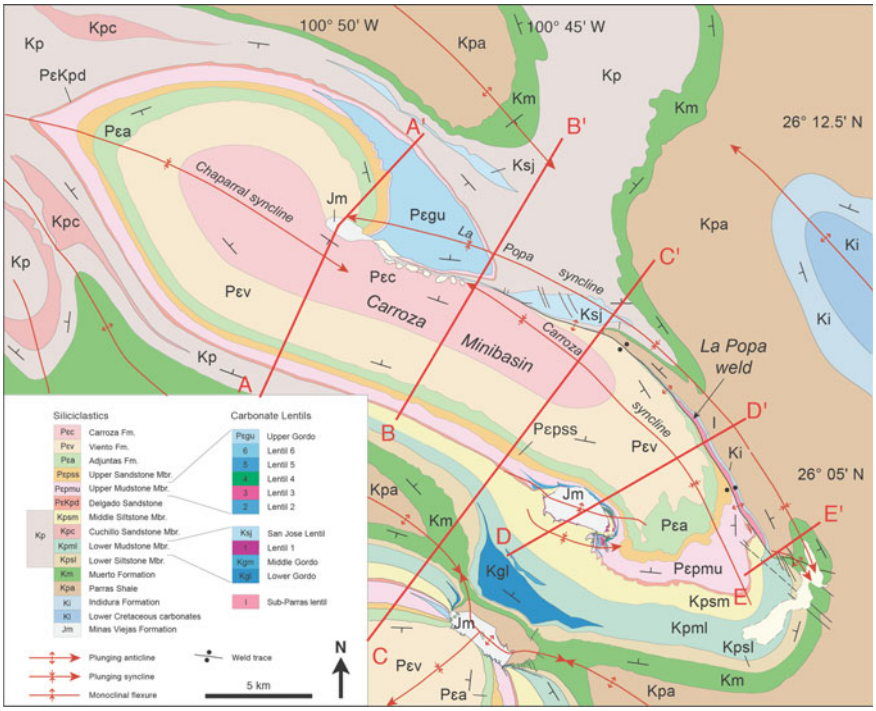

Fig. 4.1 Geologic map of La Popa salt weld, flanked by the Carroza minibasin and La Popa syncline. Cross section lines of Fig. 4.2 indicated by red lines

composite halokinetic sequences (Giles and Rowan 2012) are present along the length of the salt wall.

Deformation style and intensity in strata flanking the weld vary significantly along strike. The northwestern end of the structure consists of a diapir (Figs. 4.1 and 4.2, A–A') and the northwestern third contains remnant gypsum, with little large-scale folding of flanking strata (Fig. 4.2, B–B') and fracture intensity consistent with that of regional strata. Directly NW of the bend, the structure contains pods of gypsum linked by fault-like surfaces where the up-thrown and down-thrown blocks on opposite sides of the structure are in direct contact to form a large-scale cuspate anticlinal geometry (Fig. 4.2, C–C') with significant fracturing of host strata within 5–10 m of the weld. The southeastern half of the structure is fully welded with no remnant gypsum, forms a prominent cuspate anticlinal geometry (Fig. 4.2, D–D'), and contains a 50-m-wide zone of strata with pervasive fractures and significant discoloration and fluid-related alteration. The variable deformation was controlled by the width of the original salt wall and the amount and direction of tectonic shortening. Where shortening was orthogonal to the wall, the diapir was locally closed, but little further deformation took place. Where shortening was oblique to the trend of the wall, post-welding

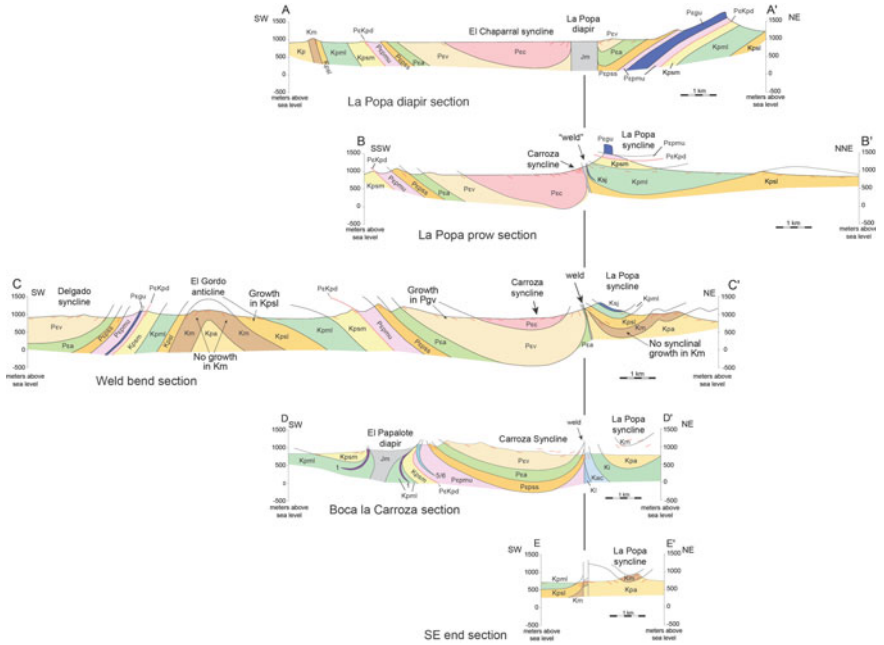

Fig. 4.2 Cross-sections of La Popa weld and salt wall. Section locations indicated in Fig. 4.1. We will visit the weld along sections D-D' and C–C' at stops 2–2 and 2–3, respectively. Cross sections from Rowan et al. (2003, 2012). AAPG © 2003, reprinted by permission of the AAPG, whose permission is required for further use

dextral strike-slip movement created extensive fracturing and shearing of the wall rock.

4.2 Excursion 2 Itinerary and Road Log

The road log begins at the Marriott Courtyard Aeropuerto Hotel, Monterrey, Mexico. Refer to Figs. 4.4 and 4.5 for locations of field trip stops for the day.

CK IK.

0 0 *Marriott Courtyard Hotel, Monterrey, Mexico. Retrace the route of Day 1 to La Popa basin, proceeding past the turnoff onto the dirt road of yesterday.*

65.8 65.8 *Turn off left (west) Highway 53 onto the dirt road to the village of San Jose de La Popa. The intersection (26.114600°/-100.647300°) is clearly marked with a sign over the highway. There is a white cement block building at the intersection. Pull over to the right side of the dirt road at an appropriate location for first stop.*

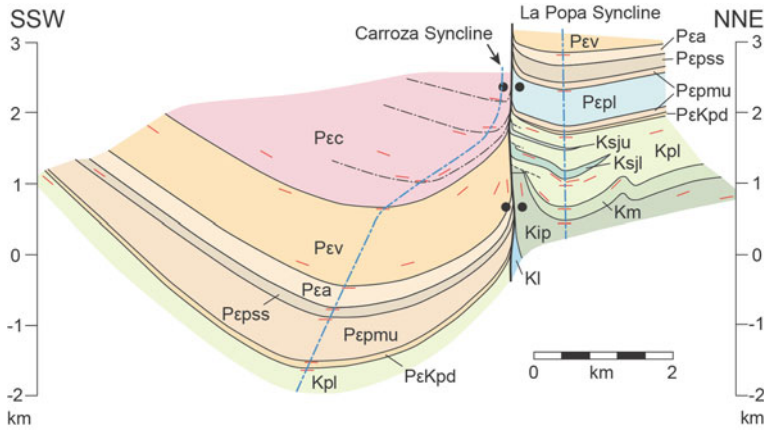

Fig. 4.3 Composite cross-section of La Popa salt weld based on cylindrical down-plunge projection along calculated synclinal fold axes that vary along strike. Short red lines are projected bedding attitudes, dashed lines are unconformities, black dash-dot lines indicate bedding in the Carroza Formation, blue dash-dot lines are synclinal axial traces and pairs of dots denote weld. Stratigraphy as in Fig. 4.2 except for Kl, Lower Cretaceous units; Kip, combined Indidura and Parras formations. From Rowan et al. (2012). Geological Society of London © 2012, reprinted by permission of the Geological Society of London, whose permission is required for further use

STOP 2.1 Overview of La Popa Weld System (26.113153°/ -100.651419°)

From this stop looking west and south in the foreground, the long, roughly continuous outcrops of the Upper Cretaceous El Toro Lentil are visible in the western foreground (Fig. 3.5c). The lentil has a near vertical to slightly overturned dip here and is overlain by slope-forming Indidura and Parras Shale turbidites. In the background are the more shallowly dipping beds (roughly 40° NE) of the Paleogene part of the Difunta Group. The high peaks are the Viento Formation. La Popa salt weld lies between El Toro Lentil and the upper Difunta Group beds. Although the weld surface has a steep southwestward dip, it is near vertical along most of its trace. Therefore, we avoid the terms *footwall* and *hanging wall* and use instead *upthrown* and *downthrown.* Thus, El Toro lentil is on the upthrown side of the weld and Difunta Group strata occupy the downthrown side of the structure.

In the right foreground, north of the dirt road leading westward and forming a low mesa, is the Muerto Formation. In the background lies the white, cliff-forming massif of the upper San Jose Lentil, on the upthrown side of the structure (Fig. 4.2, C–C').

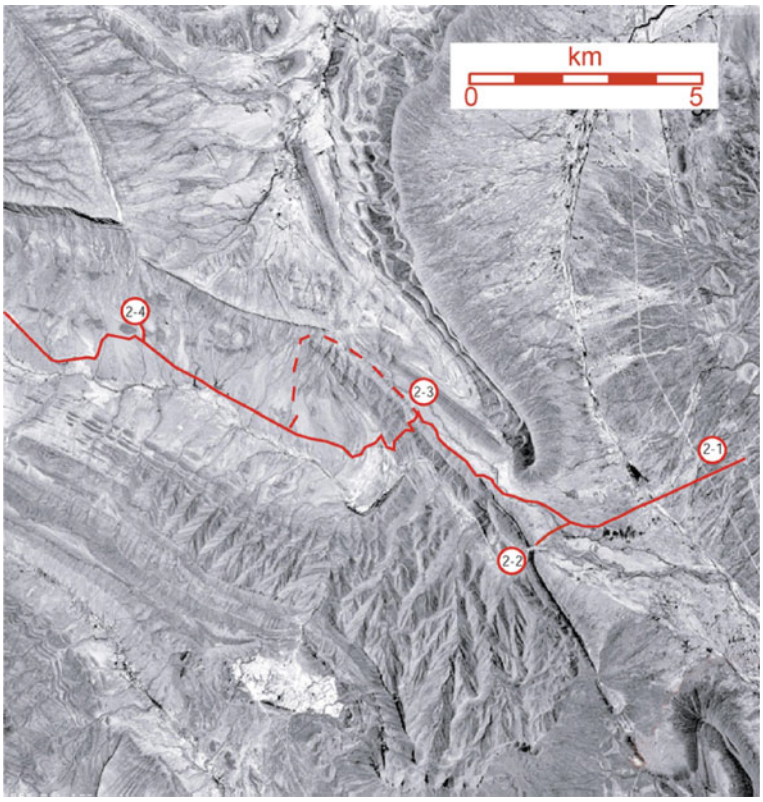

Fig. 4.4 Excursion 2 route

Estimated travel time: From the Marriott Courtyard Aeropuerto Hotel to Stop 2.1 is 1 h and ten minutes by vehicle

Estimated stop Time: 15 min

Proceed west on dirt road toward the village of San Jose de la Popa

69.6 3.8 *Intersection with 2WD track at orange cement block water tank on left (south) side of road (26.104505°/ -100.681854°). The track, flanked by barbed-wire fences beyond the water tank, bears right after a few hundred meters and continues toward a conspicuous canyon cut through El Toro Lentil called Boca la Carroza.*

70.6 1.0 *Entrance to Boca la Carroza. Park here (Do not drive past obvious road into arroyo—the sediment may be soft!).*

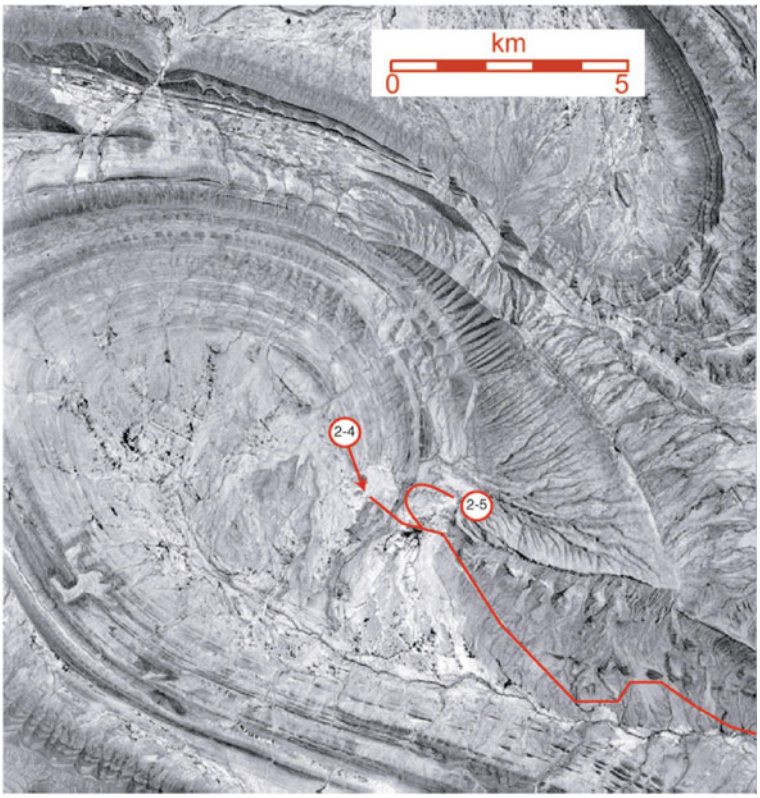

Fig. 4.5 Excursion 2 route (continued)

STOP 2–2. Boca la Carroza (26.097353°/ -100.691310°)

Exposures at Boca la Carroza display the characteristics of the southeastern half of La Popa salt weld. Here, a major drainage exits the Carroza minibasin through a short canyon cut across El Toro lentil.

Estimated driving time from Stop 2.1 to Stop 2.2 is 15 min; walking time at stop is about 15 min round trip

Estimated stop time: 1 h

Walk west along the drainage through the portal, after which the drainage bears left (south) along limestone strata on its left bank. The walk distance is 400 m. If you look up to the right (or in some of the big limestone blocks at your feet), you will see swarms of calcite-filled veins, many with en-echelon geometries (Fig. 4.6 e). The orientations are compatible with a SSW-NNE principal compressive stress, and are probably related to a small tear fault that cuts the weld at the gap (Rowan et al. 2012).

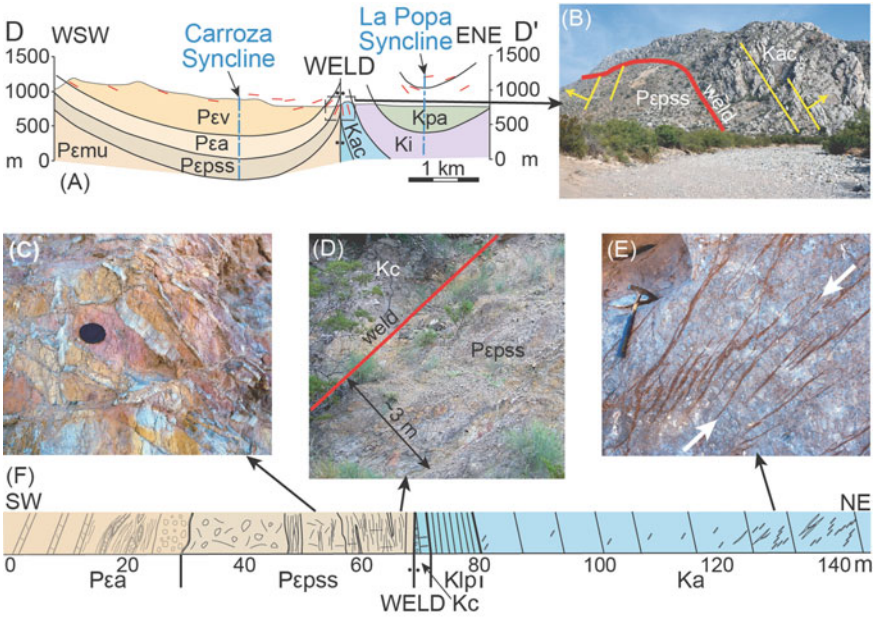

Fig. 4.6 Traverse of Boca La Carroza. **a** Cross-section with no vertical exaggeration. Short red lines show bedding dips; blue dashed lines are synclinal axial traces and pairs of dots denote complete weld. Stratigraphy as in Fig. 63 except Kac: Cupido, La Peña and Aurora formations. **b** Oblique view of inverted-V geometry with strata dipping steeply away from weld on both sides (yellow arrows indicate stratigraphic up). **c** Highly altered and pervasively fractured upper sandstone member of Potrerillos Formation (Pgpss) on downthrown side of weld, with most veins filled by gypsum. **d** Thick sandstone of upper sandstone member (Pgpss) on downthrown side of weld, sheared so that lithology and bedding are barely recognizable. Weld marked by 0.5 m wide fault gouge. Cupido Formation (Kc) on upthrown side of weld. **e** Conjugate sets of en echelon veins in Aurora Formation (Ka) on upthrown side. White arrows show orientation of σ_1, the principal compressive stress. **f** Sketch of measured section across weld. Thin lines oblique to bedding represent fractures, those parallel to bedding represent shear fabric, ellipses indicate veins and more rounded polygons are clasts. Unit symbols as in (a), except Kc, Cupido Formation; Klp, La Peña Formation; Ka, Aurora Formation. From Rowan et al. (2012). Geological Society of London© 2012, reprinted by permission of the Geological Society of London, whose permission is required for further use

La Popa weld at this locality is a fault-like plane of discontinuity. The fault zone, which has been extensively prospected north of the drainage, is brecciated across an interval 3–4 m wide. The trend of the fault on the hillside north of the portal at Boca la Carroza indicates that it dips steeply west (Figs. 4.6a and 4.7a). A minor fault in a prospect pit north of the arroyo strikes northwest and dips northeast (345, 65 NE). The fault zone juxtaposes Lower Cretaceous strata containing El Toro lentil on the east side up-thrown block against Viento Formation (Paleocene) on the west side down-thrown block. Lower Cretaceous rocks face east and are vertical to steeply northeast dipping (342, 75 NE). The Viento Formation faces west and dips moderately

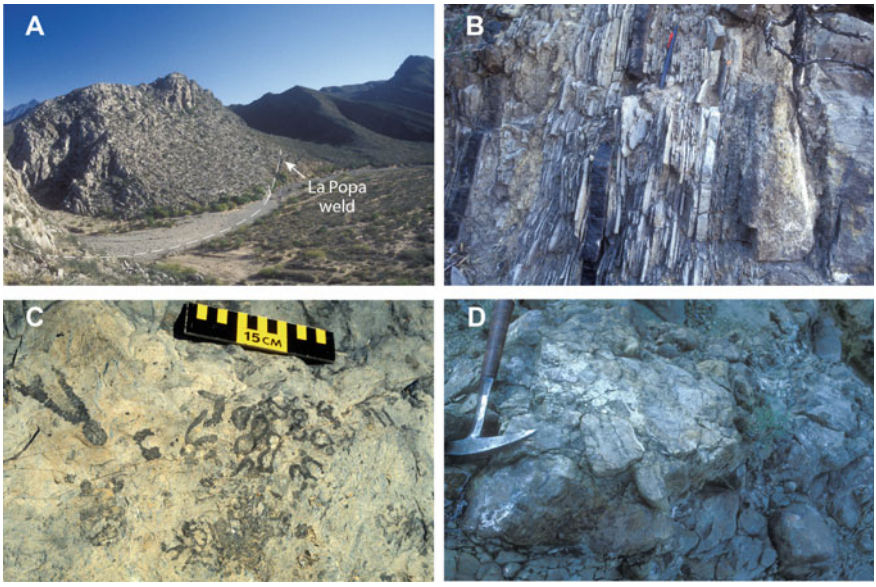

Fig. 4.7 Boca La Carroza outcrops. **a** La Popa weld on west side of El Toro Lentil at Boca La Carroza. El Toro Lentil is near vertical or dips slightly to NE (left) on upthrown side of the structure. Note beds of Viento Formation in shadows on right side of photo. Local dips here are steep to the SW (right). Trace of weld indicated by dashed line. View south. **b** La Peña Formation in contact with Cupido-equivalent strata (far right) of El Toro Lentil at Boca La Carroza. Tan bed to left of limestone at far right is the basal granule conglomerate of the La Peña, which overlies a karst surface on the limestone. Metaigneous lithic grains derived from the former salt wall are present in the conglomerate. Cavities in the karst contain infiltrated conglomerate and suggest subaerial exposure prior to the flooding event that deposited the La Peña. Stratigraphic top is to left. Pen in top center is 15 cm long. **c** Sponge biostrome in El Toro Lentil at Boca la Carroza. **d** Meta-igneous clast conglomerate in upper sandstone member of Potrerillos Formation adjacent to La Popa salt weld. Locality near arrow at arroyo margin in Fig. 4.6a

southwest (299, 61 SW). Stratigraphic juxtaposition suggests that the weld structure has normal offset at this location.

Follow the drainage as it bends around southward along the base of El Toro lentil. Key outcrops are exposed along the east side of the drainage. The outcrops are described in order from the upthrown block (the large limestone lentil), across the weld, to the siliciclastics on the downthrown (SW) side.

The carbonate and siliciclastic stratigraphic succession at Boca La Carroza east of the weld consists of Aptian through Albian strata with unique facies compared to the surrounding region (Fig. 4.8). Although described in stratigraphic order here, the first unit encountered on the traverse is the Aurora Limestone, followed by La Peña Formation, and finally Cupido Formation, before the weld is encountered. The lowermost carbonate bed, which is truncated abruptly at the weld, consists of oyster packstone with conspicuous orange-weathering meta-igneous clasts. This bed, equivalent to the Cupido Formation, is about 1 m thick and is overlain by La Peña

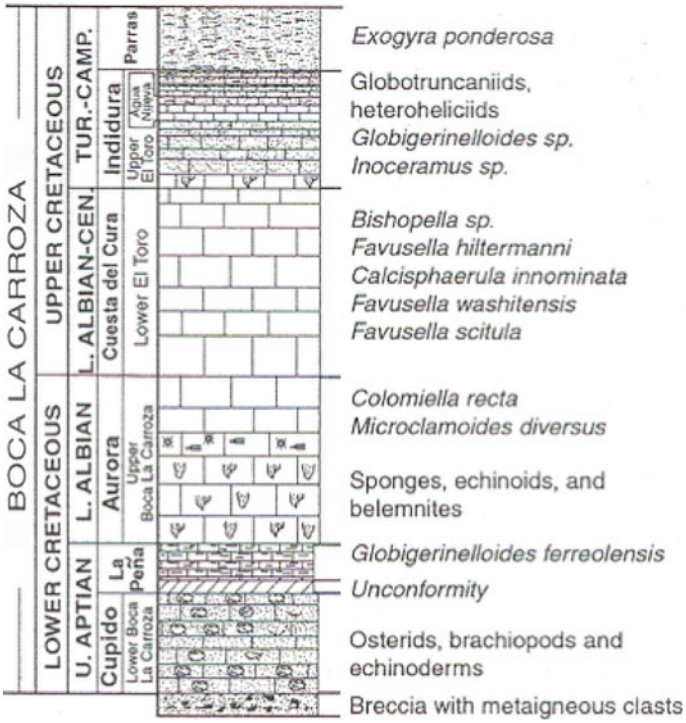

Fig. 4.8 Lithostratigraphy and biostratigraphy of upthrown side of weld at Boca La Carroza (Lawton et al. 2001). AAPG© 2001, reprinted by permission of the AAPG, whose permission is required for further use

Formation, consisting of shale with bedding-parallel black chert nodules (Fig. 4.7b). La Peña includes a basal granule-pebble conglomerate that overlies an exposure surface on the Cupido-equivalent limestone and fills cavities in the upper 30 cm of the underlying carbonate bed. The basal conglomerate contains meta-igneous granules derived from once locally exposed diapiric evaporite. Above shale of La Peña Formation, the main body of the lentil, equivalent to the Aurora Formation, consists of sponge-bearing wackestone. Sponge fossils are conspicuous in exposures along the arroyo (Fig. 4.7c).

The weld itself is a near-vertical surface between the carbonates and highly disrupted siliciclastics of the upper sandstone member of the Potrerillos Formation, which is exposed southward along the arroyo. Strata young and dip steeply away from the weld on both sides (Fig. 4.6b). There is no remnant evaporite along the weld (Fig. 4.6d), making it a complete weld (e.g., Hudec and Jackson 2011) marked by a 50 cm wide gouge zone with blocks of sandstone. Moving away from the weld, you will see ~20 m of sandstone that is intensely sheared, with abundant veins of gypsum and evidence for significant fluid alteration (Fig. 4.6c). The deformation gradually decreases over a distance of 40–50 m from the weld (Fig. 4.6f).

The upper sandstone member consists of meter-scale beds of fine- to medium-grained sandstone and pebbly sandstone with conglomeratic bases. Pebbles are primarily black chert. Olive green siltstone with pedogenic micrite nodules is interbedded with the sandstone. Depositional environments in this part of the upper sandstone member consist of tidal shoreline and coastal-plain deposits. An unusual facies near the weld, unique to this unit in La Popa basin, consists of matrix-supported conglomerate with rounded meta-igneous clasts, 20–30 cm in diameter, set in a fine-grained silty sandstone matrix (Fig. 4.7d). Beds are 1.5 m thick, thickening to 4 m downdip away from the weld. A few percent of rounded black chert pebbles are also present. These beds are interpreted as sediment gravity-flow deposits that accumulated in a debris cone or alluvial fan adjacent to La Popa salt wall. The meta-igneous clasts document salt exposure, either subaerial or submarine, during deposition of upper sandstone member beds at this locality. We infer that, as at El Papalote and El Gordo diapirs, meta-igneous blocks were present in evaporite of the salt wall prior to welding.

Retrace route back to vehicles and then along track and turn left onto main dirt road to the village of San Jose de la Popa. The road runs northwest along the salt weld at the base of a ridge to your left underlain by sandstone beds of the Viento Formation. Continue NW on the road to a tight hairpin switchback into the Viento marked by a prominent outcrop of limestone, actually in the Viento Formation.

74.0 3.4 *Hairpin curve. Just before the curve (26.121839°/ -100.716585°), turn right off the main road onto an unmaintained track that continues parallel to the strike ridge of Viento strata. The road is rough but passable in 2WD with good clearance, and ends at a turnaround 500 m NW of the turnoff (26.125139°/ -100.719638°). If in doubt, park along the main road at beginning of track and walk.*

STOP 2.3 Muerto Formation overview and weld-bend traverse (26.125139°/ -100.719638°)

This stop is the beginning of a rugged traverse, indicated by the map image of Fig. 4.9, of about 3 km NW along the drainage and up to a saddle crossed by the weld trace (Figs. 4.10c and 4.11a). Structural and stratigraphic features created by the diapiric phase of the weld are well exposed along the traverse, which is in the area of the bend in the weld. The hike requires sun protection, sturdy footwear, water and lunch. Hazards include loose rocks, sun exposure, and spiny plants. Venomous snakes are possible but extremely uncommon. The high point of the traverse, directly south of a saddle crossed by the weld (Fig. 4.9), is an excellent overview and lunch spot.

It is a good idea to shuttle a vehicle to the other end of the walking traverse, rather than retracing the walk. From the hairpin curve, the main road follows switchbacks across Viento beds on the northeast flank of the Carroza syncline, the minibasin on the downthrown side of La Popa weld. Views to the northwest are of steep Viento beds abutting the weld. The route descends across drab olive green-weathering sandstone and shale of the Viento Formation, then climbs from an arroyo crossed by a stone bridge to encounter red weathering siltstone- and shale-dominated strata of the Carroza Formation, the youngest formation of the Difunta Group. 3.25 km from the hairpin curve, the main road encounters the far end of the walking traverse at a faint

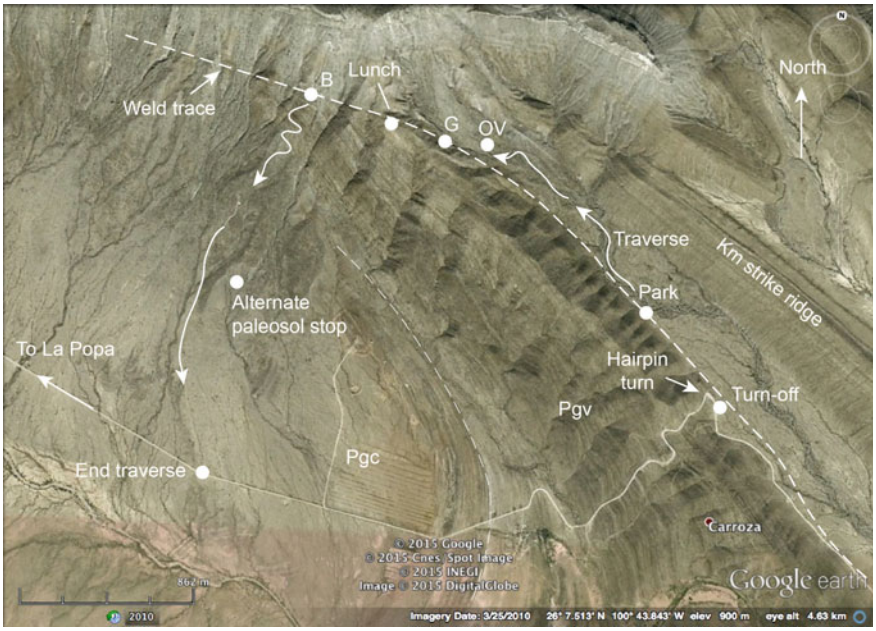

Fig. 4.9 Map of weld-bend tranverse. GPS locations of key points in traverse are in the text. Explanation: B, barite prospect; G, gypsum exposure along weld; OV, overview stop; Pgc, Carroza Formation; Km, Muerto Formation; Pgv, Viento Formation. Image from Google Earth

4WD track on the right (north) side of the road. There is a concrete telephone/power pole on the south side of the road at this point (Fig. 4.9; 26.117594°/ -100.742207°). Return to stop 2.3 after leaving a vehicle for the return shuttle.

Estimated driving time from to Stop 2.2 from Stop 2.3 is 15 min; add 10 min of walking time to the actual stop location if you have to leave vehicles on the main road. Estimated walking time to make the entire walk to the shuttle pickup point is 1.5 h

Estimated stop time: 3 h (includes lunch stop)

At the beginning of the track, just off the main dirt road, there is an outcrop of a carbonate lentil or caprock in the Viento Formation (Paleogene) along La Popa weld. To the north and west of this point, strata in the downthrown block become progressively younger as the exposed part of the weld climbs up section. The lentil is vertical here and juxtaposed across the weld against overturned Parras Shale beds dipping 80° SW. The weld surface is not very well exposed here due to talus cover, but in the road cut appears to correspond to a zone of brecciation.

From the parking/turnaround area, walk up the narrowing track until it intersects the main drainage. Follow this drainage up the strike valley; as it starts to steepen, stay in the southernmost drainage near/at the base of the ridge on your left.

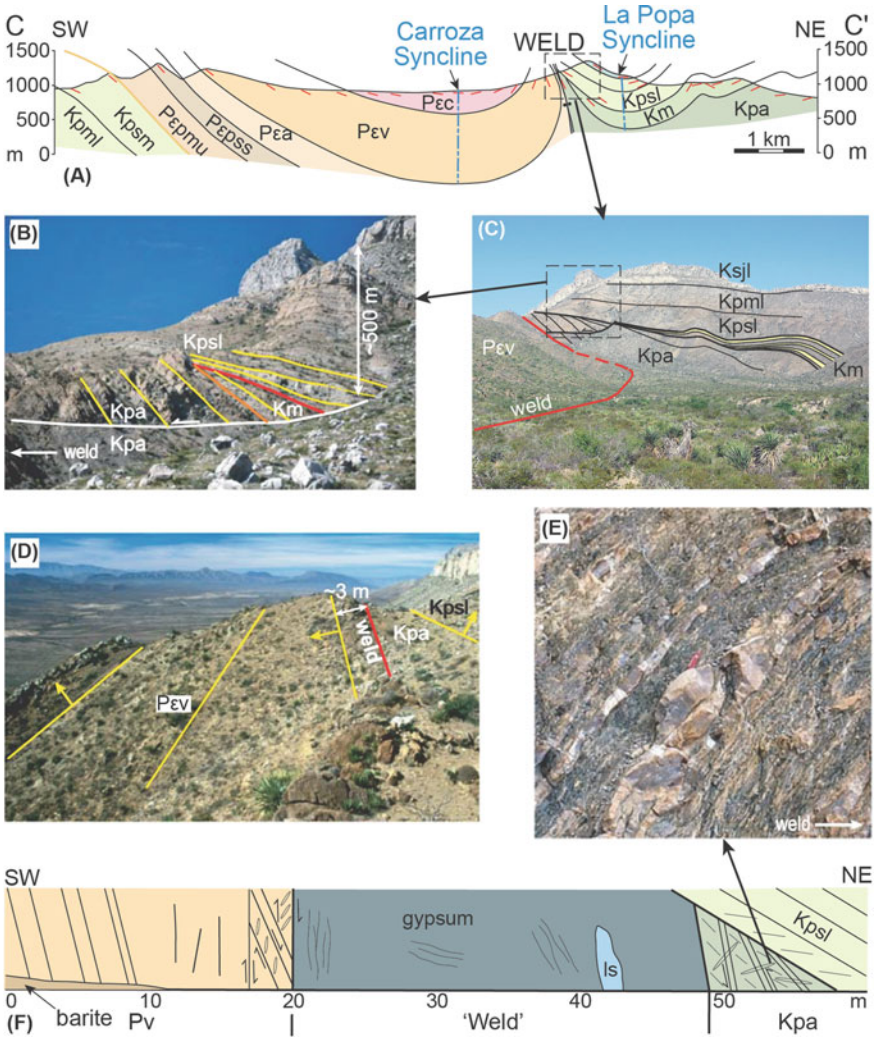

Fig. 4.10 Stop 2.3 cross section and field photos. Explanation: Stratigraphy as in Fig. 4.1. **a** Cross-section with no vertical exaggeration. Short red lines are bedding dips; blue dashed lines are synclinal axial traces. **b** Rotated normal fault with hanging-wall growth on upthrown side of weld. Red line is CHS-bounding unconformity. **c** Overview of upthrown side with tabular composite halokinetic sequence (Ksjl, Kpml and Kpsl) overlying tapered composite halokinetic sequence (Km and Kpa). Sandstones of Muerto Fm. (Km, in yellow) do not reach weld but are encased in shales. **d** Growth wedge in Viento Fm. (Pεv) on downthrown side of weld, with bedding progressively getting steeper to overturned closer to the weld. Yellow arrows denote stratigraphic up. **e** Faulted sandstones and shales with cleavage in Parras Sh (Kpa) c. 5 m from weld on upthrown side. **f** Sketch of measured section across incomplete weld with an isolated pod of gypsum. Thin lines oblique to bedding represent cleavage; ellipses represent veins with arrows showing sense of shear indicated by en echelon sets. From Rowan et al. (2012). Geological Society of London© 2012, reprinted by permission of the Geological Society of London, whose permission is required for further use

Directly up the valley, large-scale thinning of strata toward the weld is visible on the right-hand hillside (Figs. 4.10c and 4.11a). The La Popa weld runs through the ridge to the northwest on the left (south) side of the saddle (Figs. 4.10c and 4.11b, c). To the south of the weld are beds of the Viento Formation dipping approximately 65° SW. To the north of the weld are beds of the Parras, Muerto, and Potrerillos formations. The Parras and Muerto strata thin dramatically and are truncated by an unconformity at the base of the Potrerillos Formation, with more constant-thickness strata above (Figs. 4.2, C–C' and 4.10a, b).

Locally exposed within the strike valley is the uppermost Parras Shale, which here comprises dark brown to black shale and very fine-grained sandstone turbidites. The turbidite beds have sharp planar bases with local flute casts (paleocurrent directions to 112°) and Bouma sequences containing B-C-D horizons with rippled and burrowed tops. The southeast paleocurrent direction, obtained from ripples and flute casts, is parallel to the hinge of La Popa syncline on the upthrown (northeast) side of the weld.

As the arroyo begins to steepen, it is possible to climb out on the right (north) side for an overview back down the valley (OV in Fig. 4.9; 26.132497°/ -100.729646°). On the northern and eastern flanks of the Parras strike valley is a ridge underlain by thick sandstone ledges in the Muerto Formation. These strata of the upthrown block dip roughly 20° into the weld-parallel La Popa syncline to the northeast at this location. The Muerto Formation comprises thick beds of medium- to coarse-grained sandstone containing large cross sets organized into bar forms. Swaley cross-sets commonly have basal lags of oysters, high-spired gastropods and lithoclasts. The Muerto Formation comprises a succession of parasequences organized into 3 progradational parasequence-sets (Fig. 4.12; Hon 2001). The lower parasequence set is dominated by shale and siltstone and contains basal offshore shale facies above the flooding surfaces. These shoal upward into lower and middle shoreface deposits containing hummocky cross stratification with abundant *Ophiomorpha*. The upper parasequence sets are more sand prone and contain middle shoreface deposits that grade upward into upper shoreface deposits containing large scale trough cross sets, numerous lags, and fewer shale-siltstone interbeds. Overall the Muerto here displays progradation to the southeast and sandstone bodies within the parasequence sets locally thin toward the weld.

Thinning and steepening of strata on the upthrown (northern) block increase toward the weld. This thinning takes place within about 500 m of the weld trace, and the views up the valley are of an oblique section with respect to the weld. The Parras Shale is truncated at an unconformity beneath the Muerto Formation. This truncation is nicely displayed in several places northeast of the lower part of the traverse. At least one horizontal fault, which we interpret as a rotated normal growth fault in the Parras, is truncated at the unconformity beneath the Muerto Formation (Figs. 4.10 a, 4.12 and 4.13). Thinning of the Muerto takes place progressively, with each of three parasequences thinning toward the weld by low-angle onlap and erosional truncation. The Muerto pinches out within a hundred meters of the weld (Figs. 4.12 and 4.13). Each of the unconformity-bounded stratal packages (Fig. 4.12) is a wedge halokinetic sequence. The overlying Potrerillos Formation is concordant with the Muerto to

within about 200 m of the weld trace, but the contact becomes increasingly angular as the weld is approached. Angular discordance at the Muerto pinchout is 5–10°, beyond which the Potrerillos oversteps steeply dipping (70°), silt-rich Parras beds in the hanging-wall of the growth fault (Figs. 4.12 and 4.13).

As the arroyo narrows, the drainage coincides with the weld for a short distance. Here, a thin wedge of gypsum (G on Fig. 4.9; 26.132526°/ -100.730558°) about 3 m wide remains along the weld trace. The weld dips steeply northeast, as indicated by dips in both the Parras and Viento formations at this point and a line-of-sight attitude taken on the weld trace.

The unconformity-bounded halokinetic sequences of the Muerto Formation are fundamentally different from those we saw yesterday in the upper mudstone member of the Potrerillos Formation at El Papalote diapir. The Muerto Formation forms a stack of wedge halokinetic sequences that thin gradually toward the diapir and stack with the Parras Shale to form a tapered composite halokinetic sequence (Figs. 4.12 and 4.13).

At El Papalote diapir (Fig. 3.4), individual hook halokinetic sequences of the upper mudstone member stack to form a tabular composite halokinetic sequence formed during a time of slow, outer shelf deposition and in the middle siltstone and Delgado Sandstone members wedge halokinetic sequences stack to form a tapered composite halokinetic sequence during a time of prograding deltaic deposition. However, just 10 km away on the upthrown side of the weld (Fig. 4.13), the middle siltstone and Delgado Sandstone members form a tabular composite halokinetic sequence. Although sediment-accumulation rates were essentially identical in the two areas, salt-rise rate is interpreted to have been more rapid at La Popa weld because the salt wall was being squeezed by tectonic shortening (Giles and Rowan 2012).

After a bit of scrambling over boulders and then a short headwall in the arroyo, continue along a bit and then head up the steep slope to your left to a shoulder on the ridge. There is a faint trail that makes this climb easier.

From the shoulder, the view across the arroyo and weld to the northeast displays both the flat trace of the growth fault (Fig. 4.11c) and the Muerto-Parras unconformity/onlap surface (Fig. 4.11d). The growth fault is offset in one place by a younger, northeast-trending fault that drops the fault trace down to the east.

From the shoulder in the ridge, contour up and along the right slope toward the saddle along a well-used animal trail. Once at the saddle, cut back to the left (south) to the small knoll on the ridge, which is a nice lunch spot (Lunch in Fig. 4.8*; 26.133249°/ -100.734615°).*

In the distance southeast from the knoll (Fig. 4.11e), the view along the weld is of vertical beds of El Toro lentil on the upthrown block of the weld that abut SW-dipping Viento beds of the downthrown block. Also visible is the contact of the Viento (gray) and Carroza (red) formations in what is effectively a depth slice of the NW-plunging Carroza minibasin (Fig. 4.11e). Westward from the saddle, Viento beds display a fanning geometry on the downthrown (south) side of the weld (Fig. 4.10d). Steeply dipping Parras beds in the hanging wall of the rotated normal fault crop out along the north side of the weld. The Parras-Potrerillos contact lies up the slope to the north. The ridge on the north is capped by limestone of the San Jose Lentil, which is roughly

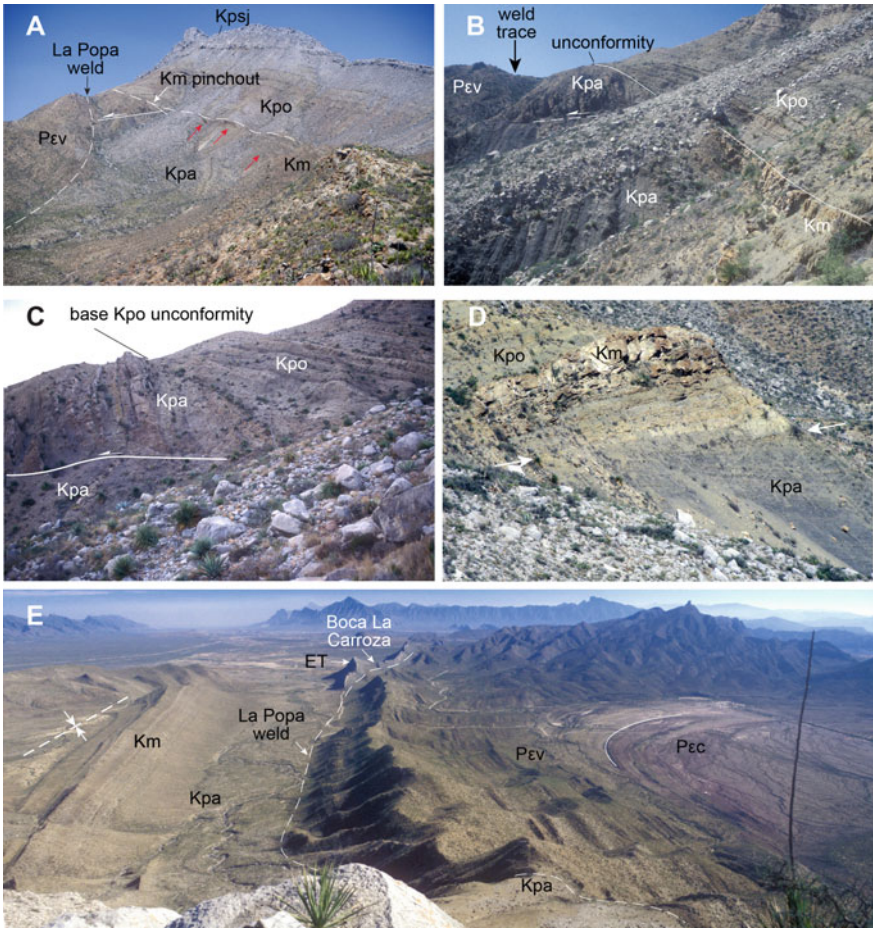

Fig. 4.11 Stratigraphic relations of La Popa salt weld. Unit symbols in photos: ET, El Toro Lentil; Kpa, Parras Shale; Km, Muerto Formation; Kpo, Potrerillos Formation; Kpsj, San Jose lentil; Pεv, Viento Formation; Pεc, Carroza Formation. **a** Growth strata in upthrown block of La Popa weld. View northwest of Muerto Formation along southwest limb of La Popa syncline. Parras Shale and lower Muerto beds are truncated beneath upper sandstone body of Muerto Formation, indicated by arrows. Potrerillos Formation and San Jose Lentil overlie Muerto Formation. Trace of weld separating Parras Shale and Viento Formation is indicated by dashed line. Beds in Viento Formation of downthrown block wall dip southwest (left). **b** Growth strata and rotated normal fault on upthrown side of La Popa weld. Steeply dipping beds of Parras Shale are cut by a flat normal fault. Muerto Formation truncates normal fault and is itself truncated by an unconformity at base of Potrerillos Formation, indicated by dashed line (truncation and Muerto pinchout are hidden behind talus). Weld crosses skyline at left of saddle (arrow). View west. **c** Detail of rotated normal fault in Parras Shale. **d** Angular unconformity and onlap surface (arrows) between Parras Shale and sandstone of Muerto Formation. Potrerillos Formation overlies Muerto. View northeast from weld. **e** View southeast of La Popa weld and Carroza minibasin from San Jose Lentil. Road in middle center follows exposed trace of weld (dashed line) to vertical beds of El Toro Lentil in distance. On left, Parras Shale and Muerto Formation dip and face northeast (left). Hinge of La Popa syncline in upthrown block indicated. In center and on right, beds of Viento Formation dip and face southwest (right). Figure 5e from Lawton et al. (2017). AAPG© 2017, reprinted by permission of the AAPG, whose permission is required for further use

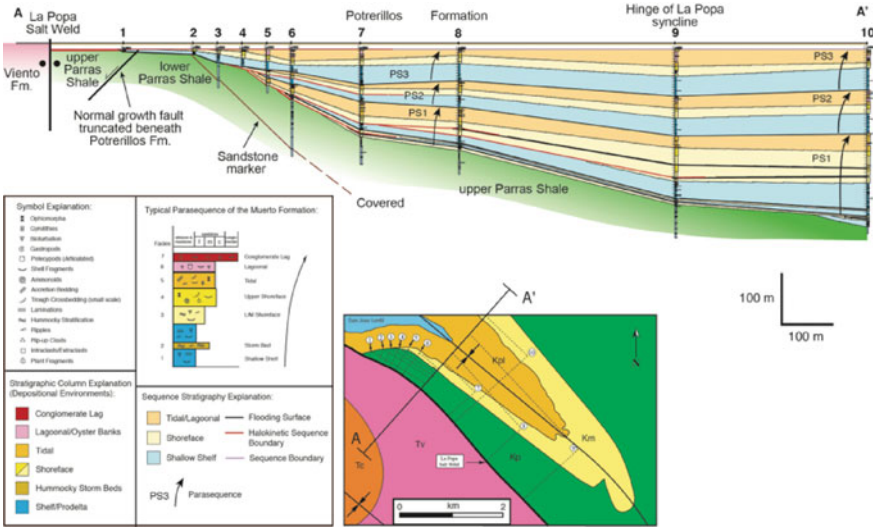

Fig. 4.12 Sequence stratigraphy of Muerto Formation northeast of La Popa weld (Hon 2001). Measured sections are projected onto a line (A-A') trending NE, perpendicular to the strike of the weld (inset map). Siltstone-sandstone parasequences (indicated by arrows) thin toward weld by onlap and erosional truncation beneath younger parasequences. The line of the section crosses the hinge of La Popa syncline in the upthrown block of the weld. Section 9 lies in the hinge, and Sect. 10 occupies the far limb of the fold. Thinning trends record bathymetry associated with the salt wall that formerly occupied the weld, but indicate that La Popa syncline postdates deposition of the Muerto Formation and was created during shortening, not by ongoing salt evacuation. Potrerillos Formation postdates a down-to-the-weld normal fault on left end of fence diagram. Kp, Parras Shale; Km, Muerto Formation; Kpl, Lower Potrerillos Formation; Tv, Viento Formation; Tc, Carroza Formation

correlative with the lowermost lentil at El Papalote diapir and dips approximately 20° to the north.

From the knoll, return to the saddle and then continue west-northwest, parallel to the weld and the strike of flanking stratigraphy.

The traverse along the weld to the west passes some stretches where there is no gypsum along the weld and others where there are pods of remnant gypsum. The presence of gypsum lenses indicates this part of the structure is incompletely welded, probably due to irregularities in the two walls of the diapir. After passing several small gullies, the traverse arrives at a small prospect with abundant barite (B in Fig. 4.9; 26.134048°/ -100.737278°). Just uphill is an exposure of gypsum about 30 m wide.

A traverse of the incomplete weld (defined as < 50 m of remnant evaporite) in this area, from the downthrown side at the barite prospect to the upthrown side up the hill, displays the following (Fig. 4.10f): (1) steeply dipping beds of the Viento Formation, with a fracture density that increases from background values over a distance of 5–10 m toward the weld; (2) a vertical contact with the gypsum, with en-echelon veins in Viento sandstones showing both flexural-slip folding and relative downward

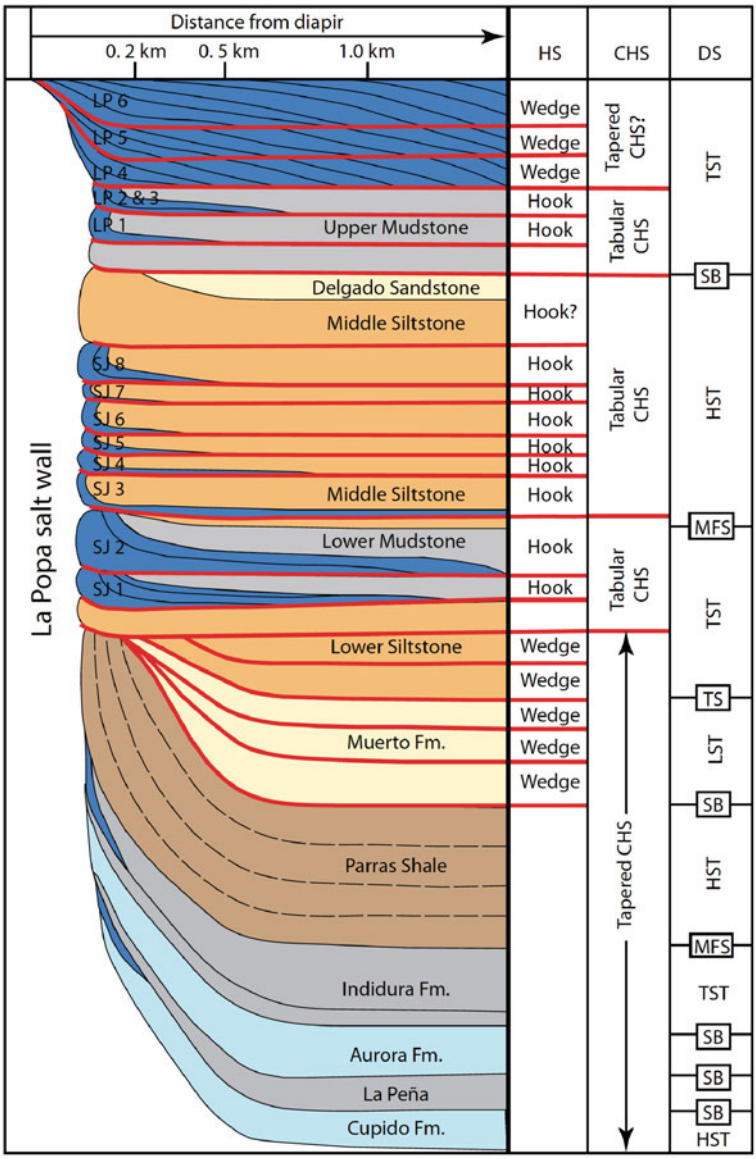

Fig. 4.13 Halokinetic sequences (HS), composite halokinetic sequences (CHS) and depositional sequence stratigraphy of the Lower Cretaceous through lower Paleogene stratigraphy exposed on the north side of La Popa Weld. Colors indicate dominant lithology of the unit: dark blue, carbonate lentil; gray regional carbonate unit and shelfal mudstone; orange, prodelta and shelfal shale; yellow, shoreface sandstone. MFS: maximum flooding surface. From Giles and Rowan (2012). Geological Society of London © 2012, reprinted by permission of the Geological Society of London, whose permission is required for further use

movement of the gypsum relative to the flanking strata (interpreted as due to slip on a halokinetic-sequence unconformity); (3) 30 m of gypsum with internal fabrics and a stringer of carbonate; (4) a steeply-dipping contact of the gypsum with black Parras Formation shales that have a cleavage compatible with flexural-slip folding, as well as small faults and fracture within 5–10 m of the gypsum (Fig. 4.10e); and (5) uphill of the gypsum, the same unconformity seen before between steeply dipping Parras Shale and moderately dipping Potrerillos strata (Fig. 4.10f).

Near the barite prospect, a large cement claim marker indicates the top of a trail that descends via*switchbacks to the base of the hill, where it encounters an old 4 wheel drive (4WD) road, which is no longer passable by vehicles.*

An optional stop in the gully to the east of the 4WD road contains good exposures of Paleocene-Eocene Carroza red beds that have been interpreted as an arid, low-gradient ephemeral fluvial system and associated overbank deposits (Buck et al. 2010; Andrie et al. 2012). The overbank deposits display paleosol horizons containing, or formerly containing, halite, gypsum, barite, and carbonate (Fig. 4.14a–c). The features of the different compound paleosol fabrics and their climatic significance are described and discussed in Buck et al. (2010).

*For optional stop walk south along the 4WD track 620 m, turn left into untracked desert and walk another 200 m into an amphitheater along the arroyo, to the Carroza exposure (*Fig. 4.9*; 26.125983°/ -100.740966°).*

Return to 4WD track, turn left (south) and walk to La Popa road. Back in the vehicles, proceed west on road approximately 3.7 km to road turnoff for following stop.

80.0 6.0 (Distance measured from hairpin curve). North of the road on the skyline, the character of the San Jose Lentil has changed here as compared to the previous stop. Here, it appears more massive and irregular than the well-bedded limestone of the lentil to the east. The change reflects an abrupt change to vertical dips that expose featureless bed bases on the north flank of the weld.

80.4 0.4 *Turn right (north) off main road onto dirt road (26.130414°/ 10 -100.769855°). This road is difficult to see from the thoroughfare. Be sure to signal your intention for the benefit of the following driver. Follow dirt road for approximately 1 km to a retention dam.*

STOP 2.4 Reservoir facies transitions in fluvial strata of growth syncline, Carroza Formation (26.137825°/ -100.768884°)

The objective of this stop is to observe the distribution of channel facies in the Carroza syncline adjacent to the salt weld. The road to the retention dam can be poor, especially where it crosses the arroyo; if in doubt, park vehicles and walk. A good trail gradually ascends from the retention dam about 1 km over the sloping terrane south of the weld. The trail crosses surficial fan deposits for the first 0.25 km, then traverses typical facies of the Carroza Formation.

Estimated driving time from shuttle stop at end of Stop 2.3 traverse to Stop 2.4 is 15* min*; add 10 min of walking time to the actual stop location if you have to leave

Fig. 4.14 Carroza paleosols. **a** Well-developed columnar structure in natric horizon, Carroza paleosol. **b** Stage II gypsum nodules in Carroza paleosol. **c** Barite rosettes in Carroza paleosol at optional stop

vehicles at the arroyo crossing. Estimated walking time to make the entire walk to the shuttle pickup point is 30 min

Estimated stop time: 1 h

Strata of the Carroza Formation consist of single-story sandstone channels with very high width/thickness ratios. The sandstone is medium-grained and contains red shale intraclasts at channel bases and grades upward to fine-grained sandstone with common horizontal lamination and parting lineation. Paleocurrent data (Waidmann 2004; Buck et al. 2010; Andrie et al. 2012) indicate highly variable paleoflow directions, probably because the parting lineation represents shallow flow on transverse and longitudinal bars; however, the resultant paleoflow direction is ESE, parallel to the hinge of the Carroza syncline. Uncommon ripple cross-lamination is present at the tops of sandstone beds, which are typically about 2 m thick. The sandstone grades to the dominant facies, which is reddish brown siltstone interpreted as floodplain deposits. Uncommon olive green-gray shale with high-spired gastropods is interbedded with the red siltstone and represents pond deposits. The olive green-gray shale facies is nowhere more than 2 m thick. Thin, very fine-grained sandstone splay deposits are common in the overbank siltstone and are recognized by the presence of climbing ripple cross-lamination. In several observed cases, splay sandstones overlie the olive gray shale facies and indicate deflection of floodwater to topographically low areas on the floodplain.

A multistory fluvial sandstone body occupies the hinge of the Carroza syncline (Fig. 4.15a, b). The three stacked sandstone bodies contain the same facies present in the single-story channel bodies. Horizontal lamination and parting lineation dominate the sedimentary structures and indicate dominantly shallow flow. The sandstone body is folded at the northern edge of its exposure, such that its northern part forms a steeply south-dipping fold limb within ~100 m of the weld (Fig. 4.15c). The asymmetry and chevron-like hinge of the syncline at this location contrast with the concentric, long-limbed style of the fold in older Carroza strata just a few km to the east. These contrasts in fold style suggest that the dominant influence on fold geometry at this location was halokinetic drape folding rather than subsidence into underlying salt. Angular truncation within the halokinetic section can be observed in the canyon north of the sandstone body (Fig. 4.15d).

Proceed west along trail, which becomes faint, to a point overlooking the arroyo.

Angular discordance and stratal truncation on the north flank of the syncline are visible in the dominantly red bed section exposed in the west wall of the arroyo (Fig. 4.15d). These strata display 50 degrees of stratal rotation within a stratigraphic section only 60 m thick (Fig. 4.16). The section here contains numerous paleosols, which are relatively rare in Carroza red beds on the opposite, south flank of the syncline. Some of the paleosols are calcareous and marked by pedogenic carbonate, whereas others appear to have been gypsic soils, consisting of gypsum nodules subsequently replaced by apatite (Buck et al. 2010). These strata represent beds that were deposited and rotated during diapiric rise of the salt wall and therefore represent nonmarine halokinetic sequences. Angular truncation took place by erosion following

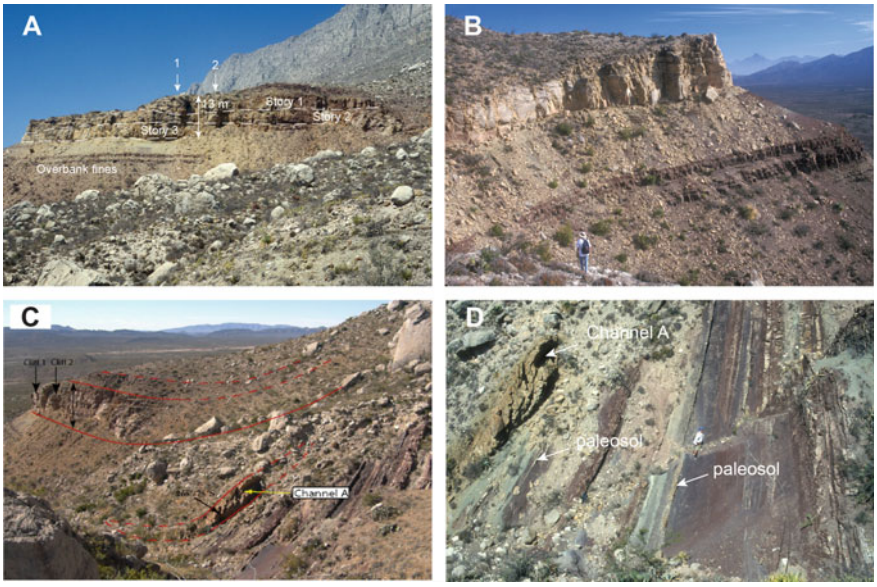

Fig. 4.15 Carroza Formation fluvial deposits. **a** Multistory fluvial sandstone body in Carroza Formation, hinge of Carroza syncline. View west. Sandstone body is 13 m thick. Arrows labeled 1 and 2 indicate cliffs of Fig. 4.15c. **b** Stacked fluvial channel sandstones in Carroza Formation adjacent to weld in hinge of La Popa syncline. View SE (back of outcrop in Fig. 4.15a. **c** Southwest view of multi-story sandstone channel above older strata that steepen abruptly near the weld. Cliffs 1 and 2 are correlative with those indicated in Fig. 4.15a. **d** Sub-vertical bedding in Carroza Formation red beds just north of multi-story channel and adjacent to the weld. These beds contain several paleosol horizons and low-angle unconformities

stratal rotation, and the numerous paleosols record more frequent episodes of exposure and non-deposition adjacent to the diapir than elsewhere in the Carroza Formation. Gypsic soils apparently were formed from sulfate derived directly from the diapir during times when it was exposed. In contrast, more typical carbonate soils likely formed during times when the diapiric sulfate was not exposed.

North of the red beds is a succession of gypsum conglomerate, apparently deposited by debris-flow processes, containing meta-igneous blocks and a carbonate-clast breccia (Fig. 4.16). These lie directly south of an exposure of massive gypsum that represents in situ diapiric material. This coarse-grained succession south of the salt wall may represent alluvial material derived directly from the diapir (Buck et al. 2010).

Retrace route to vehicles and then main road. Turn right (west).

83.1 1.1 View of La Popa Lentil (26.135526°/ -100.776391°)

From this vantage point, the beds of the Carroza Formation can be observed to dip gently into the weld surface and "diverge" or thicken toward the weld surface, unlike any other La Popa basin strata. This shift in the depocenter from the weld-parallel evacuation syncline to the weld surface itself is shown in Fig. 4.3. The 'weld' here

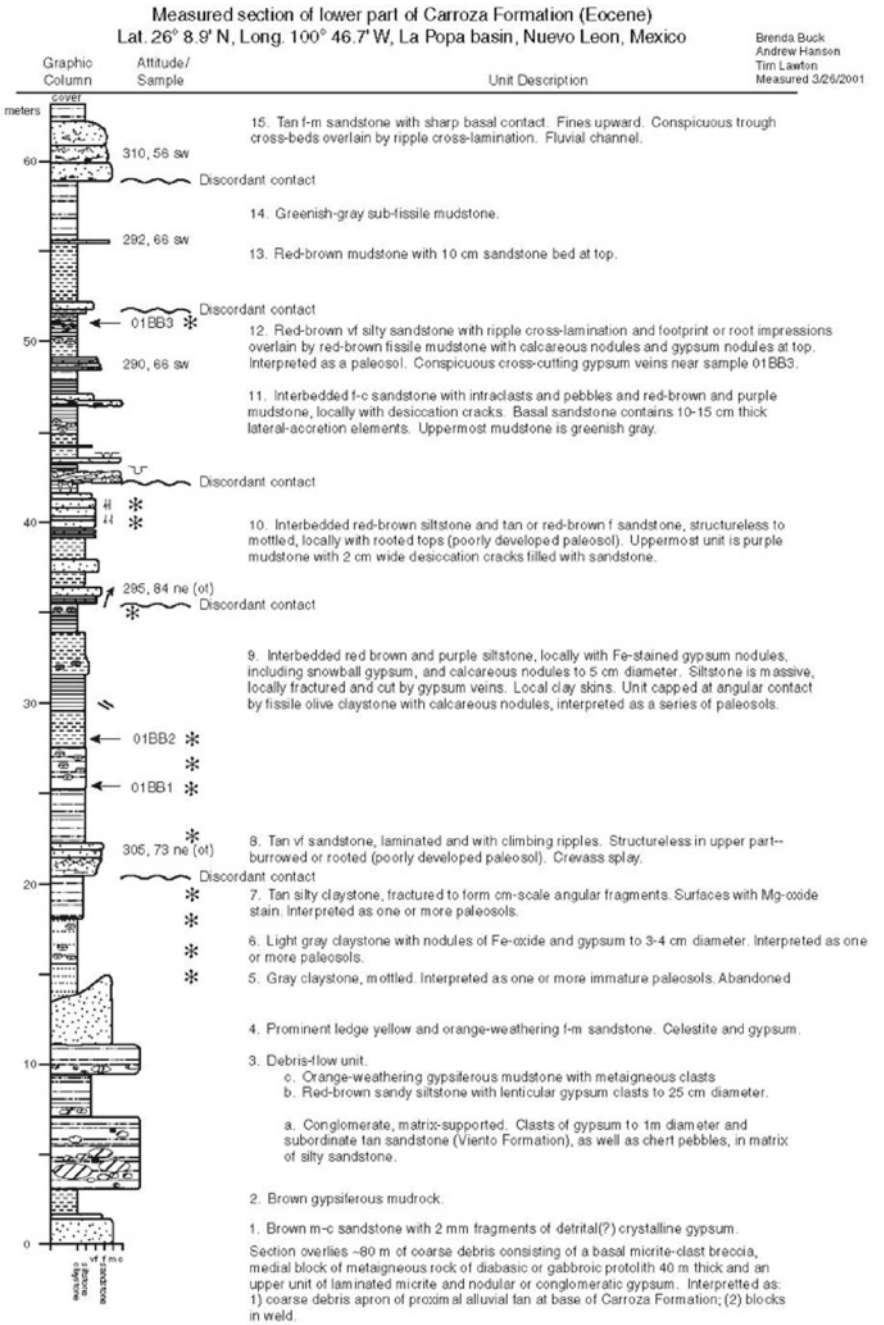

Fig. 4.16 Measured section of part of the Carroza Formation south of La Popa lentil. Stratigraphic units thin northward toward La Popa weld mainly by unconformable truncation. Incrementally steeper dips at each unconformity indicate that this is a progressive unconformity adjacent to the weld. Locations of inferred soils are indicated on section by asterisks

is not strictly a weld in that the gypsum is more than 100 m wide. Because it is narrow, it would be interpreted as a weld on seismic data, but strictly speaking, it is a narrow salt wall. Welds interpreted on seismic data are termed *apparent welds* because, without well control, it is impossible to know how much remnant evaporite is present.

On the far (northern) side of the weld, strata of the middle siltstone member of the Potrerillos Formation contain multiple interbedded carbonate lentils (Fig. 4.17a, b). Although not visible from this vantage point, each of the lentils is folded abruptly to near-vertical dips within about 100 m of the weld, forming hook halokinetic sequences and a tabular composite halokinetic sequence (see Fig. 4.13). Near the top of the slope is the Delgado Sandstone Member and above it the upper mudstone member (Fig. 4.17a, b). The latter includes several relatively thin lentils, which are in turn overlain by the thick La Popa lentil. La Popa Lentil is 550 m thick near the weld, where it is dominantly a sponge-coral reef. The face around the corner to the east (right) displays clinoforms dipping away from the weld. The change in the appearance of the San Jose Lentil from east to west along the weld results from its change in attitude from moderate north dips to vertical dips as the carbonate beds approach the weld (Fig. 4.17 c).

90.7 7.6 *Village of San Jose de la Popa. Continue westward into town on Perfecto Serna Street toward the west end of town. Continue west out of town on dirt road. Pass south of cemetery and bear left on most travelled road into an arroyo. Park in or near arroyo (26.164446°/ -100.834464°).*

91.9 1.2 *Gypsum deposit on west side of San Jose de la Popa.*

STOP 2.4a La Popa diapir (26.164446°/ -100.834464°; shown as Stop 2–4, westernmost stop, on Fig. 4.5***).***

Walk 150 m north along the arroyo; then climb out on left (west) bank and walk up the prominent gray weathering ridge onto the La Popa diapir. From this vantage point one can view the open, west-plunging segment of La Popa syncline (on the upthrown side of the weld) expressed in La Popa lentil, the upper sandstone member of the Potrerillos Formation, and the Viento Formation. The southern limb of the syncline is modified by large slump blocks of La Popa lentil that have moved down and to the south, away from the cliff face. North of the village, the lentil apparently directly overlies gypsum, which has facilitated slumping.

La Popa diapir marks the northwest termination of La Popa salt weld/wall, with a continuous succession of Carroza and Viento beds wrapping at its western end (Fig. 4.1). It contains abundant meta-igneous and black dolomite blocks. There is evidence from the air photos that this gypsum may have flowed at the surface during modern exposure.

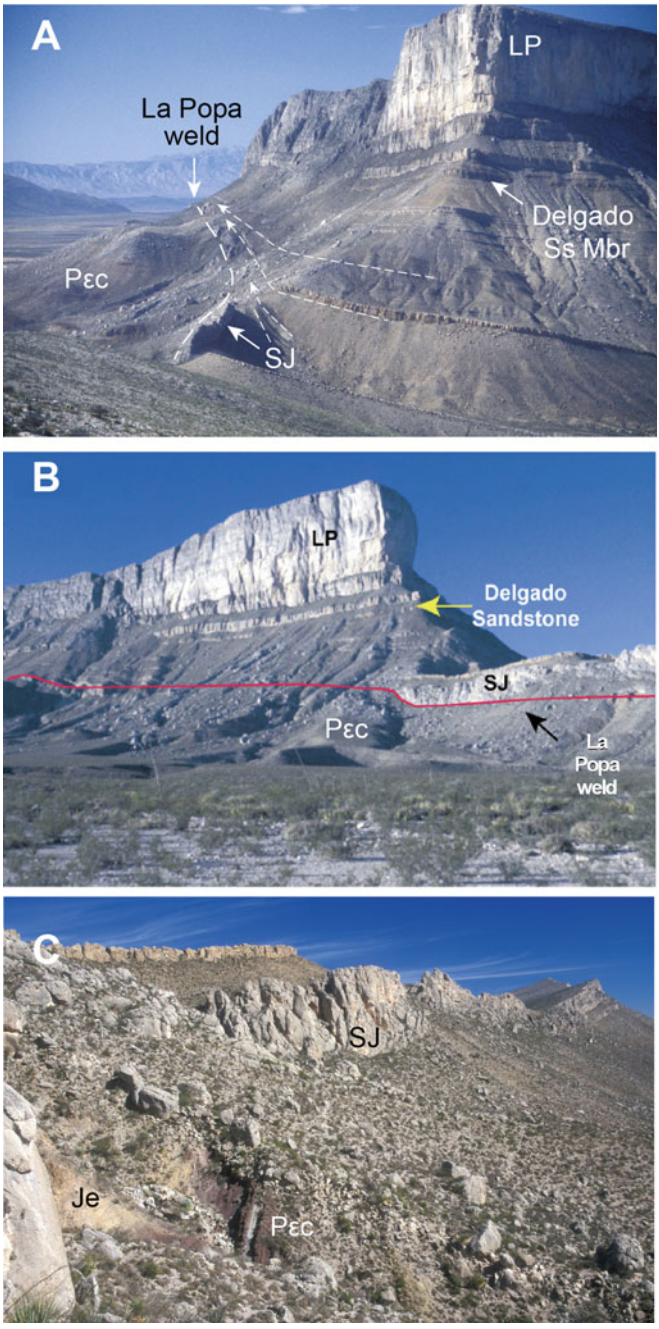
A
LP
La Popa
weld
Delgado
Ss Mbr
Pεc
SJ
B
LP
Delgado
Sandstone
SJ
Pεc
La
Popa
weld
C
SJ
Je
Pεc

◀**Fig. 4.17** Structural relations of La Popa weld. **a** View west from San Jose Lentil (road is down to the left) showing La Popa Lentil (LP) and La Popa weld. Beds north of La Popa weld dip north and steepen abruptly to vertical in vicinity of the weld, where beds converge. Carroza beds (Pɛc) in bluffs south of weld dip at low angle toward weld; San Jose Lentil (SJ) is approximately vertical, facing north. Trace of weld indicated by long dashed lines; halokinetic growth strata of Potrerillos Formation indicated by short dashed lines, with arrows indicating approximate stratal terminations. **b** View north from road to La Popa Lentil (LP) on north side of weld (red line). Beds below lentil are Potrerillos siliciclastic strata with abundant lentils (including the San Jose lentil, SJ) that rotate to vertical attitudes within 100 m of the weld. **c** View east along La Popa salt wall (road is down to the right). Beds of San Jose Lentil of upthrown block to north are vertical in foreground, but dip 20° north in distance where beds are farther from La Popa weld. Steeply south dipping beds of Carroza Formation (Pɛc) dip steeply south in arroyo. Outcrop of gypsum (Je) indicates that salt wall is not completely welded here (arroyo above Pɛc label in Fig. 4.16b)

Estimated driving time from Stop 2.4 to Stop 2.4a is 30 min, then 10 min of walking time to the actual stop location

Estimated stop time: 45 min

Retrace track along the La Popa road back to the cemetery on the north side of the road then turn northwest (26.165316°/ -100.828826°) and take the next right (north) dirt road on the west side of the cemetery (26.167032°/ -100.830299°). This road climbs the slope, curves around to the east, and arrives at La Popa lentil. Stop south of a large drainage.

Stop 2–5. Primero Canyon La Popa reef boundstone facies (26.175650°/ -100.820250°)

There are exposures of La Popa lentil reef boundstone facies in this area. Carefully descend to the base of Primero Canyon. Beautifully exposed in the canyon walls are the massive boundstone or reef core facies of La Popa lentil (Fig. 4.18a, b). The boundstone facies comprise red algal, sponge and coral framestone with interstices filled by red algal and foram grainstone (Fig. 4.18c).

Estimated driving time from shuttle stop at end of Stop 2.4a to Stop 2.5 is 20 min

Estimated stop time: 30 min

Retrace route to Highway 53 and turn right (south) to return to the Marriott Courtyard Hotel, Monterrey.

Estimated driving time from Stop 2.5 to hotel is two hours

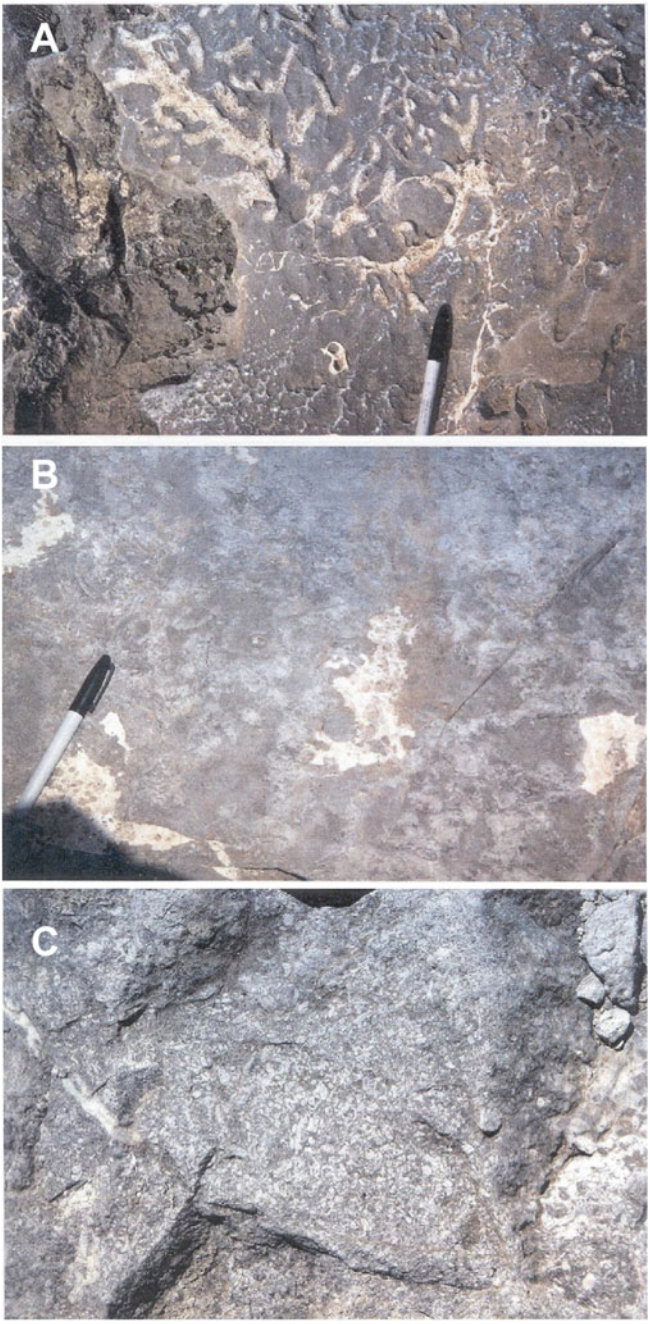

Fig. 4.18 Lithofacies of La Popa Lentil. **a** Red-algal and sponge coral framestone of La Popa Lentil. **b** Sponge and red-algal boundstone of La Popa Lentil. **c** Echinoderm and red-algal grainstone filling interstices between sponge, coral, and red-algal reefal framework

Bibliography

Alavi M (2004) Regional stratigraphy of the Zagros fold-thrust belt of Iran and its proforeland evolution. Am J Sci 304:1–20

Amezcua N, Rochin H, Esmeralda Martínez LF (2020) Preliminary strontium isotope stratigraphy of the Jurassic Minas Viejas Formation, México. Am Assoc Pet Geo Sear Discov Article #51652. https://doi.org/10.1306/51652Amezcua2020

Andrie JR, Giles KA, Lawton TF, Rowan MG (2012) Halokinetic sequence stratigraphy, fluvial sedimentology, and structural geometry of the Eocene Carroza Formation along La Popa salt weld, La Popa Basin, Mexico. In: Alsop GI, Archer SG, Hartley AJ, Grant NT, Hodgkinson R (eds) Salt tectonics, sediments and prospectivity, vol 363. Geological Society of London Special Publication, pp 59–79

Aschoff JL (2003) Sedimentation patterns within a salt-diapir influenced foreland basin: upper cretaceous to lower Paleocene Delgado Sandstone Tongue, Potrerillos Formation, La Popa Basin, Nuevo Leon, Mexico. M.S. thesis, New Mexico State University, p 259

Aschoff JL, Giles KA (2005) Salt diapir-influenced, shallow-marine sediment dispersal patterns: insights from outcrop analogs. Am Asso Petrol Geol Bull 89:447–469. https://doi.org/10.1306/10260404016

Aschoff JL, Giles KA, Lawton TF (2001) Origin of upper cretaceous (latest maastrichtian) massive, boulder-cobble conglomerates, Potrerillos Formation, La Popa basin, northeastern Mexico: incised valley fill or mega-tsunamite? Geol Soc Am Abstracts Prog 33/6:A-202

Aranda-García M (1991) El segmento San Felipe del cinturón cabalgado, Sierra Madre Oriental, estado de Durango, Mexico. Boletín De La Asociación Mexicana De Geólogos Petroleros 47:43–87

Becker F, Bechstädt T (2006) Sequence stratigraphy of a carbonate-evaporite succession (Zechstein 1, Hessian Basin, Germany). Sedimentology 53:1083–1120

Blair TC, Mcpherson JG (1994) Alluvial fans and their natural distinction from rivers based on morphology, hydraulic processes, sedimentary processes, and facies assemblages. J Sediment Res A64:450–489

Buck BJ, Lawton TF, Brock AL (2010) Evaporitic paleosols in continental strata of the Carroza Formation, La Popa Basin, Mexico: record of Paleogene climate and salt tectonics. Geol Soc Am Bull 122:1011–1026. https://doi.org/10.11/B30089.1

Campa-Uranga MF (1985) The Mexican thrust belt. In: Howell DG (ed) Tectonostratigraphic terranes of the circum-Pacific Council for Energy and Mineral Resources, Earth Science Series, 299–313

T. Lawton et al., *La Popa Basin, Nuevo León and Coahuila, Mexico*, Springer Geology,
https://doi.org/10.1007/978-3-030-79397-5

Charleston S (1981) A summary of the structural geology and tectonics of the state of Coahuila, Mexico. In: Smith CI, Katzs SB (eds) Lower Cretaceous stratigraphy and structure, northern Mexico. West Texas Geological Society Publication, pp 81–74

Chávez-Cabello G, Aranda-Gomez JJ, Molina-Garza RS, Cossio-Torres T, Arvizu-Gutiérrez IR, González-Naranjo GA (2005) La falla San Marcos: una estructura jurásica de basamento multirreactivada del noreste de México. Boletín De La Asociacion Geológica Mexicana 17:27–52

Cohen KM, Finney SC, Gibbard PL, Fan J-X (2013) updated. The ICS international chronostratigraphic chart. Episodes 36:199–204

Couch RD (2005) Style, timing and uplift history of the frontal Sierra Madre Oriental determined through analysis of growth Strata and Vitrinite reflectance. M.S. thesis, New Mexico State University, p 234

Cowley WM, Preiss WV (1997) Geology and mineral potential of diapiric inliers in the northern BURRA 1:250 000 map area. MESA Journal 5:37–45

Cuevas Leree JA (1985) Analysis of subsidence and thermal history in the Sabinas basin, northeastern Mexico. M.S., University of Arizona

De Cserna Z (1956) Tectónica de la Sierra Madre Oriental, entre Torreón y Monterrey, Mexico, D.F., Contribuciones, XX Congreso Geológico Internacional

Dickinson WR, Lawton TF (2001) Carboniferous to cretaceous assembly and fragmentation of Mexico. Geol Soc Am Bull 113:1142–1160. https://doi.org/10.1130/0016-7606(2001)113<1142:CTCAAF>2.0.CO;2

Drewes H (1988) Development of the foreland zone and adjacent terranes of the Cordilleran orogenic belt near the U.S.-Mexican border. In: Schmidt CA, Perry WJ JR (eds) Interaction of the Rocky Mountain foreland and the Cordilleran thrust front, vol. 171. Geological Society of America Memoir, Boulder Colorado, pp 447–463

Druke DC (2005) Sedimentology and Stratigraphy of the San Jose Lentil, La Popa Basin, Mexico and Its Implications For Carbonate Development in a Tectonicall Influenced Salt Basin. M.S. thesis, New Mexico State University, p 132

Eguiluz De Antuñano S (1989) La formacion Carbonera y sus implicaciones tectonicas, estados de Coahuila y Nuevo Leon. Boletín De La Sociedad Geologica Mexicana 50:3–40

Eguiluz De Antuñano S, Aranda-García M, Marrett R (2000) Tectónica de la Sierra Madre Oriental, México. Boletín De La Sociedad Geológica Mexicana 53:1–26

Eldrett JS, Minisini D, Bergman SC (2014) Decoupling of the carbon cycle during Ocean Anoxic Event 2. Geology 42:567–570. https://doi.org/10.1130/G35520.1

Fernández O, Habermüller M, Grasemann B (2020) Hooked on salt: rethinking Alpine tectonics in Hallstatt (Eastern Alps, Austria). Geology 49. https://doi.org/10.1130/G47981.1

Fitz-Díaz E, Hudleston P, Tolson G, van der Pluijm B (2014) Progressive, episodic deformation in the Mexican Fold-Thrust Belt (central Mexico): evidence from isotopic dating of folds and faults. Int Geol Rev 56:734–755. https://doi.org/10.1080/00206814.2014.896228

Fitz-Díaz E, Lawton TF, Juárez-Arriaga E, Chávez-Cabello G (2018) The Cretaceous-Paleogene Mexican orogen: Structure, basin development, magmatism and tectonics. Earth Sci Rev 183:56–84. https://doi.org/10.1016/j.earscirev.2017.03.002

Fortunato KS, Ward WC (1982) Upper Jurassic-Lower Cretaceous fan-delta complex, La Casita Formation of the Saltillo area, Coahuila, Mexico. Gulf Coast Assoc Geol Soc Trans 32:473–482

Garrison JM, Mcmillan NJ (1999) Evidence for Jurassic continental rift magmatism in northeast Mexico: Allogenic meta-igneous blocks in El Papalote diapir, La Popa basin, Nuevo Leon, Mexico. In: Bartolini C, Wilson JL, Lawton TF (eds) Mesozoic sedimentary and tectonic history of North-Central Mexico, vol 340. Geological Society of America Special Paper, Boulder, Colorado, pp 319–332

Giles KA, Lawton TF (1999) Attributes and evolution of an exhumed salt weld, La Popa basin, northeastern Mexico. Geology 27:323–326

Giles KA, Lawton TF (2002) Halokinetic sequence stratigraphy adjacent to the El Papalote diapir, northeastern Mexico. Am Asso Petrol Geol Bull 86:823–840

Giles KA, Rowan MG (2012) Concepts in halokinetic-sequence deformation and stratigraphy. In: Alsop GI, Archer SG, Hartley AJ, Grant NT, Hodgkinson R (eds) Salt tectonics, sediments and prospectivity, vol 363. Geological Society, London, Special Publication, pp 7–31

Giles KA, Druke DC, Mercer DW, Hunnicutt-Mack L (2008) Controls on Upper Cretaceous (Maastrichtian) heterozoan carbonate platforms developed on salt diapirs, La Popa basin, NE Mexico. SEPM Special Publication 89:107–124

Goldhammer RK (1999) Mesozoic sequence stratigraphy and paleogeographic evolution of northeast Mexico. In: Bartolini C, Wilson JL, Lawton TF (eds) The Western Gulf of Mexico Basin: tectonics, sedimentary basins, and petroleum systems, vol 340. Geological Society of America Special Paper, Boulder, Colorado, pp 1–58

Goldhammer RK, Lehmann PJ, Todd RG, Wilson JL, Ward WC, Johnson CR (1991) Sequence stratigraphy and cyclostratigraphy of the Mesozoic of the Sierra Madre Oriental, northeast Mexico: a field guide book. Society of Economic Paleontologists and Mineralogists Foundation, Gulf Coast Section, p 84

Götte M, Michalzik D (1992) Stratigraphic relations and facies sequences of an Upper Jurassic evaporitic ramp in the Sierra Madre Oriental (Mexico). Zentralblatt Für Geologie Und Palaontologie Teil I 1991:1445–1466

Granado P, Roca E, Strauss P, Pelz K, Muñoz JA (2018) Structural styles in fold-and-thrust belts involving early salt structures: the Northern Calcareous Alps (Austria). Geology 47:51–54. https://doi.org/10.1130/G45281.1

Gray GG, Johnson CA (1995) Structural and tectonic evolution of the Sierra Madre Oriental, with emphasis on the Saltillo-Monterrey corridor: a field guidebook: Houston, Texas. Am Assoc Pet Geol Ann Convention 17

Gray GG, Lawton TF (2011) New constraints on timing of Hidalgoan (Laramide) deformation in the Parras and La Popa basins, NE Mexico. In: Montalvo-Arrieta JC, Chávez-Cabello G, Velasco-Tapia F (eds) Volumen especial: Avances y paradigmas sobre la evolución geológica del noreste de México. Boletín de la Sociedad Geológica Mexicana, vol 63, pp 333–343

Gray GG, Eguiluz de Antuñano S, Chuchla RJ, Yurewiczu DA (1997) Structural evolution of the Saltillo-Monterrey corridor, Sierra Madre Oriental: applications to exploration challenges in fold-thrust belts-a field guidebook: Privately Published, p 20

Gray GG, Pottorf RJ, Yurewicz DA, Mahon KI, Pevear DR, Chuchla RJ (2001) Thermal and chronological record of syn- to post-Laramide burial and exhumation, Sierra Madre Oriental, Mexico. In: Bartolini C, Buffler, RT, Cantu Chapa A (eds) The Western Gulf of Mexico Basin: tectonics, sedimentary basins, and petroleum systems, vol 75. American Association of Petroleum Geologists, Memoir, Tulsa, Oklahoma, pp 159–181

Gray GG, Villagomez D, Pindell J, Molina-Garza RS, O'sullivan P, Stockli D, Farrel W, Blank D, Schuba J (2020) Late Mesozoic and Cenozoic thermotectonic history of eastern, central and southern Mexico as determined through integrated thermochronology, with implications for sediment delivery to the Gulf of Mexico. In: Dawson I, Hull JNF, Pindell J (eds) The basins, orogens and evolution of the Southern Gulf of Mexico and Northern Caribbean. The Geological Society of London, Special Publication, London, p 504. https://doi.org/10.6084/m9.figshare.c.4991948.

Groves IM, Carman CE, Dunlap WJ (2003) Geology of the Beltana willemite deposit, Flinders Ranges, South Australia. Econ Geol 98:797–818

Guzman EJ, de Cserna Z (1963) Tectonic history of Mexico. In: Childs OE, Beebe BW (eds) Backbone of the Americas-tectonic history from pole to pole, vol 2. American Association of Petroleum Geologists, Memoir, Tulsa, Oklahoma, pp 113–129

Hearon TEI, Rowan MG, Giles KA, Kernan RK, Gannaway CE, Lawton TF, Fiduk JC (2015) Allochthonous salt initiation and advance in the northern Flinders and eastern Willouran ranges, South Australia: using outcrops to test subsurface-based models from the northern Gulf of Mexico. Am Assoc Pet Geol Bull 99:293–331. doi: https://doi.org/10.1306/08111414022

Hennings PH (1994) Structural transect of the southern Chihuahua fold belt between Ojinaga and Aldama, Chihuahua, Mexico. Tectonics 13:1445–1460

Hitzman MW, Broughton D, Selley D, Woodhead J, Wood D, Bull S (2012) The Central African Copperbelt: diverse stratigraphic, structural, and temporal settings in the world's largest sedimentary copper district. Soc Econ Geol Spec Publ 16:487–514

Hon KD (2001) Salt-influenced growth-stratal geometries and structure of the Muerto formation adjacent to an ancient secondary salt weld, La Popa Basin, Nuevo León, Mexico. M.S. thesis, New Mexico State University, p 97

Hudec MR, Jackson MPA (2007) Terra infirma: understanding salt tectonics. Earth Sci Rev 82:1–28

Hudec MR, Jackson MPA (2011) The salt mine; a digital atlas of salt tectonics, vol 99. American Association of Petroleum Geologists, Memoir, p 305

Hudec MR, Norton IO, Jackson MPA, Peel FJ (2013) Jurassic evolution of the Gulf of Mexico salt basin. Am Asso Petrol Geol Bull 97:1683–1710

Hunnicutt L (1998) Tectonostratigraphic interpretation of Upper Cretaceous to lower Tertiary limestone lentils within the Potrerillos Formation surrounding El Papalote diapir, La Popa basin, Nuevo Leon, Mexico. M.S. thesis, New Mexico State University, p 181

Imlay RW (1937) Geology of the middle part of the Sierra de Parras, Coahuila, Mexico. Geol Soc Am Bull 48:587–630

Imlay RW, Herman G (1984) Upper Jurassic ammonites from the subsurface of Texas, Louisiana, and Mississippi. In: Ventress WPS, Bebout DG, Perkins BF, Moore CH (eds) The Jurassic of the Gulf rim. Gulf Coast Section, Society of Economic Paleontologists and Mineralogists Foundation, Proceedings of the Third Annual Research Conference, Austin, Texas, pp 149–170

Juárez-Arriaga E, Lawton TF, Ocampo-Díaz YZE, Stockli DF, Solari L (2019) Sediment provenance, sediment-dispersal systems, and major arc-magmatic events recorded in the Mexican foreland basin, North-Central and Northeastern Mexico. Int Geol Rev 61:2118–2142. https://doi.org/10.1080/00206814.2019.1581848

Juárez-Arriaga E, Lawton TF, Stockli DF, Solari L, Martens U (2019) Late Cretaceous-Paleocene stratigraphic and structural evolution of the central Mexican fold and thrust belt, from detrital zircon (U-Th)/(He-Pb) ages. J S Am Earth Sci 96. https://doi.org/10.1016/j.jsames.2019.102264

Kroeger KF, Stinnesbeck W (2003) The Minas Viejas Formation (Oxfordian) in the area of Galeana, northeastern Mexico: significance of syndepositional volcanism and related barite genesis in the Sierra Madre Oriental. In: Bartolini C, Buffler RT, Blickwede J (eds) The Circum-Gulf of Mexico and the Caribbean: hydrocarbon habitats, basin formation, and plate tectonics, vol 79. American Association of Petroleum Geologists Memoir, pp 515–528

Krutak, PR (1967) Structural geology of the Sierra de la Gavia, Coahuila, Mexico. Geol Soc Am Bull 78:59–75

Laudon RC (1984) Evaporite diapirs in the La Popa basin, Nuevo León, México. Geol Soc Am Bull 95:1219–1225

Laudon RC (1996) Salt dome growth, thrust fault growth, and syndeformational stratigraphy, La Popa basin, northern Mexico. Trans Gulf Coast Assoc Geol Soc 46:219–228

Lawton TF (2000) Inversion of Late Jurassic-Early Cretaceous extensional faults of the Bisbee basin, southeastern Arizona and southwestern New mexico. In: Lawton TF, Mcmillan NJ, Mclemore VT (eds) Southwest passage-a trip through the Phanerozoic, vol 51. New Mexico Geological Society, Guidebook, pp 95–102

Lawton TF, Amato JM (2017) U-Pb ages of salt diapir xenoliths, La Popa basin: implications for salt age in onshore Mexico salt basins. Lithosphere 9:745–758. https://doi.org/10.1130/L658.1

Lawton TF, Buck BJ (2006) Implications of diapir-derived detritus and gypsic paleosols in Lower Triassic strata near the Castle Valley salt wall, Paradox basin, Utah. Geology 34:885–888. https://doi.org/10.1130/G22574.1

Lawton TF, Clemons RE (1992) Klondike basin - late Laramide depocenter in southern New Mexico. New Mex Geol 14:1–17

Lawton TF, Giles KA (1997a) El Papalote diapir, La Popa basin. In: Soegaard K, Giles KA, Vega FJ, Lawton TF (eds) Structure, stratigraphy, and paleontology of late cretaceous-early tertiary Parras-La Popa Foreland Basin Near Monterrey, Northeast Mexico. AAPG Annual Convention, Dallas, Texas, Field Trip #10, pp 55–74

Lawton TF, Giles KA (1997b) Influence of intermittent salt diapirism and Madrean thrusting on Late Cretaceous-Paleogene sedimentation patterns, La Popa basin. AAPG Abstracts Meeting, Dallas Annual Convention, Mexico

Lawton TF, Molina-Garza RS (2014) U-Pb geochronology of the type Nazas Formation and superjacent strata, northeastern Durango, Mexico: implications of a Jurassic age for continental-arc magmatism in north-central Mexico. Geol Soc Am Bull 126:1181–1199. https://doi.org/10.1130/B30827.1

Lawton TF, Vega FJ, Giles KA, Rosales-Dominguez C (2001) Stratigraphy and origin of the La Popa basin, Nuevo Leon and Coahuila, Mexico. In: Bartolini C, Buffler RT, Cantú-Chapa A (eds) The Western Gulf of Mexico Basin: tectonics, sedimentary basins, and petroleum systems, vol 75. American Association of Petroleum Geologists Memoir, Tulsa, Oklahoma, pp 219–240

Lawton TF, Shipley KW, Aschoff JL, Giles KA, Vega FJ (2005) Basinward transport of Chicxulub ejecta by tsunami-induced backflow, La Popa basin, northeastern Mexico, and its implications for distribution of impact-related deposits flanking the Gulf of Mexico. Geology 33:81–84

Lawton TF, Sierra-Rojas MI, Martens U (2020) Stratigraphic correlation chart of Carboniferous–Paleogene rocks of Mexico, adjacent southwestern United States, Central America, and Colombia. In: Martens U, Molina Garza RS (eds) Southern and Central Mexico: basement framework, tectonic evolution, and provenance of Mesozoic–Cenozoic Basins. Geological Society of America, Boulder, Colorado, Special Paper 546. https://doi.org/10.1130/s2020.2546(05)

Longoria JF (1984) Mesozoic tectonostratigraphic domains in east-central Mexico. In: Westermann GEG (ed) Jurassic-Cretaceous biochronology and paleogeography of North America. Geological Society of America Special Paper 27, pp 171–193

Lopez R, Cameron KL, Jones NW (2001) Evidence for Paleoproterozoic, Grenvillian, and Pan-African age Gondwanan crust beneath northeastern Mexico. Precambr Res 107:195–214

Lopez-Ramos E (1982) Geología de México, México, DF, Consejo Nacional de Ciencia y Technología, p 454

Marrett RJ, Aranda-García M (1999) Structure and kinematic development of the Sierra Madre Oriental fold-thrust belt, Mexico. In: Wilson JL, Ward WC, Marrett RA (eds) Stratigraphy and structure of the Jurassic and cretaceous platform and basin systems of the sierra Madre oriental, Monterrey and Saltillo areas, Northeastern Mexico-a Field Book and Related Papers. South Texas Geological Society, San Antonio, pp 69–98

Martini M, Fitz E, Solari L, Camprubí A, Hudleston PJ, Lawton TF, Tolson G, Centeno-García E (2012) The Late Cretaceous fold-thrust belt in the Peña de Bernal-Tamazunchale area and its possible relationship to the accretion of the Guerrero terrane. In: Aranda-Gomez JJ, Tolson G, Molina-Garza RS (eds) The Southern Cordillera and beyond, vol 25. Geological Society of America Field Guide, pp 19–38

Marton G, Buffler RT (1994) Jurassic reconstruction of the Gulf of Mexico basin. Int Geol Rev 36:545–586

Mcbride EF, Weidie AE, Wolleben JA, Laudon RC (1974) Stratigraphy and structure of the Parras and La Popa basins, northeastern Mexico. Geol Soc Am Bull 84:1603–1622

Mckee JW, Jones NW, Long LE (1984) History of recurrent activity along a major fault in northeastern Mexico. Geology 12:103–107

Mckee JW, Jones NW, Anderson TH (1988) Las Delicias basin: a record of late Paleozoic arc volcanism in northeastern Mexico. Geology 16:34–40

Millán-Garrido H (2004) Geometry and kinematics of compressional growth structures and diapirs in the La Popa basin of northeast Mexico: insights from sequential restoration of a regional cross section and three-dimensional analysis Tectonics, 23, TC5011. https://doi.org/10.1029/2003TC001540

Padilla Y, Sánchez RJ (1982) Geologic evolution of the Sierra Madre Oriental between Linares, Concepción del Oro, Saltillo y Monterrey; Mexico [Ph. D. dissert.]: Austin, Texas, The University of Texas, p 217

Padilla Y, Sánchez RJ (1985) Las estructuras de la Curvatura de Monterrey, Estados de Coahuila, Nuevo León, Zacatecas y San Luís de Potosí. Instituto de Geología Revista, 6:1–20

Pindell JL (1985) Alleghenian reconstruction and subsequent evolution of the Gulf of Mexico, Bahamas, and proto-Caribbean. Tectonics 4:1–39

Pindell J, Weber B, Hale-Erlich W, Cossey S, Bitter M, Molina Garza RS, Graham R, Erlich RN (2020) Strontium isotope dating of evaporites and the breakup of the Gulf of Mexico and Proto-Caribbean Seaway. In: Martens U, Molina Garza RS (eds) Southern and Central Mexico: basement framework, tectonic evolution, and provenance of Mesozoic–Cenozoic Basin. Geological Society of America, Boulder, Colorado, Special Paper 546. https://doi.org/10.1130/2020.2546(12)

Pulham, AJ, Peel FJ, Rives T, Delph B, Salel J-F, Nicholson T, Wu J, Requejo R (2019) The age of the Louann Salt; insights from historic isotopic analyses in salt stocks from the onshore interior salt basins of the northern Gulf of Mexico. In: Fiduk JC, Rosen NC (eds) Salt tectonics, associated processes, and exploration potential: revisited 1989–2019. 37th Anual GCSSEPM Foundation Perkins-Rosen Research Conference, Houston, Texas, pp 64–66

Quintero-Legorreta O, Aranda-García M (1985) Relaciones estructurales entre el anticlinorio de Parras y el Anticlinorio (Sierra Madre Oriental) en la región de Agua Nueva, Coahuila. Instituto De Geología Revista 6:21–36

Sandwell DT, Dietmar Müller R, Smith WHF, Garcia E, Francis R (2014) New global marine gravity model from CryoSat-2 and Jason-1 reveals buried tectonic structure. Science 346:65–67

Rowan MG (in press) The ocean-continent transition of late synrift salt basins: extension and evaporite deposition in the southern Gulf of Mexico and global analogs. From the Guajira Desert to the Apennines, and from Mediterranean Microplates to the Mexican Killer Asteroid. Geological Society of America Special Paper, Boulder, Colorado

Rowan MG, Vendeville BC (2006) Foldbelts with early salt withdrawal and diapirism: physical model and examples from the northern Gulf of Mexico and the Flinders Ranges, Australia. Mar Pet Geol 23:871–891

Rowan MG, Lawton TF, Giles KA, Ratliffe RA (2003) Near-salt deformation in La Popa basin, Mexico, and the northern Gulf of Mexico: a general model for passive diapirism. Am Asso Petrol Geol Bull 87:733–756

Rowan MG, Lawton TF, Giles KA (2012) Anatomy of an exposed vertical salt weld and flanking strata, La Popa Basin, Mexico. In: Alsop GI, Archer SG, Hartley AJ, Grant NT, Hodgkinson R (eds) Salt tectonics, sediments and prospectivity. Geological Society of London Special Publication 363, pp 33–57

Rowan MG, Muñoz JA, Giles KA, Roca E, Hearon TE IV, Fiduk JC, Ferrer O, Fischer MP (2020) Folding and fracturing of rocks adjacent to salt diapirs. J Struct Geol 141. https://doi.org/10.1016/j.jsg.2020.104187

Salvany JM, Bastida J (2004) Análisis litoestratigráfico del Keuper Surpirenaico central. Revista De La Sociedad Geológica De España 17:3–26

Scott RW (1984) Significant fossils of the Knowles Limestone, Lower Cretaceous, Texas. In: Ventress WPS, Bebout DG, Perkins BF, Moore CH (eds) The Jurassic of the Gulf rim. Gulf coast section, society of economic paleontologists and mineralogists foundation, proceedings of the 3rd annual research conference, Austin, Texas, pp 333–346

Seager WR, Mack GH (1986) Laramide paleotectonics of southern New Mexico. In: Peterson JA (ed) Paleotectonics and sedimentation in the Rocky Mountain region, United States. American Association of Petroleum Geologists Memoir 41, pp 669–685

Servais M, Cuevas-Pérez E, Monod O (1986) Une section de Sinaloa a San Luis Potosi: nouvelle approche de l'evolution du mexique nord-occidental. Bulletin De La Société Géologique De France 8:1033–1047

Shipley KW (2004) Ejecta-bearing deposits at the cretaceous-tertiary boundary and their implications for timing of Hidalgoan (Laramide) Folding, La Popa Basin, Nuevo Leon, Mexico. M.S. thesis, New Mexico State University, p 146

Smith CI (1981) Review of the geologic setting, stratigraphy, and facies distribution of the Lower Cretaceous in northern Mexico. In: Lower cretaceous stratigraphy and structure, Northern Mexico. West Texas Geological Society, Field Trip Guidebook, Publication 81–74, pp 1–27

Snedden JW, Galloway WE (2019) The Gulf of Mexico Sedimentary Basin. Cambridge University Press, Cambridge, p 326. https://doi.org/10.1017/9781108292795

Soegaard K, Ye H, Halik N, Daniels AT, Arney J, Garrick S (2003) Stratigraphic evolution of latest Cretaceous to early Tertiary Difunta foreland basin in northeast Mexico: influence of salt withdrawal on tectonically induced subsidence by the Sierra Madre Oriental fold and thrust belt. In: Bartolini C, Buffler RT, Blickwede J (eds) The Circum-Gulf of Mexico and the Caribbean: hydrocarbon habitats, basin formation, and plate tectonics. American Association of Petroleum Geologists Memoir 79, Tulsa, Oklahoma, pp 364–394

Suppe J, Sàbat F, Muñoz JA, Poblet J, Roca E, Vergés J (1997) Bed-by-bed fold growth by kink-band migration: Sant Llorenç de Morunys, eastern Pyrenees. J Struct Geol 19:443–461

Suter M (1984) Cordillerean deformation along the eastern edge of the Valles-San Luís de Potosí States carbonate platform, Sierra Madre Oriental fold-thrust belt, east-central Mexico. Geol Soc Am Bull 95:1387–1397

Suter M (1987) Structural traverse across the Sierra Madre oriental fold-thrust belt in east-central Mexico. Geol Soc Am Bull 98:249–264

Tardy M, Carfantan J-C, Rangin C (1986) Essay de sinthèse sur la structure du Mexique. Bulletin De La Société Géologique De France 8:1025–1031

Tardy M, Lapierre H, Freydier C, Coulon C, Gill JB, Mercier de Lepinay B, Beck C, Martinez RJ, Talavera MO, Ortiz HE, Stein E, Bourdier JL, Yta M (1994) The Guerrero suspect terrain (the Greater Antilles and the Western Cordillera of Colombia): a late Mesozoic intra-oceanic arc accreted to cratonal America during the Cretaceous. Tectonophysics 230:49–73

Thompson RM, Morrison MA, Hendry GL, Parry SJ (1984) An assessment of the relative roles of crust and mantle in magma genesis: an elemental approach. Roy Soc Lond Philos Trans Ser A 310:549–590

Vega FJ (1989) La presencia del Eocene merino en la cuenca de la Popa (Grupo Difunta), Nuevo Leon: orogenia post-Ypresiana: Universidad Nacional Autonoma de Mexico, Instituto de Geologia. Revista 8:67–70

Vega FJ, Lawton TF (2011) Upper Jurassic (Lower Kimmeridgian-Olvido) carbonate strata from the La Popa Basin diapirs, NE Mexico. Boletín De La Sociedad Geológica Mexicana 63:313–321

Vega FJ, Mitre-Salazar LM (1997) Stratigraphy and deformational history at the La Popa basin, northeastern Mexico: Geological Society of America Abstracts with Programs, 29/2, p 49

Vega FJ, Perrilliat MC (1989) On a new species of Venecardia from the lower Eocene in northeastern Mexico (Difunta Group). Tulane Studies in Geology and Paleontology 22:101–106

Vega-Vera FJ, Mitre-Salazar LM, Martínez-Hernández E (1989) Contribución al conocimiento de la estratigrafía del Grupo Difunta (Cretácico Superior-Terciario) en el noreste de México. Universidad Nacional Autonóma De México, Instituto De Geología, Revista 8:179–187

Vega FJ, Perrilliat M, Duarte-Torres L, Durán-Herrera G, Rivas-García R, Aguilar-Piña M, Ventura JF (2007) Eocene strata from the Sabinas Basin and their bearing in sedimentary basin correlation in NE Mexico. Boletín De La Sociedad Geológica Mexicana 59:115–123

Vendeville BC, Jackson MPA (1992) The rise of diapirs during thin-skinned extension. Mar Pet Geol 9:331–353

Wall JR, Murray GE, Diaz GT (1961) Occurrence of intrusive gypsum and its effects on structural forms in Coahuila marginal folded province of northeastern Mexico. Am Asso Petrol Geol Bull 45:1504–1522

Waidmann BR (2004) Geometries of Strata in a Salt-withdrawal Basin as Predictors of Shortening-driven Diapir Tectonics: Carroza Formation, La Popa Basin, Nuevo León, Mexico. M.S. thesis, New Mexico State University, p 131

Weislogel AL, Lawton TF (2000) Facies assemblages of the tidally-influenced deltaic system of the Maastrichtian Muerto Formation, La Popa basin, Mexico: an analogue for the Gulf of Mexico subsurface. Trans Gulf Coast Assoc Geol Soc 50:669–678

Wilson JL, Ward WC (1993) Early Cretaceous carbonate platforms of northeastern and east-central Mexico. In: Simo JA, Scott RW, Masse JP (eds) Cretaceous carbonate platforms. American Association of Petroleum Geologists Memoir, 56, pp 35–49

Yarnold JC (1993) Rock-avalanche deposits in dry climates and the effect of flow into lakes: insights from the mid-Tertiary sedimentary breccias near Artillery Peak, Arizona. Geol Soc Am Bull 105:345–360

Ye H (1997) The arcuate Sierra Madre Oriental orogenic belt, NE Mexico: tectonic infilling of a recess along the southwestern North American continental margin. Structure, Stratigraphy and Paleontology of Late Cretaceous-Early Tertiary Parras-La Popa Foreland Basin near Monterrey, Northeast Mexico. AAPG-Field trip 10, pp 82–115